Spring 1-1-2003

Principles of Chemical Reactivity on the Diels-Alder Reaction in Ionic Liquids and Lewis Acid Catalysis using Large-Scale Computations

Orlando Acevedo

Principles of Chemical Reactivity on the Diels-Alder Reaction in Ionic Liquids and Lewis Acid Catalysis using Large-Scale Computations

A Dissertation

Presented to the Bayer School

of Natural and Environmental Sciences

Duquesne University

In partial fulfillment of

the requirements for

the degree of Doctor of Philosophy

by

Orlando Acevedo

May 2003

Name	**Orlando Acevedo**
Dissertation Title	**Principles of Chemical Reactivity on the Diels-Alder Reaction in Ionic Liquids and Lewis Acid Catalysis using Large-Scale Computations**
Degree	Doctor of Philosophy
Date	May 3, 2003

APPROVED _____
Dr. Jeffrey D. Evanseck
Dissertation Director
Associate Professor of Chemistry and Biochemistry

APPROVED _____
Dr. Jeffry D. Madura
Chairman, Dept. of Chemistry and Biochemistry
Associate Professor of Chemistry and Biochemistry

APPROVED _____
Dr. Bruce Beaver
Associate Professor of Chemistry and Biochemistry

APPROVED _____
Dr. Daniel A. Singleton
Professor of Chemistry, Texas A&M University

APPROVED _____
Dr. David W. Seybert
Dean, Bayer School of Natural and Environmental Sciences
Professor of Chemistry and Biochemistry

ACEVEDO, ORLANDO (Ph.D., Chemistry)

PRINCIPLES OF CHEMICAL REACTIVITY ON THE DIELS-ALDER REACTION IN IONIC LIQUIDS AND LEWIS ACID CATALYSIS USING LARGE-SCALE COMPUTATIONS (May 2003)

Abstract of a dissertation at Duquesne University

Disseration supervised by Professor Jeffrey D. Evanseck

No. of pages in text: 195

My Ph.D. dissertation describes three different external influences on pericyclic reactions: **(1) ionic liquids, (2) Lewis acids and (3) bis(oxazoline)-Cu(II) complexes**. (1) Ionic liquids deliver enhanced rates and *endo/exo* selectivities on the Diels-Alder reaction. The goal is to establish a firm understanding of the molecular interactions that give rise to the observed rate and selectivity enhancements. In order to accomplish our goal, we have used density functional theory methodology, specifically the Becke three parameter with Lee, Yang and Parr corrections at the 6-31G(d), to describe short-range effects, and have created new force field parameters using CHARMM to allow faster classical computations and explore bulk phase effects. (2) Lewis acids are known to influence strongly the rate, regio, *endo/exo*, diastereofacial and enantio selectivities of the Diels-Alder reaction. Specifically, asymmetric catalysis using chiral Lewis acids provides a crucial tool in the enantioselective synthesis of chiral organic compounds. Uncovering the differential forces between the ground and transition structures with chiral Lewis

acids is a perquisite step towards the creation of more effective enantioselective catalysts. Our efforts focus upon a novel combination of two specific intermolecular interactions between boron Lewis acids and Diels-Alder transition structures. Quantum mechanical calculations along with kinetic isotope effects are used in conjunction to elucidate these specific interactions. (3) Cu(II) functions effectively as a Lewis acidic center that has proven to control the stereoselectivity of a wide range of organic reactions. Specifically, bis(oxazoline) copper(II) complexes operate as enantioselective Lewis acid catalysts for carbocyclic and hetero Diels-Alder reactions. We have used quantum mechanical calculations in order to determine how ligand field strength influences Cu(II) coordination and ultimately the stereoselectivity of organic reactions.

To my parents.

ACKNOWLEDGEMENTS

I would like to thank Jeffrey D. Evanseck for his ability to inspire in me the pursuit of science and for his guidance and encouragement over the years. I feel lucky to have had him as an advisor and as a friend. The direct contribution he has made to my intellectual growth cannot be minimized. Jeff listened to my ideas with an open mind, encouraged me during difficult times, and inspired me by being a role model for the entire group.

I thank Jeffry D. Madura for his guidance and for making my transition to Duquesne University a welcomed one. His support during my studies is greatly appreciated, as well as the valuable advice and help in my research.

I thank Evanseck's research group members who have been to me a family away from home. Over the years we have developed relationships that will endure and I will always remember all the fond memories in the ERG. I would especially like to thank Jason DeChancie, Mike Gomez , Sue Kong, Anne Loccisano, Alba Macias , Sarah Mueller and Amy Waligorski for their help and friendship. I give a special thanks to Jason DeChancie for all his help on Chapter 6 of this thesis.

I thank Madura's research group members for their assistance and friendship. I would like to thank, especially, Pranav Dalal, Tom Dick and Emilio Esposito.

I gratefully acknowledge the Department of Chemistry and Biochemistry at Duquesne University for supporting me financially and allowing me the opportunity to be in charge of millions of dollars worth of computer equipment, even if it meant countless hours of being on the phone with IBM and SGI. I acknowledge the National Energy and Technology Laboratory (NETL) for financial support over the last year and a half of my Ph.D. research.

I express great gratitude towards my parents who have supported me throughout my entire life, no matter which endeavor I would have chosen. I know my father would have been proud of my accomplishments; his guidance is directly responsible my success. Finally, I thank my wife Chantel, for her love and enduring support throughout the years.

Contents

List of Figures

List of Schemes

List of Tables

Chapter 1

Introduction

The Diels-Alder reaction, first discovered in 1928,[1] is one of the most commonly utilized carbon-carbon bond forming processes in organic synthesis.[2,3] Its significance is so great, that Otto Diels and Kurt Alder were awarded the Nobel Prize in 1950 for its discovery.[2,3] In 1960, Yates and Eaton reported that an approximate rate acceleration of 10^5 was observed for the Diels-Alder reaction between anthracene and maleic anhydride in the presence of aluminum chloride.[4] This study greatly extended the range of Diels-Alder reactions that could be carried out under mild conditions. Their work, along with a subsequent study by Inukai and Kojima,[5] initiated efforts by several research groups to improve the rate as well as selectivity of Diels-Alder reactions by focusing upon the external conditions of the reaction, such as high temperature and pressure, Lewis acids, aqueous solutions, stable cation radicals, microwave radiation, lithium perchlorate,

chromatographic absorbents, ionic liquids and micelles.[6] The present understanding of how to control this important reaction is formed from a huge amount of experimental work, yet there are a number of unresolved problems that need further scientific investigation to develop a complete understanding of the Diels-Alder reaction. First, the recently reported rate and *endo/exo* stereoselective enhancement of Diels-Alder reactions by ionic liquids[7,8] is so new that no systematic investigation has been attempted to explain the molecular origins of its effect. Second, Lewis acids are known to influence strongly the rate, regio, *endo/exo*, diastereofacial and enantio selectivities of the Diels-Alder reaction[9,10], however, uncovering the differential forces between the ground and transition structures with chiral Lewis acids is a perquisite step towards the creation of more effective enantioselective catalysts. Technology is evolving at an astounding rate, rapidly increasing the performance of computers at all levels. Advancements in microprocessor performance has brought down the cost of computers and reduced their size. Improvements in interconnect devices has helped to make high-performance power more accessible and affordable, with more open system architectures that contribute to enhanced scalability. The ability to network the computing power of smaller systems to find solutions to large computational problems has allowed for great scientific insight, which has been difficult to determine by experiment.. Given the synthetic value and current understanding of external effects on the Diels-Alder reaction coupled with advances in computer technology and algorithm development, it is important to further investigate the factors causing dramatic rate acceleration and *endo/exo* selectivity from both ionic liquids and Lewis acids. In this work, a computational and experimental study is undertaken to provide the necessary microscopic details to uncover the molecular

origins of rate and selectivity enhancements by ionic liquids, Lewis acids and bis(oxazoline) copper(II) complexes for the Diels-Alder reaction.

1.1 The Diels-Alder Reaction

1.1.1 Mechanistic Aspects of the Diels-Alder Reaction

The Diels-Alder reaction involves a [4+2] cycloaddition of a diene and a dienophile to produce a cycloadduct. Using the Woodward-Hoffman rules and the concept of secondary orbital interactions,[11] the preferred product can be easily predicted.[12] The mechanism, however, has been the subject of long debate, documented in a series of papers by Houk.[13,14] As shown in Figure 1.1, both a concerted mechanism, involving a single, aromatic transition structure and a stepwise reaction path have been proposed. In the concerted mechanism, there is partial formation of the two new bonds in the single transition structure. The two bonds can form to the same extent, in which it is referred to as a synchronous and concerted reaction. If the two bonds form to different extents, then the reaction is asynchronous. The other mechanism is called a stepwise process, which involves the formation of an intermediate diradical due to a single bond being formed between the diene and the dienophile. The second bond forms subsequently to give the product.

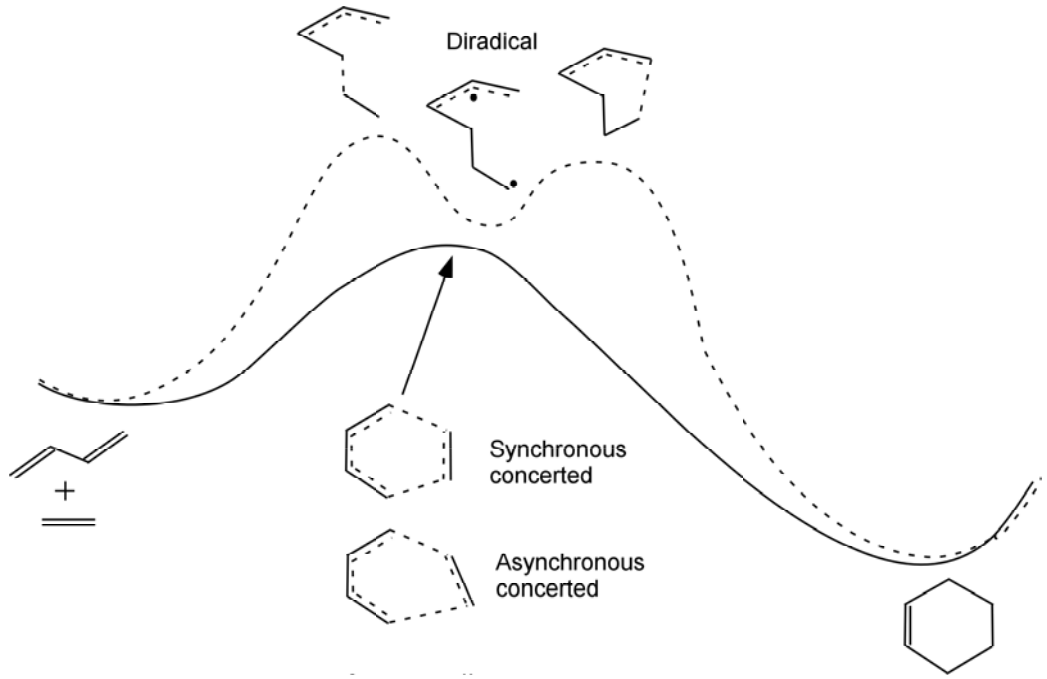

Figure 1.1. *The energy diagram for concerted and stepwise mechanisms of the Diels-Alder reaction between butadiene and ethene.*

R. B. Woodward and coworkers constructed the currently accepted asynchronous concerted mechanism, based on a study of the Cope rearrangement.[15] The transition structure of this interconversion appeared to be related to the Diels-Alder reaction. Since the Diels-Alder reaction could form either product from the Cope rearrangement, it was assessed that the transition structures should be similar. M. Dewar opposed this mechanism on the basis of the relative rates of several Diels-Alder reactions.[13,16] He promoted a symmetric cyclic pseudoaromatic transition state. Even though it is now well established that Diels-Alder cycloadditions proceed through a concerted reaction mechanism, external influences, such as Lewis acid activation, can switch the mechanism to a stepwise reaction.[17] A more in-depth and critical review concerning the mechanistic aspects of the Diels-Alder reaction have been reported.[2,18] External influences on

concerted reactions and their impact on the mechanism of pericyclic reactions continues to be our area of interest in research.

1.1.2 Regio- and Stereoselectivities

Reactivity of the Diels-Alder reaction has been reasonably explained by the Woodward-Hoffmann (WH) rule[12] and Fukui's frontier-orbital theory (FMO).[19] The WH rule is a symmetry conservation rule. A symmetry element, such as a plane or rotation axis is retained throughout reaction paths for "symmetry-allowed" reactions. In general, geometric distortions in the course of reaction is avoided to stay on the minimum-energy trajectory. Reactions between conjugated systems with $(4n + 2)$ π electrons lie on a "symmetry-allowed" path, but a system with $4n$ π electrons belong to a "symmetry-forbidden" path. FMO is based on a perturbative treatment of two reactants and is under kinetic control.

In the Diels-Alder reaction, a preference for formation of the *endo* product is typically, however not exclusively, observed.[11] Although several theories have been proposed to explain the observed selectivity, none is firmly established. Initially, Alder created the rule of "maximum accumulation of unsaturation" which is one of the more popular explanations attributing the *endo* preference to the secondary π-orbital overlap. Several researchers such as Woodward-Hoffmann,[12] Houk,[20] Salem,[21] Alston,[22] Singleton[23] and Yamabe[24] have investigated specific secondary orbital overlaps to rationalize this preference.

Briefly, secondary orbital interactions are the transition structure terms that do not involve covalent bond making or breaking. From FMO theory, the diene HOMO and

dienophile LUMO coefficients allow for a number of positive overlaps, or stabilizing interactions, where three of the individual secondary orbital interactions are considered. The classical secondary orbital interactions defined by Woodward and Hoffmann (WH) resulted from the FMO treatment of butadiene dimerization. The interaction defined from independent theoretical studies of the butadiene and acrolein reaction by Salem, Houk, and Alston is referred to as SAH in Figure 1.2. Finally, Singleton proposed the [4+3] secondary orbital interactions (S43) involving bond making/breaking centers.

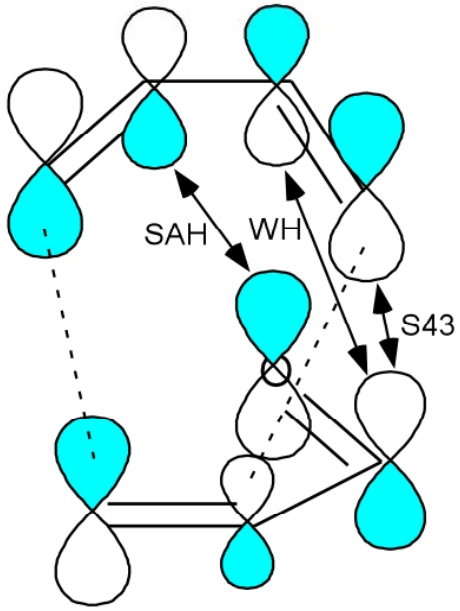

Figure 1.2. *Woodward-Hoffmann (WH), Salem, Houk, and Alston (SAH) and Singleton's [4+3] (S43) secondary orbital interactions in a Diel-Alder reaction between butadiene and acrolein.*

Secondary orbital interaction interpretations are known to be controversial.[11,24,25] Hence, other explanations invoke primary overlap,[26] the differential volumes of activation[27] and different polarities of the transition states.[28] The origin of regiochemical preference and *endo* selectivity continues to be a debated subject.

1.1.3 Solvent Effects

Solvent effects on Diels-Alder reactions are well known[29] and have attracted much attention in the past few years, because of the noticeable improvement in rate acceleration and stereoselectivity. Recent papers devoted to the theoretical treatment of solvation effects, have made progress in clarifying the role of solvent participation in Diels-Alder reactions.[28,30,31] Experimental studies have also been carried out,[32] but because of limitations due to intercorrelations between the empirical parameters, which renders the explanation of the precise role of each solute-solvent interaction term difficult, little clarification has been shown. In the Diels-Alder reaction, the role of the solvent has been assumed to be static,[33] hence its effect is basically given through the contribution of the solvation energy to the total free energy of the reactants and the transition structures. Recent theoretical papers, though, show that direct participation of solvent molecules may occur in which a few critical solvent molecules can bind to the transition structure and lower the activation energy.[31] It is also likely that the electric field created by the solvent changes the shape of the potential energy surface and can modify the position of the stationary points. The reaction path itself can be perturbed, especially when Lewis acids are involved.[17] Although this may an extreme case, it reinforces the need for a thorough study on the solvent effects on Diels-Alder reactions. Particularly when using ionic liquids and Lewis acids in solutions, many theoretical challenges to better understand the microscopic details that provide enhanced rates and selectivities are presented.

1.2 Ionic Liquids

Room temperature ionic liquids are a novel and exciting class of solvents that have the potential to accelerate and control a vast range of organic, inorganic, and enzymatic reactions in an environmentally safe manner.[7,8] Unfortunately, only a few systematic studies addressing the microscopic details on how ionic liquids influence chemical reactivity and selectivity have been reported.[34] Ionic liquids are distinct from the well-studied molten salts or melts. Ionic liquids are defined as material containing only ionic species, with a melting point at or below room temperature.[7,8] In sharp contrast to molten salts or melts, ionic liquids can be fluid at temperatures as low as 204 K, are colorless, have low viscosities, high conductivity, negligible vapor pressure, excellent thermal and chemical stabilities, are recyclable, non-explosive, easy to prepare, active at room temperature, and tolerate impurities such as water.[35]

It is known that many salts form liquids near room temperature.[36] It also has been pointed out in a recent review that there are no reliable ways to predict the precise melting point of organic salts or identify which salts have melting points near room temperature.[36] The melting point suppression of ionic liquids has been attributed to replacing inorganic cations with larger and unsymmetrical organic cations. Invariably, ionic liquids are either organic salts or mixtures containing at least one organic component. Osteryoung, Wilkes and Hussey have independently developed ionic liquids that are fluid at room temperature.[7,8] The most commonly used salts are those with alkylammonium, alkylphosphonium, N-alkylpyridinium, and N,N'-dialkylimidazolium cations. Most developments and derivatives of neutral ionic liquids have been based upon 1-ethyl-3-methyl-imidazolium chloride (EMIC), **1**, and N-1-butylpyridinum chloride

(BPC), **2**. Other molecular systems, typically derivatives of **1** and **2**, have been recently created and evaluated.

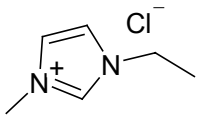

1

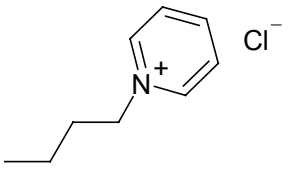

2

Ionic liquids are truly designer solvents, in that the cation or the anion may be changed in order to affect the relative solubilities of the reactants and products, the reaction kinetics, the liquid range of the solvent, the cost of the solvent, the intrinsic catalytic behavior of the media, and air stability of the system.[8] Consequently, many issues must be considered when trying to understand how ionic liquids deliver rate enhancement and increased stereoselectivity for important chemical reactions.

An attractive property of ionic liquids is that their Lewis acidity can be varied with the composition of the liquid.[37] Acidity variations can be used to induce substantial changes in the coordination of complex solutes present. For example, when aluminum halide, AlX_3, is combined with an organic salt, $[R]^+[X]^-$, the constituents of the resulting ionic liquid are determined by their molar ratio, *a/b*, according the following reactions which proceed essentially to completion.

$$b[R]^+[X]^- + aAlX_3 \rightarrow a[R]^+[AlX_4]^- + (b-a)[R]^+[X]^- \qquad (a/b<1) \qquad (1.1)$$

$$b[R]^+[X]^- + aAlX_3 \rightarrow (2b-a)[R]^+[AlX_4]^- + (b-a)[R]^+[Al_2X_7]^- \qquad (1<a/b<2) \qquad (1.2)$$

If *a/b* is less than 1, then these melts consist essentially of $[R]^+[AlX_4]^-$ and $[R]^+[X]^-$, and are known as "basic" melts because they contain halide ions that are not bound to aluminum. When *a/b* is greater than 1, but less than 2, $[R]^+[AlX_4]^-$ and $[R]^+[Al_2X_7]^-$ are the principle constituents of the system, and are known as "acidic" melts, since

$[R]^+[Al_2X_7]^-$ is a halide acceptor. Very small amounts of $[X]^-$ and $[Al_2X_7]^-$ are always present in acidic and basic ionic liquids due to the following autosovolysis reaction:

$$2[R]^+[AlX_4]^- \rightleftarrows [R]^+[Al_2X_7]^- + [R]^+[X]^- \quad (1.3)$$

The equilibrium constant for Equation 1.3 has been measured for both EMIC-$AlCl_3$ and BPC-$AlCl_3$ and lies in the range of 10^{-16} to 10^{-17} at 40°C.

To understand the impact of ionic liquids on chemical reactivity, from a microscopic viewpoint, it is necessary to identify the anions present at a given $AlCl_3$ mole fraction and study the intermolecular interactions possible with the organic reactants. Raman,[38] ^{27}Al-NMR[39] and mass spectra[40] all indicate that when *a/b* is less than 1 in a pure ionic liquid that $[AlX_4]^-$ is the only chloroaluminate(III) species present. ^{27}Al-NMR spectra of BPC-$AlCl_3$ ionic liquids as a function of composition at temperatures in the region of 28-55°C consist of a single peak, which broadens considerably as more aluminum(III) chloride is added.[41] At temperatures of 65-76°C the spectrum of *a/b* = 1.4 resolves into two peaks, one broad and the other sharp, which were assigned to $[Al_2Cl_7]^-$ and $[AlCl_4]^-$, respectively. Similar results have been reported for the EMIC-$AlCl_3$ ionic liquid. Negative-ion FAB mass spectra of EMIC-$AlCl_3$ ionic liquids have also shown peaks due to both $[Al_2Cl_7]^-$ and $[AlCl_4]^-$ ions with *a/b* > 1.[42] X-ray diffraction studies of the BPC-$AlCl_3$ ionic liquid (*a/b* = 1 and 2) demonstrate the presence of the tetrahedral $[Al_2Cl_7]^-$ and $[AlCl_4]^-$ ions constructed from a two corner-sharing $[AlCl_4]^-$ tetrahedral. Unambiguous evidence for the presence of the $[Al_3Cl_{10}]^-$ ion in EMIC-$AlCl_3$ ionic liquids has been provided by the negative-ion FAB mass spectrum (*a/b* = 1.9), and by the infrared spectrum (*a/b* = 3 at 200°C).[43] In addition, the infrared spectrum demonstrated the presence of $[Al_2Cl_6]$, indicating that it is unlikely that

chloroaluminate(III) species heavier than $[Al_3Cl_{10}]^-$ ions make any contribution to the structure of these ionic liquids at any composition. The experimental results have been used to construct a density functional and molecular mechanical study to understand the possible ion-ion and ion-substrate interactions that may influence the reaction pathway for chemical reactions.

1.3 Lewis Acids

Since Lewis acids are known to influence strongly the rate and stereoselectivities, using a chiral Lewis acid for asymmetric catalysis, it is possible to use them in the enantioselective synthesis of chiral organic compounds.[3,9,10,44,45] However, for many reactions, the factors leading to enantioselective catalysis by chiral Lewis acids have not been thoroughly studied and mechanistic details are not completely understood.

Recently, E. J. Corey and coworkers have reported an understanding for the Diels-Alder selectivities and stereochemical preferences by conformational restriction of the Lewis acid-carbonyl complexes.[9,44,46,47] In x-ray crystallographic studies of α, β-unsaturated aldehyde complexes with fluorine and alkyl ether containing boron Lewis acids, it was shown that a conformational preference occurs when the formyl group and B-F or B-O bond are coplanar.

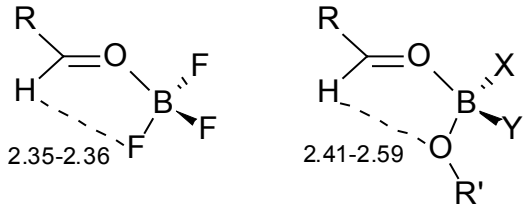

Scheme 1.1. *Examples of the formyl C-H···F and C-H···O hydrogen bond. Distances are in Å.*

Scheme 1.1 shows x-ray crystal structures of boron trifluoride complexes with benzaldehyde, methacrolein, 2,3-methylene-dioxybenzaldehyde and dimethylformamide (DMF), investigated by Corey.[9,48] The H···F distances of 2.35-2.36 Å are within the sum of the van der Waals radii of 2.67 Å. The O···H distances of 2.41-2.59 Å in x-ray crystal structures of [catecholborane· $(DMF)_2]^{+}\cdots Br^{-}$ and [2-(N,N-dimethylamino)phenoxyboron· $(DMF)_2]^{+}\cdots I^{-}$ are also below the van der Waals radii of 2.72 Å.[48] It has been proposed that this conformational preference is due to an electrostatic interaction known as a nontraditional (O=C-H···X) hydrogen bond.[46,48,49] Usually the hydrogen atom in the formyl group lacks the electrophilicity required for hydrogen bonding, but in this special case it is enhanced when coordinated to the boron Lewis acid. In addition, the coordination enhances the nucleophilicity of the heteroatom, which acts as a hydrogen bond acceptor.[50] This theory is based on the ground state conformation, but it is possible to expand upon this work by considering the impact of significant interactions between Lewis acids and organic partners that could develop at the transition structure.

Our work looks at the Diels-Alder reaction between acrolein and butadiene with the Lewis acid BF_2OCH_3 (see Scheme 1.2).

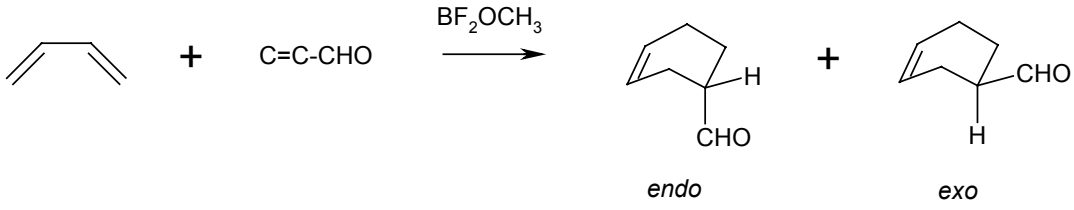

Scheme 1.2. *Diels-Alder reaction between butadiene and acrolein with the Lewis acid BF_2OCH_3..*

This study will emphasize the enhanced coordination of the Lewis acid to its organic partners and two novel nontraditional interactions that develop at the transition structure.

These results will provide further insight into how Lewis acids influence chemical reactions.

1.4 Bis(oxazoline) Copper(II) Complexes

Our efforts provide an interpretation for the remarkable reactivity and selectivity by the copper (II) based catalytic system, and present a basis to design more reactive catalysts that can be extended to other organic reactions and give greater flexibility in the nature of the diene, as well as the substitution pattern on the dienophile. David Evans and co-workers have designed and synthesized copper(II)-based Lewis acid catalysts that demonstrate the kinetic and synthetic advantages of such systems. The majority of C2-symmetric bis(oxazoline)-Cu(II) complexes catalyze Diels-Alder reactions, such as α,β-unsaturated carbonyl compounds with electron rich olefins, with high diastero- and enantioselectivity of 94-96%. A mechanistic understanding of how the copper(II) catalysts deliver their rate and stereoselective power is lacking. It is important to understand the energetics and transition structures in order to determine how Cu(II) catalysts impacts the Diels-Alder reaction, since other organic reactions, (i.e., enol amination, ene, and Michael) are impacted significantly as well.[51]

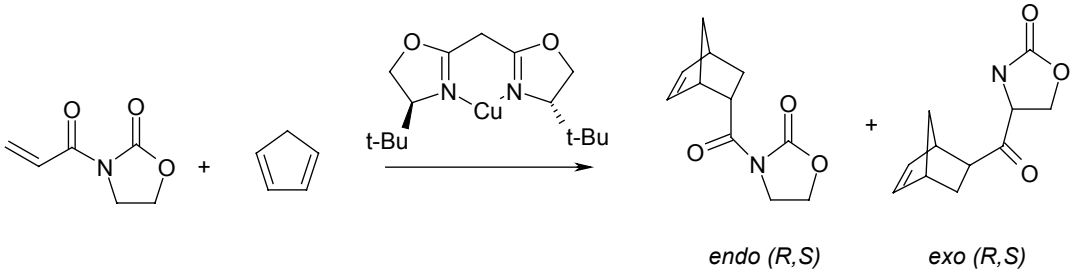

Scheme 1.3. *Diels-Alder reaction between acrylimide and cyclopentadiene in the presence of the bis(oxazoline)-copper(II) (S,S) Lewis acid catalyst with representative products of the favorable stereochemical outcome (S) and unfavorable outcome of (R).*

In the Diels-Alder reaction of cyclopentadiene and acrylimide, bis(oxazoline)-Cu(II) coordinates to the carbonyl oxygens of acrylimide resulting in a "twisted" planar conformation that locks the dienophile in place. The C2-like symmetry of bis(oxazoline)-Coppper(II) is proposed to block one face of the dienophile, thus controlling the selectivity. Additionally, ligand field effects directly influences the planarity of the dienophile, contributing to the overall selectivity observed. Computational assessment of the bis(oxazoline)-Cu(II) catalyzed Diels-Alder transition structures have not been reported to date.

1.5 Objectives of Thesis

Due to the impact of the Diels-Alder reaction on the utility and understanding of organic chemistry and the ability of large-scale computing, it is both important and timely to provide physical insight into how external factors (catalysts or solvent) influence the rate enhancement or stereoselectivity of chemical reactions. This Ph.D. dissertation investigates three different external influences, which are known experimentally and poorly understood theoretically, by using large-scale quantum mechanical computations and large-scale molecular dynamics simulations. The external influences upon chemical reactivity and stereochemistry are ionic liquids, Lewis acid catalysts and bis(oxazoline) copper(II) catalysts. In each of the categories it is necessary to understand the microscopic details and intermolecular interactions in order to access their role in the rate and selectivity enhancement.

(1) Ionic liquids deliver enhanced rates and *endo/exo* selectivities on the Diels-Alder reaction. The goal is to establish a firm understanding of the molecular interactions

that give rise to the observed rate and selectivity enhancements. In order to accomplish our goal, we have used density functional theory methodology to describe short-range effects, and have created CHARMM parameters to allow faster classical computations and explore bulk phase effects.

(2) Lewis acids are known to influence strongly the rate, regio, *endo/exo*, diastereofacial and enantio selectivities of the Diels-Alder reaction. Specifically, asymmetric catalysis using chiral Lewis acids provides a crucial tool in the enantioselective synthesis of chiral organic compounds. Uncovering the differential forces between the ground and transition structures with chiral Lewis acids is a perquisite step towards the creation of more effective enantioselective catalysts. Our efforts focus upon a novel combination of two specific intermolecular interactions between boron Lewis acids and Diels-Alder transition structures. Quantum mechanical calculations along with kinetic isotope effects are used in conjunction to elucidate these specific interactions.

(3) Cu(II) functions effectively as a Lewis acidic center that has proven to control the stereoselectivity of a wide range of organic reactions. Specifically, bis(oxazoline) copper(II) complexes operate as enantioselective Lewis acid catalysts for carbocyclic and hetero Diels-Alder reactions. We have used quantum mechanical calculations in order to determine how ligand field strength influences Cu(II) coordination and ultimately the stereoselectivity of organic reactions and to investigate organizing elements. The influence of the bis(oxazoline) copper(II) complex upon the Diels-Alder reaction has been explained in terms of three critical factors: the impact of metal coordination geometry, dienophile conformation (s-cis vs. s-trans) and the bis(oxazoline) substituents.

Our calculations provide new insight into the effects of external influences on the geometry, flexibility and energy of the Diels-Alder transition structures and the influence of these factors on rate and selectivity. This thesis will contribute to the understanding of the stereochemical and catalytic issues of solvent effects, in terms of ionic liquids, and important local electrostatic interactions, in terms of Lewis acid complexation to the Diels-Alder reaction, that should establish opportunities in the design of future asymmetric catalytic systems.

1.6 References

(1) Diels, O.; Alder, K. *Justus Liebigs Ann. Chem.* **1928**, *460*, 98.

(2) Nicolaou, K. C.; Snyder, S. A.; Montagnon, T.; Vassilikogiannakis, G. *Angew. Chem. Int. Ed.* **2002**, *41*, 1668.

(3) Oppolzer, W. In *Comprehensive Organic Synthesis*; Trost, B. M., Ed.; Pergamon Press: Oxford, 1991; Vol. 5, p 315.

(4) Yates, P.; Eaton, P. *J. Am. Chem. Soc.* **1960**, *82*, 4436.

(5) Inukai, T.; Kojima, T. *J. Org. Chem.* **1967**, *32*, 872.

(6) Pindur, U.; Lutz, G.; Otto, C. *Chem. Rev.* **1993**, *93*, 741.

(7) Welton, T. *Chem. Rev.* **1999**, *99*, 2071; Seddon, K. R. *J. Chem. Tech. Biotechnol.* **1997**, *68*, 351.

(8) Freemantle, M. In *C&EN*, 2001, pp 21.

(9) Corey, E. J. *Angew. Chem. Int. Ed.* **2002**, *41*, 1650.

(10) Dalko, P. I.; Moisan, L. *Angew. Chem. Int. Ed.* **2001**, *40*, 3726.

(11) Garcia, J. I.; Mayoral, J. A.; Salvatella, L. *Acc. Chem. Res.* **2000**, *33*, 658.

(12) Woodward, R. B. H.; Hoffmann, R. *The Conservation of Orbital Symmetry*; VCH: Weinhein, 1985.

(13) Houk, K. N.; Gonzalez, J.; Li, Y. *Acc. Chem. Res.* **1995**, *28*, 81.

(14) Goldstein, E.; Beno, B.; Houk, K. N. *J. Am. Chem. Soc.* **1996**, *118*, 6036; Storer, J. W.; Raimondi, L.; Houk, K. N. *J. Am. Chem. Soc.* **1994**, *116*, 9675; Li, Y.; Houk, K. N. *J. Am. Chem. Soc.* **1993**, *115*, 7478.

(15) Woodward, R. B.; Katz, T. J. *Tetrahedron* **1959**, *5*, 70.

(16) Dewar, M. J. S. *Tetra. Lett.* **1959**, *5*, 16.

(17) Tanaka, J.; Kanemasa, S. *Tetrahedron* **2001**, *57*, 899.

(18) Sauer, J.; Sustmann, R. *Angew. Chem. Int. Ed.* **1980**, *19*, 779.

(19) Fukui, K. *Theory of Orientation and Stereoselection*; Springer-Verlag: Heidelberg, Germany, 1970.

(20) Houk, K. N. *Tetrahedron Letters* **1970**, *30*, 2621.

(21) Salem, L. *J. Am. Chem. Soc.* **1968**, *90*, 553.

(22) Alston, P. V.; Ottenbrite, R. M.; Cohen, T. *J. Org. Chem.* **1978**, *43*, 1864.

(23) Singleton, D. A. *J. Am. Chem. Soc.* **1992**, *114*, 6563.

(24) Yamabe, S.; Nishihara, Y.; Minato, T. *J. Phys. Chem. A* **2002**, *106*, 4980.

(25) Birney, D. M.; Houk, K. N. *J. Am. Chem. Soc.* **1990**, *112*, 4127; Suárez, D.; Sordo, J. A. *Chem. Commun.* **1998**, *3*, 385.

(26) Hearndon, W. C.; Hall, L. H. *Tetra. Lett.* **1967**, 3095.

(27) Blokzijl, W.; Blandamer, M. J.; Engberts, J. B. F. N. *J. Am. Chem. Soc.* **1991**, *113*, 4241; Gajewski, J. J. *J. Org. Chem.* **1992**, *57*, 5500.

(28) Ruiz-López, M. F.; Assfeld, X.; García, J. I.; Mayoral, J. A.; Salvatella, L. *J. Am. Chem. Soc.* **1993**, *115*, 8780.

(29) Reichardt, C. *In Solvents and Solvent Effects in Organic Chemistry*; VCH: Weinheim, 1998.

(30) Acevedo, O.; Evanseck, J. D. *Org. Lett.* **2003**, *5*, 649; Chandrasekhar, J.; Shariffskul, S.; Jorgensen, W. L. *J. Phys. Chem. B* **2002**, *106*, 8078.

(31) Kong, S.; Evanseck, J. D. *J. Am. Chem. Soc.* **2000**, *122*, 10418.

(32) Cativiela, C.; García, J. I.; Mayoral, J. A.; Avenoza, A.; Peregrina, J. M.; Roy, M. A. *J. Phys. Org. Chem.* **1991**, *4*, 48; Cativiela, C.; García, J. I.; Mayoral, J. A.; Royo, A. J.; Salvatella, L.; Assfeld, X.; Ruiz-lopez, M. F. *J. Phys. Org. Chem.* **1992**, *5*, 230.

(33) Blake, J. F.; Jorgensen, W. L. *J. Am. Chem. Soc.* **1991**, *113*, 7430.

(34) Acevedo, O.; Evanseck, J. D. In *Ionic Liquids as Green Solvents: Progress and Prospects*; Estill, D. R., Ed.; ACS Symposium Series, 2003; Margulis, C. J.; Stern, H. A.; Berne, B. J. *J. Phys. Chem. B* **2002**, *106*, 12017; de Andrade, J.; Böes, E. S.; Stassen, H. *J. Phys. Chem. B* **2002**, *106*, 3546; Morrow, T. I.; Maginn, E. J. *J. Phys. Chem. B* **2002**, *106*, 12807; Takahashi, S.; Suzuya, K.; Kohara, S.; Koura, N.; Curtiss, L. A.; Saboungi, M. L. *Z. Phys. Chem.* **1999**, 209; Hébant, P.; Picard, G. *J. Mol. Struc. (Theochem)* **1995**, *358*, 39; Picard, G.; Bouyer, F. C.; Leroy, M.; Bertaud, Y.; Bouvet, S. *J. Mol. Struc. (Theochem)* **1996**, *368*, 67; Ribeiro, M. C. C.; Almeida, L. C. J. *J. Chem. Phys.* **2000**, *113*, 4722; Bock, C. W.; Trachtman, M.; Mains, G. J. *J. Phys. Chem.* **1994**, *98*, 478.

(35) Fannin Jr., A. A.; Floreani, D. A.; King, L. A.; Landers, J. S.; Piersma, B. J.; Stech, D. J.; Vaughn, R. L.; Wilkes, J. S.; Williams, J. L. *J. Phys. Chem.* **1984**, *88*, 2614.

(36) Larson, A.; Holbrey, J. D.; Tham, F. S.; Reed, C. A. *J. Am. Chem. Soc.* **2000**, *122*, 7264.

(37) Hussey, C. L. *Pure & Appl. Chem.* **1988**, *60*, 1763.

(38) Gale, R. J.; Gilbert, B. P.; Osteryoung, R. A. *Inorg. Chem.* **1978**, *17*, 2728.

(39) Wilkes, J. S.; Frye, J. S.; Reynolds, G. F. *Inorg. Chem.* **1983**, *22*, 3870.

(40) Ackermann, B. L.; Tsarbopoulos, A.; Allison, J. *Anal. Chem.* **1985**, *57*, 1766; Wicelinski, S. P.; Gale, R. J.; Pamidimukkala, K. M.; Laine, R. A. *Anal. Chem.* **1988**, *60*, 2228.

(41) Gray, J. L.; Maciel, G. E. *J. Am. Chem. Soc.* **1981**, *103*, 7147.

(42) Franzen, G.; Gilbert, B. P.; Pelzer, G.; Depauw, E. *Org. Mass Spectrom.* **1986**, *21*, 443.

(43) Abdul-Sada, A. K.; Greenway, A. M.; Seddon, K. R.; Welton, T. *Org. Mass Spectrom.* **1989**, *24*, 917.

(44) Ryu, D. H.; Lee, T. W.; Corey, E. J. *J. Am. Chem. Soc.* **2002**, *124*, 9992.

(45) Matthias, B.; Corey, E. J. *Org. Lett.* **2001**, *3*, 1559; Fringuelli, F.; Piermatti, O.; Pizzo, F.; Vaccaro, L. *Euro. J. Org. Chem.* **2001**, *3*, 439; Jorgensen, K. A. *Angew. Chem. Int. Ed.* **2000**, *39*, 3558; Otto, S.; Engberts, J. B. F. N. *Pure Appl. Chem.* **2000**, *72*, 1365; Dias, L. C. *J. Braz. Chem. Soc.* **1997**, *8*, 289; Ishihara, K.; Yamamoto, H. *Cattech* **1997**, *1*, 51; Ghosez, L. *Pure Appl. Chem.* **1996**, *68*, 15; Oh, T.; Reilly, M. *Org. Prep. Proceed. Int.* **1994**, *26*, 129; Weinreb, S. M. In *Comprehensive Organic Synthesis*; Trost, B. M., Ed.; Pergamon Press: Oxford, 1991; Vol. 5, p 451; Boger, D. L. In *Comprehensive Organic Synthesis*; Trost, B. M., Ed.; Pergamon Press: Oxford, 1991; Vol. 5, p 451; Roush, W. R. In *Comprehensive Organic Synthesis*; Trost, B. M., Ed.; Pergamon Press:

Oxford, 1991; Vol. 5, p 513; Sweger, R. W.; Czarnik, A. W. In *Comprehensive Organic Synthesis*; Trost, B. M., Ed.; Pergamon Press: Oxford, 1991; Vol. 5, p 551; Carruthers, W. *Cycloaddition Reactions in Organic Synthesis*; Pergamon Press: New York, 1990; Fringuelli, F.; Tatichi, A.; Wiley: New York, 1990.

(46) Corey, E. J.; Rohde, J. J.; Fischer, A.; Azimioara, M. D. *Tetrahedron Lett.* **1997**, *38*, 33.

(47) Corey, E. J.; Rohde, J. J. *Tetrahedron Lett.* **1997**, *38*, 37; Corey, E. J.; Barnes-Seeman, D.; Lee, T. W. *Tetrahedron Lett.* **1997**, *38*, 1699; Corey, E. J.; Barnes-Seeman, D.; Lee, T. W. *Tetrahedron Lett.* **1997**, *38*, 4351.

(48) Corey, E. J.; Lee, T. W. *Chem. Commun.* **2001**, *15*, 1321.

(49) Alkorta, I.; Rozas, I.; Elguero, J. *Chem. Soc. Rev.* **1998**, *27*, 163.

(50) Qian, W.; Krimm, S. *J. Phys. Chem. A* **2002**, *106*, 6628; Qian, W.; Krimm, S. *J. Phys. Chem. A* **2002**, *106*, 11663.

(51) Johnson, J. S.; Evans, D. A. *Acc. Chem. Res.* **2000**, *33*, 325.

Chapter 2

Methodology

A description of the computational tools used to compute the structure, vibrational and thermodynamic properties of organic reactions is presented. The basics of quantum mechanical calculations, from Hartree-Fock and density functional theory, are reviewed. A critical assessment of hybrid density functional theory (DFT) is made due to its reported success on pericyclic processes, computational efficiency and lack of dispersion forces. A practical, user-friendly description on how to carry out large-scale computations (QM and MM) is provided. An overview of the technique behind force field parameterization is discussed. The principles of molecular dynamic (MD) simulations and methods are described. Secondary kinetic isotope effects are reviewed as a method that allows transition structures to be studied and compared directly to experimental data.

2.1 Quantum Mechanical Calculations

2.1.1 Schrödinger Equation

The intuitive location to start a discussion of quantum mechanics lies in the non-relativistic, time-independent Schrödinger equation:[1,2]

$$H\Psi = E\Psi \tag{2.1}$$

The H is the Hamiltonian operator, Ψ is the wave function and E is the energy for a system of M nuclei and N electrons. The Hamiltonian operator operates upon the wave function in such a way that it returns the wave function back multiplied by the energy. The Hamiltonian operator is typically written:

$$H = -\frac{\hbar^2}{2m}\nabla^2 + V \tag{2.2}$$

The Hamiltonian operator is comprised of two parts, the kinetic and potential energies to the total energy. The first part of the Hamiltonian is the kinetic energy operator. The potential energy depends on the electrostatic interactions between the electron and the nucleus and the interaction between the electron and other electrons. The potential is independent of time. For a single electron and a single nucleus with Z protons the potential energy operator is:

$$V = -\frac{Ze^2}{4\pi\varepsilon_0 r} \tag{2.3}$$

For a harmonic oscillator approximation the operator takes the form:

$$V = \frac{1}{2}kx^2 \tag{2.4}$$

Solving the Schrödinger equation for atoms with more than one electron has many complications. It is possible to calculate the Schrödinger equation exactly for small

systems, such as the helium atom, comprised of just two electrons and one nucleus. For this problem, some considerations are made, where the two electrons can interact with the nucleus but not with each other. So this three-particle system can now be solved exactly using the separation of variables method, where the Hamiltonian can be divided into parts dependent only on subsets of the coordinates. This is an example of perturbation theory, which is best applied when the differences between the real and simple problems are small. However for more complicated systems, electron spin must be accounted for in the computation. It is not possible to solve the Schrödinger equation exactly beyond the single nuclei and two electron system, but the Schrödinger equation can be simplified by the Born-Oppenheimer approximation.[3] Since nuclei have a much larger mass compared to electrons, it is reasonable to assume that they move more slowly. This means that the electrons can adjust almost instantaneously to any changes in the positions of the nuclei, so by holding the position of the nuclei fixed, the electronic wave function depends only on the positions of the nuclei and not the momentum. The original Hamiltonian for nuclei and electrons is written as

$$H = -\sum_{i=1}^{N}\frac{1}{2}\nabla_i^2 - \sum_{A=1}^{M}\frac{1}{2M_A}\nabla_A^2 - \sum_{i=1}^{N}\sum_{A=1}^{M}\frac{Z_A}{r_{iA}} + \sum_{i=1}^{N}\sum_{j>i}^{N}\frac{1}{r_{ij}} + \sum_{A=1}^{M}\sum_{B>A}^{M}\frac{Z_A Z_B}{R_{AB}} \qquad (2.5)$$

The ∇_i is the Laplacian operator, Z is the nuclear charge, r_{iA} is the distance between nuclei and electron, r_{ij} is the distance between electrons and R_{AB} is the distance between nuclei. The first term in the equation is the kinetic energy of the electrons, the second term is the kinetic energy of the nuclei, the third term is the columbic attraction, the fourth term is the electron-electron repulsion, and the fifth term is the nuclear-nuclear repulsion, in accordance to Equation 2.5, respectively. By applying the Born-Oppenheimer approximation, the kinetic energy of the nuclei is zero and the repulsion of

between nuclei can be considered constant. This leads to the electronic version of the Hamiltonian (H_{elec}):

$$H_{elec} = -\sum_{i=1}^{N} \frac{1}{2} \nabla_i^2 - \sum_{i=1}^{N} \sum_{A=1}^{M} \frac{Z_A}{r_{iA}} + \sum_{i}^{N} \sum_{j>i}^{N} \frac{1}{r_{ij}} \tag{2.6}$$

This gives a new Schrödinger equation:

$$H_{elec} \Phi_{elec} = E_{elec} \Phi_{elec} \tag{2.7}$$

Practical considerations of Equation 2.7 are reviewed further in the chapter, under the Thermodynamic Quantities sections. Typical electronic energies, zero point energies, potential energy surfaces and vibrations are covered in detail.

2.1.2 Variational Principle

The variational theorem states that the wave function, Ψ, that gives the lowest eigenvalue of energy provides the closest approximation to the system's true ground state. The expectation value, which is considered the average, of a quantity such as energy is found with the Hamiltonian operator by calculating the following integrals:

$$E = \frac{\int \Psi^* H \Psi d\tau}{\int \Psi^* \Psi d\tau} \tag{2.8}$$

The two integrals are performed over all space and use of the conjugate notation (Ψ^*) indicates that the wave function may be a complex number, although any number, real or complex, may be considered. When wave function is normalized,

$$\int | \Psi |^2 \, d\tau = 1 \tag{2.9}$$

then the denominator in Equation 2.8 will equal one, but only if the wave function is well-behaved. This means if integration is carried out over all space, the probability of

finding each particle must be one. The Ψ must follow the antisymmetry principle, which states that a many-electron wave function must be antisymmetric with respect to the interchange of the coordinate (both space and spin) of any two electron, if the solution to the Schrödinger equation is to be valid for electronic structure calculations.

In most electronic structure calculations, the desired outcomes are the molecular orbitals. For the many-body problems there is no correct solution, therefore it is necessary to decide whether one proposed wave function is better than another. Fortunately, using the variational theorem is a perfect fit. Since the energy calculated from an approximation to the true wave function will always be greater than the true energy. Hence, the better the wave function, the lower the value for the energy.

$$\frac{\int \phi^* H \phi d\tau}{\int \phi^* \phi d\tau} \geq E_{gs} \tag{2.10}$$

2.1.3 The Hartree-Fock Equation

Because the systems of interest are polyelectronic, the presence of interactions between the electrons are expressed as Coulomb and exchange integrals. The Coulomb interaction arises from the electrostatic repulsion between pairs of electrons. The other contribution to the energy is the exchange interaction, which has no classical counterpart. This arises from the motions of electrons with parallel spins since they are correlated. This is a manifestation of the Pauli principle, given that two electrons occupying the same region of space with parallel spins would have the same set of quantum numbers. In order to find the best wave function (lowest in energy) for the system, the orbital picture of the system needs to be retained, where single electrons are assigned to individual spin

orbitals, χ. The problem is to find a solution which simultaneously enables all electronic motions to be taken into account, hence a change in the spin orbital for one electron influences the behavior of an electron in another spin orbital. If a single electron in a spin orbital in the field of the nuclei and the other electrons in their fixed spin orbitals (mean field approximation), the Hamiltonian operator can be further simplified to:

$$H_{core} = -\frac{1}{2}\nabla_1^2 - \sum_{A=1}^{M}\frac{Z_A}{r_{1A}} \tag{2.11}$$

Where the label '1' in the subscripts is used to represent the coordinates of a single electron, Z_A is the nuclear charge and r_{1A} is the distance between the electron and nucleus. Given that all electron motions are separated in this approximation, the many-electron wave function is represented as a sum of the products of one-electron wave functions in the form of a Slater determinant.

$$\Psi = \frac{1}{\sqrt{N!}}\begin{vmatrix} \chi_1(1) & \chi_2(1) & \ldots & \chi_N(1) \\ \chi_1(2) & \chi_2(2) & \ldots & \chi_N(2) \\ \ldots & \ldots & \ldots & \ldots \\ \chi_1(N) & \chi_2(N) & \ldots & \chi_N(N) \end{vmatrix} \tag{2.12}$$

The $\chi_l(N)$ is the spin orbital of the Nth electron, where the function depends on both space and spin coordinates. The $\frac{1}{\sqrt{N!}}$ term is the normalization constant. This is the simplest form of an orbital wave function that satisfies the antisymmetry and Pauli spin principle.

The Hartree-Fock equations have been derived and presented before.[2,4] Briefly, the Fock operator, f_i, an effective one-electron Hamiltonian for an electron in a polyelectronic system, takes on the standard eigenvalue form:

$$f_i\chi_i = \varepsilon_i\chi_i \tag{2.13}$$

The ε_i term is the energy of the specific electron.

In setting up these equations, it is important to recall that each electron is assumed to move in a fixed field comprising the nuclei and the other electrons. It leads to the approach used, in which solving the equation for one electron will affect the solutions for the other electrons in the system. This strategy is called the self-consistent field (SCF) approach. In essence, a set of trial solutions χ_i are obtained, then are used to calculate the Coulomb and exchange operators. The Hartree-Fock equations are solved, giving a second-set of solutions which are used in the next iteration. The SCF method gradually lowers the total energies until the results for all the electrons are unchanged, which is said to be self-consistent.

In Hartree-Fock theory, electron correlation is mainly neglected which tends to be a major drawback when calculating the energetics of systems. This is due to the energy of the system being described by the sum of the one-electron spin orbitals. So the probability of finding an electron at a particular point in space is independent of the probability of finding any other electron at that point in space. This is responsible for much of the poor performance when applied to systems with electron conjugation. However Hartree-Fock provides good structures and allows quantum-chemical calculations to be sufficiently fast to allow their application to more realistic problems.[5]

2.1.4 Basis Sets

Basis sets are composed of atomic functions. To construct these functions according to Hartree-Fock theory, it would seem that the Slater type orbitals would be a clear choice. However, Slater functions are not the best choice for molecular orbital

calculations because some of the integrals are very difficult to evaluate when the atomic orbitals are centered on different nuclei. The solution is to replace the Slater orbitals by functions based on Gaussians. A Gaussian has the function in the form of $\exp(-\alpha r^2)$ and ab initio calculations use basis functions comprising integral powers of x, y and z.

$$x^a y^b z^c \exp(-\alpha r^2) \tag{2.14}$$

α determines the radial extent of a Gaussian function. A major advantage of using Gaussian functions is that the product of two Gaussians can be expressed as a single Gaussian. So in a two-electron integral, the product of $\phi_\mu(1)\phi_\nu(1)$ where ϕ_μ and ϕ_ν may be on different centers, can be replaced by a single Gaussian function that is centered at the appropriate point.

Along with these advantages, comes some disadvantages, when compared to Slater type functions. In comparing the 1s Slater function and the best Gaussian approximation, Figure 2.1 shows that the Gaussian functions do not have the cusp at the origin that the Slater functions do and they also decay towards zero more quickly. This means that the Gaussian functions underestimate the long-range overlap between atoms and the charge and spin density at the nucleus. The errors by a single Gaussian functions leads to large inaccuracies. However, a workaround for this problem is to represent each atomic orbital as a linear combination of Gaussian functions, of the form:

$$\phi_\mu = \sum_{i=1}^{L} d_{i\mu}\phi_i(\alpha_{i\mu}) \tag{2.15}$$

where $d_{i\mu}$ is the coefficient of the primitive Gaussian function ϕ_i, which has exponent $\alpha_{i\mu}$. L is the number of functions in the expansion.

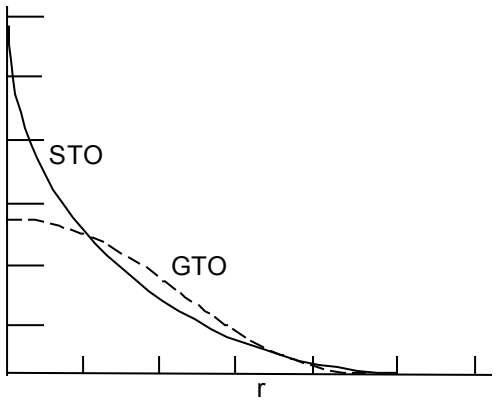

Figure 2.1. *The 1s Slater type orbital and the best Gaussian counterpart. The atomic radius is given by r.*

A Gaussian function that permits both the coefficient and the exponent to vary during a calculation is referred to as an uncontracted or primitive Gaussian. However, this requires a significant computational effort, so basis sets typically consist of contracted Gaussian functions. In the contracted Gaussian function, the coefficients and exponents are pre-determined and remain constant throughout the calculation. A minimal basis set contains only the number of functions required to describe all the filled orbitals in each atom (*1s*, *2s* and *2p*, etc.). Increasing the number of basis functions per atom makes the basis set larger, which impose fewer constraints on the electron and more accurately approximates exact molecular orbitals.[2,6] Split valence basis sets, such as 3-21G and 6-31G have two sizes of basis functions for each valence orbital. For example, in the 3-21G basis set, three Gaussian functions are used to describe the core orbitals. Three Gaussians are used by the valence electrons, where the contracted parts are described by two Gaussians for the inner valence and one Gaussian for the outer valence. Introduction of polarization functions into the basis sets allows a higher angular quantum number, so they correspond to *p* orbitals for hydrogen and *d* orbitals for first and second row elements. A common polarized basis set is the 6-31G(d),[7,8] which indicates the use of

polarization functions on the heavy (non-hydrogen) atoms. Another improvement to the basis set is the use of highly diffuse functions, denoted by using a '+', hence 6-31+G(d). Diffuse functions allow orbitals to occupy a larger region of space, this is useful for anions and molecules containing lone pairs with have a significant amount of electron density away from the nuclear center.[6]

Basis set flexibility provides a better description of intermolecular interactions tailored to the need imposed upon by the system being studied. The split-valence and polarization basis set 6-31G(d) has been used in this work as the primary basis set used. Larger basis sets have been used, such as 6-311G(3df), which is a triple zeta basis set. This means that extra valence functions (3 sizes of s and p functions) are added to the 6-31G(d). The 3df places 3 d functions and 1 f function on the heavy atoms. This larger basis set is used to confirm that the 6-31G(d) basis set is adequate in representing many of the model calculated in this thesis.

2.1.5 Computational Approximations

Advances in computational chemistry allow for the determination of stationary points by various approximations to the Schrödinger equation.[5,8-12] Complete discussions and excellent reviews of the different methods can be found in the literature.[1,2,13] Over the years, the Diels-Alder reaction between 1,3-butadiene and ethylene has become a prototype reaction to evaluate the accuracy of many different levels of theory. A "level of theory" involves the specific combination of a computational method and basis set. For example, the RHF/3-21G level of theory, involves the restricted Hartree-Fock method with the 3-21G basis set. Ken Houk and his research group have pioneered many

ideas concerning the fundamental ideas of pericyclic reactions by combining theory and experiment.[5,8,11,14-17] For the Diels-Alder reaction, the results from various methods and basis sets (levels of theory) are summarized in Table 2.1, where the experimental activation energies ($\Delta E^{\neq}$) and energies of reaction (ΔE_{rxn}) are compared to that computed.

Table 2.1. *Transition structure geometries, activation energies and reaction energies of the concerted Diels-Alder reaction of 1,3-butadiene and ethylene. Energies are reported in kcal/mol, distances in angstroms, and angles in degrees.*

Method	R_{C1-C5}	$\phi_{C2-C1-C5}$	$\Delta E^{\neq}$	ΔE_{rxn}	Ref.
RHF/3-21G	2.210	101.6	35.9	-43.1	18
RHF/6-31G(d)	2.201	102.6	47.4	-36.0	12,17
MP2/6-31G(d)	2.286	101.6	20.0	-45.9	12,17
MP4SDTQ/6-31G(d)[a]	2.286	101.6	22.4	-47.5	19
BLYP/6-31G(d)	2.292	102.6	22.8	29.8	20
B3LYP/6-31G(d)	2.273	102.4	24.8	-36.3	12
CASSCF/3-21G	2.217	101.9	37.3		21
CASSCF/6-31G(d)	2.223	103.1	40.7		21
UQCISD(T)/6-31G(d)[b]	2.223	103.1	29.4		21
RQCISD(T)/6-31G(d)[b]	2.223	103.1	25.5		21
Experimental			26.5 ± 2.0	-38.4	5,22

Table contents extracted from References [5] and [8]. [a]Single point on the MP2/6-31G(d) optimized geometries.[b]Single point on the CASSCF/6-31G(d) optimized geometries.

Two distinct observations from the computations emerge. First, the activation energies are sensitive to the level of theory chosen. The computed activation energies range from 47.4 to 20.0 kcal/mol, as compared to the 26.5 ± 2.0 kcal/mol found by experiment.[5,22] Restricted Hartree-Fock (RHF) activation energies are too high, reinforcing the need to include electron correlation in energy evaluations. Second-, third- and fourth-order Møller-Plesset values are too low, thus overstating the effect of electron correlation. In addition, the CASSCF method overestimates the activation energies, illustrating well-known issues with the selection of the active space orbitals.[23] Gradient corrected, nonlocal density functional methods, such as the B3LYP (Becke three

parameter exchange functional[24] and the nonlocal correlation functional of Lee, Yang, and Parr[25]), have gained popularity due to computer time efficiency and results that match experimental data closely.[8] Quadratic configuration interaction methods which include the effects of single and double substitutions and in the case of QCISD(T), triple substitutions, provide reasonable energies of concerted and stepwise pathways of Diels-Alder activation energies.[9,21] The second observation is that key geometric parameters are relatively insensitive to the level of theory used for the computations. For example, the breaking/forming bond lengths between the C1 and C5 atoms fall within the narrow range of 2.201 to 2.292 Å, as shown in Table 2.1. The results suggest that the *geometries* of pericyclic transition structures can be calculated at lower levels of theory such as RHF/3-21G and that more demanding methods that incorporate the effects of electron correlation, can be used to evaluate the *energies* of the stationary points. A common notation used is *energy-method/energy-basis-set//geometry-method/geometry-basis-set*, such as MP4/6-311+G(d,p)//RHF/3-21G(d). This specifies that an MP4 single point energy calculation using the 6-311+G(d,p) basis set was performed on a structure previously optimized with Hartree-Fock theory at the 3-21G(d) basis set.

2.2 Density Functional Theory

2.2.1 Introduction

Density functional theory (DFT) is an approach to the electronic structure of atoms and molecules, based on the electron density distribution $n(r)$, instead of the many-electron wave function $\Psi(r_1, r_2, r_3...)$.[26] DFT has seen a dramatic surge of interest in recent publications, and has subsequently been employed to obtain thermochemical data,

molecular structures, force fields and frequencies.[1,27] It has also shown good agreement with experimental techniques, such as assignments of NMR, photoelectron, ESR and UV spectra. The strength of DFT lies in its ability to provide a balance between modest accuracy and computational time when dealing with systems comprised of greater than 20 atoms.

There are several similarities between DFT and the Hartree-Fock approach. In Hartree-Fock theory, the multi-electron wave function is expressed as a Slater determinant constructed from a set of N (number of electrons) single-electron wave functions. DFT considers single-electron functions, as well, however whereas Hartree-Fock theory calculates the full N-electron wave function, DFT only attempts to calculate the total electronic energy and the electronic density distribution. A limitation of DFT compared to traditional methods, is that in a traditional method an arbitrary level of accuracy can in principle be obtained for any system only limited by computational resources, while DFT depends on adequate knowledge of the exchange correlation energy functional. The exchange correlation potential describes the effects of the Pauli principle and the Coulomb potential beyond a pure electrostatic interaction of the electrons. More accurate forms are being developed, but there is no known systematic way to achieve an arbitrarily high level of accuracy.[28]

2.2.2 Hohenberg-Kohn and Kohn-Sham

The starting point of DFT is the notion that the energy of electronic system can be expressed in terms of its density. A formal proof was developed in 1964 by Hohenberg and Kohn, showing that the ground-state energy of an electronic system is uniquely

defined by its density, although the exact functional dependence of the energy on density remained unknown.[26] Hence, there is a one-to-one mapping between the potential, the particle density and the ground state wave function. This shows that the exact electron density could be found through the variation theorem. Given the density, only one potential and wave function correspond to that density, so the wave function Ψ_0 is a functional of potential, $\upsilon(r)$, and a functional of particle density, $\rho(r)$.

$$\Psi_0 = \Psi_0[\upsilon(r)] = \Psi_0[\rho(r)] \tag{2.16}$$

Kohn and Sham suggested a practical way to solve the Hohnberg-Kohn theorem for a set of interacting electrons is by approximating the function $F[\rho(r)]$ in the equation[29]

$$E[\rho(r)] = \int V_{ext}(r)\rho(r)dr + F[\rho(r)] \tag{2.17}$$

where the first term arises from the interaction of the electrons with an external potential $V_{ext}(r)$ and $F[\rho(r)]$ is the sum of kinetic energy of all electrons and contribution from interelectron interactions. Their approximation of $F[\rho(r)]$ separates the function into the sum of three terms, the kinetic energy $E_{KE}[\rho(r)]$, electron-electron Coulombic energy $E_H[\rho(r)]$, and the exchange correlation $E_{XC}[\rho(r)]$.

$$F[\rho(r)] = E_{KE}[\rho(r)] + E_H[\rho(r)] + E_{XC}[\rho(r)] \tag{2.18}$$

In order to solve the kinetic energy term, the idea was borrowed from the Hartree-Fock expression for kinetic energy in terms of exact orbitals where electrons do not interact. Kohn and Sham proved that it is possible to construct a system of non-interacting electrons which have the exact same electron density of the real molecular system of interacting electrons. The second term, $E_H[\rho(r)]$, also known as the Hartree electrostatic energy arises from the classical interaction between two charge densities, which are summed over all possible pairwise interactions. Combining these two terms and including

the electron-nuclear interaction leads to the full expression for the energy of a N-electron system. The final term, the exchange correlation $E_{XC}[\rho(r)]$, contains not only the contributions from exchange and correlation but also a contribution due to the difference between true kinetic energy of the system and $E_{KE}[\rho(r)]$. The ground-state electronic energy writing out all the terms explicitly is

$$E[\rho(r)] = \sum_{i=1}^{N} \int \psi_i(r) \left(-\frac{\nabla^2}{2} \right) \psi_i(r) dr + \frac{1}{2} \iint \frac{\rho(r_1)\rho(r_2)}{|r_1 - r_2|} dr_1 dr_2 - \sum_{A=1}^{M} \int \frac{Z_A}{|r - R_A|} \rho(r) dr + E_{XC}[\rho(r)] \quad (2.19)$$

2.2.3 Exchange-Correlation Approximation

As seen in Equation 2.19, the key between obtaining valid results depends, for density functional theory, in the exchange-correlation functional. Depending on which approximations to the exhange-correlation function are implemented determines how accurate the results will be.[1] The most popular and simplest approximation is the local density approximation (LDA).[29] This approximation is based upon a uniform electron gas model where the electron density is constant throughout all space. Assuming that the charge density varies slowly throughout a molecule so that a localized region behaves like a uniform gas, $E_{XC}[\rho(r)]$ for this system can be obtained by integrating over all space:

$$E_{XC}^{LDA}[\rho(r)] = \int \rho(r) \varepsilon_{XC}(\rho(r)) dr \quad (2.20)$$

where $\varepsilon_{XC}(\rho(r))$ is the exchange and correlation energy per electron in the uniform electron gas, as a function of electron density $\rho(r)$.

Despite its simplicity, the local density approximation performs well, particularly for metallic systems including organometallic species.[30] However, LDA has been shown to be inadequate for some problems.[31] An improved version of the LDA called local spin-density approximation (LSDA) has been created.[28] LSDA is an extension of DFT, similar to same way that restricted and unrestricted Hartree-Fock extensions were developed in order to model appropriately systems with unpaired electrons. The LSDA uses different orbitals and different densities with the net spin density being the difference between the density of up-spin and down-spin electrons. This proved to work well for bond lengths and vibrations, but not for dipole moments[32] or predictions of molecular binding energies,[33] which tend to be overestimated.

To overcome this overbinding character of the LSDA, a new method has been introduced that uses gradient-corrected, 'non-local' functionals which depend upon the gradient of the density at each point in space and not just on its value. The lowest-order gradient correction of exchange is in the form:

$$\beta \frac{(\nabla \rho)^2}{\rho^{4/3}} \tag{2.21}$$

Many alternatives for gradient-corrected exchange and correlation functionals have been reported, which go beyond the lowest-order gradient correction, and are referred to collectively as generalized gradient approximations (GGA).[28]

The gradient correction to the exchange functional proposed by Becke in 1988, was a greatly improved functional, which takes into consideration the exchange energy for rare gases in addition to the known behavior for the uniform electron gas.[34] Known as B-88, this exchange functional depends on both density and density gradient. The B-88 functional was a great improvement in that the asymptotic exchange energy behavior

could be reproduced exactly. Other popular correlation functionals include the Lee, Yang and Parr (LYP),[25] Perdew-86,[35] and Perdew and Wang (PW91).[36] These GGAs yield good thermochemistry, with average errors of the order of 6 kcal/mol in standard thermochemical test.[28] GGAs are also useful in the energetics and structures of hydrogen-bonded systems, but start to break down when taking into account dispersion interactions.[37]

While pure DFT methods calculate E_{XC} by pairing an exchange functional with a correlation functional, the use of a hybrid functional that contains some proportion of exact (HF) exchange, improves the deficit of GGA's severe underestimation of activation barriers for some reactions due to neglect of Coulomb "self-interaction" of the electrons.[24,38] The most popular is the Becke three parameter functional (B3) including the semiempirical combination of exact exchange, the local spin density approximation and gradient correction. This provides a better approach for calculating the electronic structure of atoms and molecules.

Modern DFT functionals are the result of the combination of exchange and correlation functionals, in Becke's original paper his own gradient correction for exchange was used in conjunction with a gradient correction developed by Perdew and Wang. A more popular scheme is the B3LYP, the Becke three parameter functional, where the non-local correlation is provided by Lee, Yang and Parr (LYP) and the standard local correlation functional due to Vosko, Wilk and Nusair (VWM). The model is takes form in the equation:

$$E_{XC}^{B3LYP} = (1-a_0)E_X^{LSDA} + a_0 E_X^{HF} + a_X \Delta E_X^{B88} + a_C E_C^{LYP} + (1-a_C)E_C^{VWN} \qquad (2.22)$$

The first three terms are the exchange contributions and the last two terms describe the correlation energy. The empirical coefficients a_0, a_X and a_C are obtained by least-squares fitting to experimental data. Their values are $a_0 = 0.20$, $a_X = 0.72$ and $a_C = 0.81$.[1] The B3LYP functional is used in this thesis for all density functional calculations for its increased accuracy in predicting molecular structures and properties and its improved speed over traditional methods, such as the Møller-Plesset method.

A major drawback for DFT is the lack of inclusion of dispersive forces. Dispersive forces are due to instantaneous dipoles which arise during the fluctuations in the electron clouds. This instantaneous dipole can induce a dipole in a neighboring atom, which gives an attractive inductive effect. These forces may be necessary to adequately model a particular system, which could lead to over- or underestimation of the energetic predictions with DFT.

2.2.4 Application of DFT to the Diels-Alder reaction

Since the focus of this thesis is on the influence of external factors on Diels-Alder reactions, it is natural to focus on density functional theory's ability to predict properly the energetics and structures of this reaction. DFT has been successfully applied to pericyclic reactions, where comparison of results from different DFT calculations with extensive results from Hartree-Fock calculations and other molecular orbital based methods on the Diels-Alder reaction has confirmed the accuracy of these methods.[5,8,9] An extensively studied reaction is the Diels-Alder reaction between butadiene and acrolein. The calculated activation energy for Hartree-Fock predicts a value of 47.4 kcal/mol, while MP2/6-31G(d) calculations predict 17.6 kcal/mol.[8] It is well-known that Hartree-Fock tends to overestimate the activation energy while MP2 underestimates it. In order to

predict accurate energies near the experimental value of 24.8 kcal/mol, it is important to include electron correlation energy. B3LYP/6-31G(d) gives an activation energy of 25 kcal/mol, which is in excellent agreement with experiment.[8]

The study of transition structures for the stepwise, diradical pathway and the concerted pathway has been an area of concern for years.[15] It is now well-established that Diels-Alder cycloadditions proceed through a concerted mechanism, nevertheless how inclusion of Lewis acid activation impacts the mechanism of these reactions continues to be an area of ongoing research.[39] How the B3LYP method predicts these reactions is relevant to the discovery of these mechanisms. Results from DFT methods, specifically the B3LYP/6-31G(d), has confirmed the experimental estimates for the energy of concert, for a concerted pathway.[8] Recently, a more direct validation of computational results has provided a direct comparison of high precision primary and secondary kinetic isotope effects with predictions from DFT.[14,39] These reactions show an excellent agreement between theory and experiment. This lends confidence in DFT's ability to predict transition structures, since significant errors would arise in the calculated geometries if there were large deviations from the measured isotope effects.

The application of DFT to the Diels-Alder reaction in this thesis is important for several reasons. The first of which, is DFT's inclusion of electron correlation. This is necessary in this study since the Diels-Alder reactions are carried out in polar solvents and in the presence of Lewis acids. Second, the high computational efficiency of DFT allows systems of interest to be calculated with out imposing heavy constraints on the size of the reaction. Finally, the importance of the Diels-Alder reaction to organic

synthesis dictates that the origins of the rate and stereoselectivity be thoroughly understood for the design of new asymmetric catalysts and applications.

2.3 Thermodynamic Quantities

Thermochemical quantities may be extracted from a potential energy surface (PES) in terms of internal energy, E, enthalpy, H, or Gibbs free energy G. The procedure described here is based upon the implementation in the Gaussian software package.[40] By default, thermochemistry analysis is carried out at 298.15 K and 1 atmosphere of pressure, which is easily modified.[6,41] The equations used to compute thermochemical data from a PES can be found in most standard thermodynamic textbooks. In this specific implementation, there are two important assumptions that induce error into the computed thermochemical quantities. First, the equations used assume non-interacting particles, which is tantamount to an ideal gas treatment. Second, it is also assumed that the first and higher excited states are inaccessible. Both assumptions have the potential to introduce error into the computed thermochemical quantities, but in general do not impact the majority of molecular systems of interest.

The stationary points obtained by computational procedures on the PES are for vibrationless molecular systems. The electronic Hamiltonian used in ab initio calculations gives the total electronic energy, E_{elec}. A real molecule, however, has vibrational energy even at 0 K, which is the quantum mechanical zero-point energy (*ZPE*), $\frac{1}{2}h\nu$. At absolute zero, the internal energy, E_0, is defined as the computed electronic energy plus the zero-point energy.

$$E_0 = E_{elec} + ZPE \tag{2.23}$$

Thermal corrections to the computed internal energy are necessary in order to obtain energies at temperatures that are directly comparable to experiment.[42] The thermal corrections to the internal energy are determined by contributions from the translational (q_t), electronic (q_e), rotational (q_r) and vibrational (q_v) partition functions. The internal thermal energy correction term is the sum of all four contributions. It is important to realize that thermal energy corrections already include the zero-point energy through the vibrational partition function contribution, so it is not added redundantly.

$$E_{thermal}^{temp} = E_t + E_r + E_v + E_e \tag{2.24}$$

The internal energy at a specific temperature is then determined by the sum of the internal thermal energy correction term and the computed electronic energy. Take 298 K as an example.

$$E_{298} = E_{thermal}^{298} + E_{elec} \tag{2.25}$$

Absolute thermodynamic quantities are difficult to compute accurately, and rarely reported in computational chemistry.[43] Rather, differences in the thermochemical quantities are used to improve the accuracy and agreement with experiment. Two thermodynamic quantities are of common interest are defined in Figure 2.2.

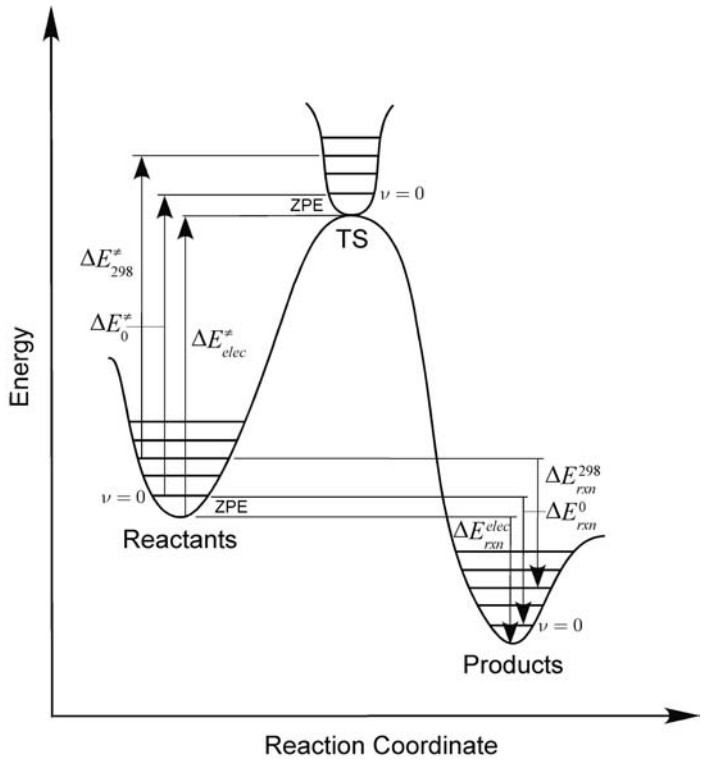

Figure 2.2. Computed thermodynamic quantities.

The first thermodynamic quantity involves the activation energy, $\Delta E^{\neq}_{298}$, which is the internal energy difference between the transition structure and the ground state reactants at a specified temperature.

$$\Delta E^{\neq}_{298} = E^{TS}_{298} - E^{react}_{298} \tag{2.26}$$

The second quantity typically referred to is the energy of reaction, ΔE^{298}_{rxn}, which is the energy of the products minus the energy of the reactants.

$$\Delta E^{298}_{rxn} = E^{product}_{298} - E^{react}_{298} \tag{2.27}$$

It is possible to use standard thermodynamic equations to convert the thermally corrected internal energy into enthalpies and Gibbs free energies at the same temperature. To determine the enthalpy, the thermodynamic definition of enthalpy is used.

$$H = E + PV \tag{2.28}$$

At constant pressure and temperature, and using the ideal gas approximation, the enthalpy difference, can be related to the difference in internal energy. Therefore, the change in enthalpy will be computed correctly when the number of moles of gas changes during the course of the reaction.

$$\Delta H = \Delta E + P\Delta V$$
$$\Delta H = \Delta E + (\Delta n)RT \tag{2.29, 2.30}$$

The enthalpy of activation and enthalpy of reaction is determined as with the internal energy terms discussed earlier.

$$\Delta H_{298}^{\neq} = \Delta E_{298}^{\neq} + (\Delta n)RT$$
$$\Delta H_{rxn}^{298} = \Delta E_{rxn}^{298} + (\Delta n)RT \tag{2.31, 2.32}$$

Entropy corrections to the computed enthalpy change are necessary in order to obtain the Gibbs free energy. The entropy corrections are determined by contributions from the translational (q_t), electronic (q_e), rotational (q_r) and vibrational (q_v) partition functions. The entropy correction term is the sum of all four terms.

$$S_{total} = S_t + S_r + S_v + S_e \tag{2.33}$$

By utilizing the definition of the Gibbs free energy, it is possible to relate it to the enthalpy. In addition the computed enthalpy change at the same temperature gives the change in the Gibbs free energy.

$$G = H - TS$$
$$\Delta G = \Delta H - T\Delta S \qquad (2.34, 2.35)$$

The Gibbs free energy of activation and Gibbs free energy of reaction are determined as with the enthalpy and internal energy terms discussed previously.

$$\Delta G_{298}^{\neq} = \Delta H_{298}^{\neq} - T\Delta S_{298}^{\neq}$$
$$\Delta G_{rxn}^{298} = \Delta H_{rxn}^{298} - T\Delta S_{rxn}^{298} \qquad (2.36, 2.37)$$

In a Gaussian vibrational analysis output, as modified and shown in Table 2.2 several important pieces of information are printed to make the proper corrections for thermochemical quantities at stationary points. Gaussian provides absolute thermochemical quantities, which follow from the discussion above. The units are in hartrees.

Table 2.2. *Example of Gaussian output. The different thermodynamic quantities.*

Sum of electronic and zero-point Energies $= E_{elec} + ZPE = E_0$
Sum of electronic and thermal Energies $= E_{elec} + E_{thermal}^{298} = E_{298}$
Sum of electronic and thermal Enthalpies $= E_{elec} + H_{thermal}^{298} = H_{298}$
Sum of electronic and thermal Gibbs FreeEnergies $= E_{elec} + G_{thermal}^{298} = G_{298}$

2.4 Assessment of Computed Results

Derivatives are required for energy minimizations.[1] The direction of the first derivative of the energy indicates where the minimum lies, while the second derivative gives the curvature of the function. The first derivative is used to lower the energy of the

system by moving each atom in response to the forces acting on it. The second derivative predicts where the function is either a minimum (positive curvature, normal vibration) or maximum (negative curvature, imaginary frequency). The Taylor series expansion of the energy, $V(x)$, about the point x_o can be used to understand how stationary points are classified. Approximations are commonly made to this series expansion.

$$V(x) = V(x_o) + (x - x_o)V'(x_o) + (x - x_o)^2 V''(x_o)/2 + \cdots \tag{2.38}$$

Vibrational analysis must be carried out on stationary points, where the first derivatives, $V'(x_o)$, are equal to zero and the potential at $V(x_o)$ is assumed to be zero. By ignoring higher order terms, the harmonic approximation results.

$$V(x) = \frac{1}{2}V''(x_o)\Delta(x - x_o)^2 \tag{2.39}$$

This representation gives a useful way of understanding how the second derivative is related to the force constant (curvature) and how to assign the type of stationary point (sign).

The number of negative eigenvalues resulting after vibrational analysis on the Hessian matrix distinguishes the different types of stationary points. For a ground state, all of the eigenvalues correspond to real vibrations of the molecule, thus are all positive quantities and can be observed by experiment. The transition structure is special since it has a single negative eigenvalue describing the vibration at the transition structure. Of interest is the first-order saddle point, where energy passes through a maximum for movement along the reaction pathway that connects two minima, but is a minimum for displacements in all other directions perpendicular to the path. It is vital to check that the Hessian matrix at any proposed saddle point has the required single negative eigenvalue.

The vibration has an imaginary or negative frequency, since as the molecules move along the reaction path, the energy decreases as the reactants and products are approached. The curvature of such vibrational behavior is negative. Thus, the name of negative frequency is commonly used. This is opposite to the energetic behavior of ground state molecules, where displacements from the equilibrium position result in energetic increases. Molecules that have more than one imaginary frequency results in an uninterpretable system. The relationship between the frequency of vibration and force constant is well known. The vibrational frequency, ν, is proportional to the square root of the force constant, *k*, divided by the reduced mass, μ.

$$\nu = (2\pi)^{-1}(k/\mu)^{1/2} \tag{2.40}$$

2.5 Kinetic Isotope Effect

Comparison of high-precision experimental kinetic isotope effects (KIEs) with high-level transition structure/KIE calculations is an extremely powerful tool for defining the mechanism and transition state geometry of organic reactions.[17,20,39,44] The analysis of secondary kinetic isotope effects has been particularly valuable for the investigation of pericyclic reactions.[14,39,45] A starting point for understanding isotope effects is the approximation of the potential energy for the stretching of a C-H bond as a simple harmonic function.[1,46]

$$E = h\nu(\upsilon + 1/2) \qquad \text{Where } \nu = (2\pi)^{-1}(k/\mu)^{1/2} \tag{2.41, 2.42}$$

The electronic energy curve of a molecule is a set of vibrational energy levels ($\upsilon = 0,1,2,..$), where k is the force constant for the molecular vibration and μ is the

reduced mass. At room temperature, 99% of molecules are in their 0^{th} vibrational level. By using the value $\upsilon = 0$ in Equation 2.41, the vibrational energy of the molecules is equal to ½ hν. This energy is called the zero point energy, which is the foundation behind isotope effects.

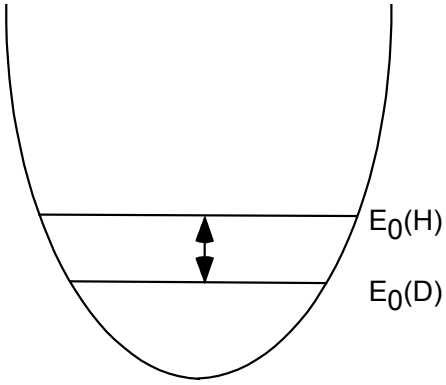

Figure 2.3. *Zero point energies associated with H and D nuclei.*

Substitution of an atom, such as hydrogen or carbon, by its isotope does not effect the electronic structure. Since mass appears in the denominator of Equation 2.42, the heavier isotope has a lower zero point energy, as shown in Figure 2.3. In order to calculate the difference in zero point energy, E_0, between C-H and C-D bonds, the energy for each bond can be determined from the wavelength of the infrared radiation absorbed the corresponding bonds. For example, the C-H stretching vibration is about 3000 cm^{-1}.[46]

$$E_0(H) = ½ h\nu = (½)\ 3000\ cm^{-1} = 1500\ cm^{-1} \quad (2.43)$$

For a C-D bond,

$$E_0(D) = ½ h\nu = (½)\ 2200\ cm^{-1} = 1100\ cm^{-1} \quad (2.44)$$

Then the difference is

$$\Delta E_0 = 1500\ cm^{-1} - 1100\ cm^{-1} = 400\ cm^{-1} \cong 1.15\ kcal/mol \quad (2.45)$$

This dissociation energy difference shows that the activation energy for C-D dissociation should be about 1.15 kcal/mol smaller than for the C-H dissociation. Rate constants for C-H dissociation (k_H) and for C-D dissociation (k_D) are given by

$$k_H = A_H \exp(-E_a(H)/RT)$$
$$k_D = A_D \exp(-E_a(D)/RT) \qquad (2.46, 2.47)$$

If the preexponential factors A_H and A_D are identical, then the ratio k_H/k_D can be calculated. Specific to this research and typically looked at for the determination of transition structures are secondary kinetic isotope effects. Secondary KIEs involve a C-H(D) undergoes a bond change, such that is seen at a transition structure, but is not broken. The magnitude of secondary kinetic isotope effects are thought to increase as the transition structure changes from reactant-like to product-like.

In a Diels-Alder reaction, when a deuterium is substituted for hydrogen at the diene or dienophile terminus, a secondary KIE can be measured. During the course of sp^2 to sp^3 hybridization change, a C-H out-of plane bending mode changes from a low frequency to a higher one (Scheme 2.1(a)). This leads to an increased zero point energy along the reaction path, normally leading to an inverse 2°-KIE. Secondary KIEs are typically divided into two categories: *normal* ($k_H/k_D > 1$) where the KIE effects are seen for hybridization changes of the type $sp^3 \rightarrow sp^2$ or $sp^2 \rightarrow sp$, and *inverse* ($k_H/k_D < 1$) where the KIE effects are seen for hybridization changes in the opposite direction $sp \rightarrow sp^2$ or $sp^3 \rightarrow sp^2$.

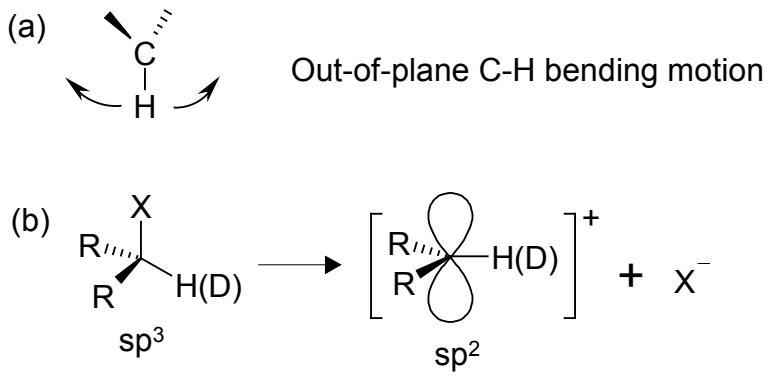

Scheme 2.1. *(a) "Out-of-plane" C-H bending motion for a transition state. (b) Normal 2° kinetic isotope effect, where the carbon orbital used for C-H bonding changes from an sp^3 hybrid to an sp^2 hybrid.*

To compute the kinetic isotope effects, it is necessary to obtain force constants from frequency calculations characterizing the system. The force constant matrices together with optimized geometries are used by the program QUIVER[47] is used to calculate the secondary KIEs based on statistical mechanics and classical transition state theory,[48] using the Bigeleisen-Mayer formalism.[49] Force constants obtained by frequency calculations are used to determine a ratio of partition functions, where $u = h\upsilon/kT$.

$$\frac{k_H}{k_D} = \frac{\nu_H^{\ddagger}}{\nu_D^{\ddagger}} \frac{\prod^{3N-6} \frac{u_H}{u_D}}{\prod^{3N^{\ddagger}-7} \frac{u_H^{\ddagger}}{u_D^{\ddagger}}} \frac{\prod^{3N-6} \frac{[1-\exp(-u_H)]}{[1-\exp(-u_D)]}}{\prod^{3N^{\ddagger}-7} \frac{[1-\exp(-u_H^{\ddagger})]}{[1-\exp(-u_D^{\ddagger})]}} \frac{\exp\left(\sum^{3N-6} \frac{(u_H-u_D)}{2}\right)}{\exp\left(\sum^{3N^{\ddagger}-7} \frac{(u_H^{\ddagger}-u_D^{\ddagger})}{2}\right)} \tag{2.48}$$

To account for the anharmonicity of molecular vibrations, QUIVER scales the force constants obtained from the ab initio calculations by an empirical scaling factor. The scaling factor used through out this thesis was 0.9614, which is appropriate for the B3LYP/6-31G(d) level of theory.[44] Scaling factors for different methods in recent publications use the scaling factor values of 0.8953 for HF/6-31G(d) and 0.9427 for MP2/6-31G(d).[44,50] Raw frequency values computed at the different methods, are known to contain systematic error. In the Hartree-Fock level, the errors arise due to the neglect

of electron correlation, arising in overestimations of approximately 10-12%.[6] The use of a scaling factor has been demonstrated to produce very good agreement with experiment for a wide range of systems.

2.6 Classical Calculations

Due to the resources required and the limitations on computer size and speed, quantum mechanical (QM) methods typically treat a relatively small number of atoms. The high dependency of the computer time on the number of basis functions makes it impossible to treat large systems.[51,52] These QM methods are no longer feasible when modeling biochemical systems, which may contain 20,000 atoms or more. Empirical energy functions suit the demands imposed by computational studies of these larger systems. Classical calculations are based on the application of mathematical equations to describe the relationship of chemical structure to energy.[1,13] The mathematical equations include relatively simple terms to describe the physical interactions that dictate the interactions between atoms. The major difference between classical calculations and quantum mechanical calculations, is that these empirical force fields use atomistic models, in which atoms are the smallest particles in the systems rather than electrons and nuclei used in quantum mechanics. This allows for a reasonable amount of computer resources to be allocated in order to achieve the number of energy calculations required on the systems in their appropriate environment, i.e., solvent. Traditional electronic structure algorithms calculate eigenstates associated with discrete energy levels. This leads to a diagonalization problem that has cubic scaling in the computational effort. Because of the steep scaling of computational effort with system size *N*, traditional high-

accuracy quantum chemical methods such as CCSD(T) scales at $O(N^7)$.[52] Even MP2 methods scale at $O(N^5)$.[52] DFT uses electron density a function of three spatial dimensions, which has the ability to reduce computational resources necessary as compared to other ab initio methods that include electron correlation. However, DFT still typically scales at $O(N^3)$.[51] The most expensive computation in standard molecular mechanics calculations is the evaluation of the nonbonded energy. Exact computation requires $O(N^2)$ operations, which is not realistic for large-scale systems.[1] Traditionally, cutoff methods have represented all atoms sufficiently far away from an atom of interest as not being present at all, assuming that their effects would be negligible. Although it is possible that accuracy suffers, the operation count is reduced to $O(N)$.

2.6.1 Parameter Optimization

In cases where it is necessary to extend the force field used for simulation, in order to treat new molecules, a systematic procedure is needed to obtain and optimize the new force field parameters consistent with the existing ones.[53] The first step of the parameterization process is to select the appropriate model. If the system is composed of small organic molecules, such is the case in this thesis, then the model compound may be the molecules themselves. However, it may be desirable to select several smaller model compounds that can be connected to create the final, desired molecule. This is advantageous when adequate experimental data exists for the smaller compounds, specifically in the Cambridge Crystal Database,[54] although QM data can be substituted in the absence of such data. The model compounds should be of size that is accessible to QM calculations, typically using methods varying from HF, B3LYP to MP2, while using a basis set no smaller than 6-31G(d).

Upon choosing the appropriate model compounds, it is now necessary to provide the topology information, which is comprised of connectivity, atom types and partial atomic charges. Typically, molecules that are present in the force field which closely mimic the model compounds of interest are selected and initial information is extracted. This simplifies the process, while keeping the new model compound in line with the existing force field. Partial charges could be assigned from a Mulliken population analysis, although the use of CHELPG charges typically give a better representation.[55] It is imperative that care be taken to assign a total charge on the molecule of zero, or –1 for anions and +1 for cations. At this point the information required by CHARMM or other force fields to create the molecule is present, but the parameters necessary to perform the energy calculations need to be determined.

In order to create the appropriate force field parameters, it is necessary to look at the potential energy function equation, which include the terms necessary to describe the physical interactions that dictate the structure and properties of the system. In this thesis, the CHARMM force field was used, so efforts will be focused upon this particular force field.[56] The potential energy function is represented by the following equation.

$$U(R)=\sum_{bonds}K_b\left(b-b_0\right)^2+\sum_{angle}K_\theta\left(\theta-\theta_0\right)^2+\sum_{UB}K_{UB}\left(S-S_0\right)^2+$$
$$\sum_{dihedrals}K_\chi\left(1+\cos\left(n\chi-\delta\right)\right)+\sum_{impropers}K_{imp}\left(\varphi-\varphi_0\right)^2+ \qquad (2.49)$$
$$\sum_{nonbonded}\varepsilon_{ij}\left[\left(\frac{R\min_{ij}}{r_{ij}}\right)^{12}-\left(\frac{R\min_{ij}}{r_{ij}}\right)^{6}\right]+\frac{q_iq_j}{r_{ij}}$$

The internal terms, such as bonds, angles, dihedrals, Urey-Bradley and impropers are associated with covalently connected atoms, and the external influences such as the van

der Waals (VDW) and columbic interactions are represented by the nonbonded terms. The terms in the 3D structure are the bond lengths, b, the valence angles, θ, the dihedral or torsion angles, χ, and the distances between the atoms, r_{ij}. K_b and K_θ are the force constants associated with the bond and angle terms, respectively, with the other K's representing their respective force constants in the force field. The harmonic approximation is sufficient to describe accurately the bond, angle, Urey-Bradley and impropers terms for MD simulations performed at room temperature.

Adjustment of the bond and angle equilibrium values are generally straightforward, although minimized structures generally do not have bond lengths and angles that correspond directly to the equilibrium parameters.[53] Force constants are optimized by reproducing experimental or QM vibrational spectra. The parameters should be able to reproduce the assignments of the frequencies as well as their numerical values. Dihedrals parameters are optimized on the basis of conformational energies. The use of QM data allows for the calculation of entire energy surfaces which models correctly the minima and maxima. Ultimately, the empirical energy surface associated with the rotation of a torsion angle will contain contributions from all the terms in the potential energy surface, so it is important that several iterations are repeated to obtain a final, consistent set of parameters. Energy from the global minima (fully optimized structure) with no dihedral constraints should be used to offset the entire surface with respect to zero for both the QM and MM data. The dihedral parameters can then be optimized to maximize the agreement between empirical data and target surface. It is often helpful to include additional dihedrals with different multiplicities to get a more

accurate fit, although the force constant and phase both need to be adjusted to contribute properly to the potential energy surface.

As an example of parameterization of the potential energy surface, the rotation of butadiene's torsional angle is considered. The rotation is about the central bond in the molecule (refer to Scheme 2.2).

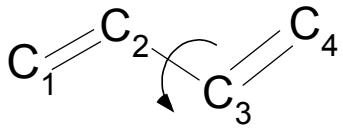

Scheme 2.2. *Rotation about the C1-C2-C3-C4 dihedral angle for 1,3-butadiene.*

As seen in Figure 2.4, new parameters for the dihedral angle have been developed and compared to several QM methods, from HF to MP2.[57] CHARMM now models the system well, with two maxima (at 0° and 100°) and two minima (at 40° and 180°). The relative enthalpy observed for the gauche-trans barrier (ΔH_{298} at 100° - ΔH_{298} at 180°) experimentally was 5.88 ± 0.09 kcal/mol[58] which agrees best with MP2 at 5.28 kcal/mol. The relative experimental enthalpy for the gauche-trans difference (ΔH_{298} at 100° - ΔH_{298} at 40°) was 2.76 ± 0.07 kcal/mol[58] compared to the MP2 value of 2.67 kcal/mol. There is excellent agreement between the molecular mechanic minimizations, quantum mechanical minimizations and experimental data, with a deviation of less than one kcal/mol at the different energy barriers.

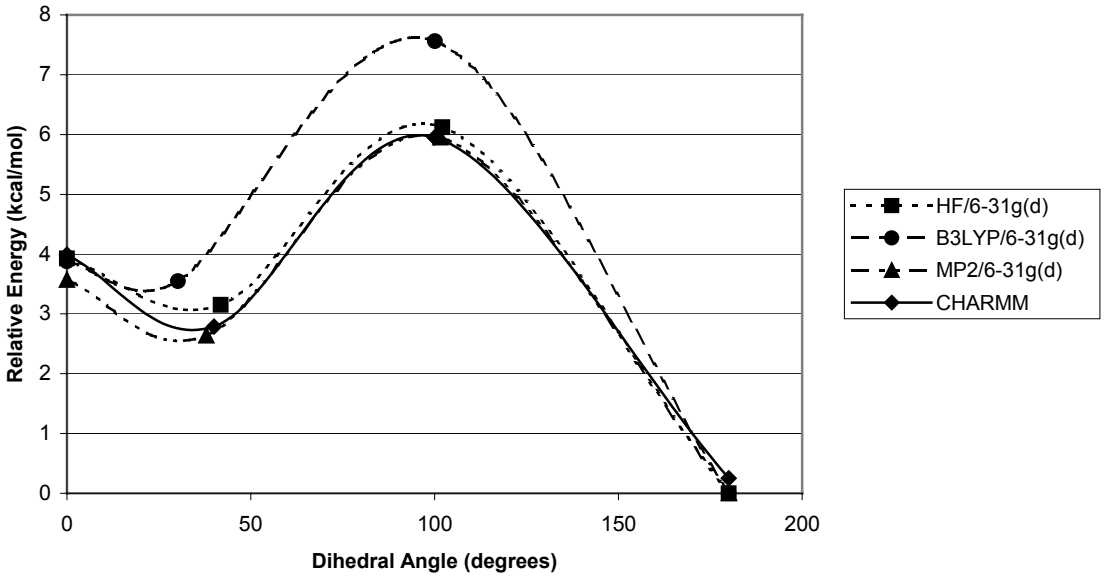

Figure 2.4. *Potential energy surface of butadiene torsional rotation comparing optimized CHARMM parameters to several quantum mechanical methods.*

When the bond, angle and dihedral angles are not providing satisfactory agreement with the target data, the inclusion of improper and Urey-Bradley terms can be added. Improper terms are used to improve conformity with out-of-plane distortions associated with planar groups.

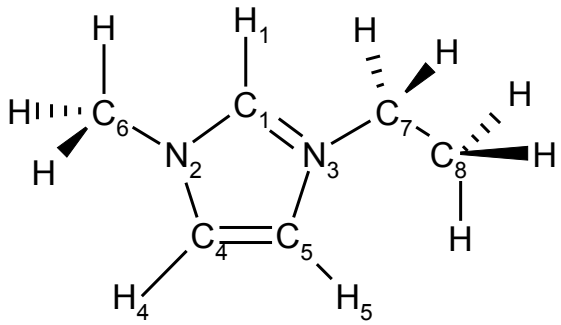

Scheme 2.3. *1-Ethyl-3-methylimidazolium cation.*

In Scheme 2.3, a cation from an ionic liquid solvent in this thesis requires that the H_1, H_4 and H_5 hydrogens are kept in the plane of the ring to properly model the system. The use of impropers typically improve agreement with respect to out-of-plane distortions associated with planar groups (Wilson wags). Urey-Bradley terms are useful for the

proper assignment of symmetric and asymmetric stretching modes, for example, in methyl groups.

The van der Waals and Lennard-Jones (LJ) parameters tend to be the most difficult to optimize.[53] For the most part, using existing VDW parameters based on atoms already in the force field is the simplest solution, and yields satisfactory results. In cases where the VDW parameters require optimization, typically only a few atoms need to be corrected, for example in this thesis, Al and Cl. It is essential that partial charges be rechecked for agreement with target data if VDW parameters are included. Validation needs to be made by rechecking the VDW parameters and partial charges in a consecutive fashion.

2.6.2 Molecular Dynamics

In molecular dynamics (MD), there are two basic assumptions, 1) the simulated system is governed by the laws of classical mechanics and 2) the explicit simulation of the electronic degrees of freedom is not necessary but can be summarized as effective interactions between atoms.[59] Successive configurations of the system are generated by integrating Newton's laws of motion, as shown for a one-dimension system:

$$\frac{d^2x_i}{dt^2} = \frac{F_{x_i}}{m_i} \tag{2.50}$$

The result is a trajectory that specifies how the positions and velocities of the particles vary with time. One of the most important restrictions of molecular mechanical methods based on a classical force field is the inability to describe chemical reactions, isomerizations or excited states, unless specifically parameterized for such processes.

In general, a simulation starts with an initial velocity u_i and the initial spatial coordinates x_i. The integration is comprised of many small stages, each separated by a fixed time. The total force on each particle in the configuration at a time, t, is calculated as the vector sum of its interactions with other particles. The force determines the acceleration of the particles, which are combined with the positions and velocities at a time, t, to calculate the positions and velocities at the next time step. The force is assumed to be constant during the time step. The new forces and positions are determined, leading to new positions and velocities over and over again as time is propagated.

For the subsequent integrations, several algorithms are available of which the Verlet algorithm is one of the most widely used.[60] The Verlet algorithm uses the positions and accelerations at time, t, and the positions from the previous step to calculate the new positions:

$$x_i(t+\Delta t) = 2x_i(t) - x_i(t-\Delta t) + a_i(t)\Delta t^2 \tag{2.51}$$

$$v_i(t) = \frac{x_i(t+\Delta t) - x_i(t-\Delta t)}{2\Delta t} \tag{2.52}$$

where Δt is the integration time step, x_i is the position of atom i . The coordinates at time $t + \Delta t$ are recurrently calculated from the coordinates at $t - \Delta t$ and acceleration at t. The lack of an explicit velocity term in the equations makes it difficult to obtain the velocities, so they are not available until the positions have been computed at the next step.

2.6.3 Potentials of Mean Force

In order to incorporate solvent effects in molecular dynamic simulations, an approach is to use the potential of mean force (PMF) method. PMF describes how free energy changes as a particular coordinate is varied, for example, in a Diels-Alder reaction, the separation of the diene from the dienophile. Since the primary focus is the behavior of the solute in solution, the free energy change can be described using PMF by incorporating the solvent effects as well as the intrinsic interaction between two particles.

Potentials of mean force may be determined using molecular dynamics or Monte Carlo simulations. A drawback is to the method is that the simulations do not adequately sample regions where the radial distribution function differs drastically from the most likely value.[1] A common method to overcome this deficiency is the use of umbrella sampling. This allows unfavorable states to be sample sufficiently, with a modification of the potential function, by including a weighing factor.

In a recent article, Jorgensen et. al calculated free energy profiles for Diels-Alder reactions of cyclopentadiene with acrylonitrile, methyl vinyl ketone and 1,4-naphthoquinone in gas phase and aqueous solution with Monte Carlo simulations in a mixed quantum and molecular mechanics (QM/MM) environment using PMF.[61] AM1 treatment was used for the solute in the presence of 500 TIP4P water molecules. Excellent agreement for the solvent effect upon the Diels-Alder reactions was observed between the calculations and experiment, with differences of 1 kcal/mol or less.[61] These results along with several earlier papers by Jorgensen's research group, shows the potential of mean force as an excellent technique for modeling solutes in solvent.[62]

2.6.4 Periodic Boundary Conditions

The treatment of boundary effects is crucial to simulations methods. Periodic boundary conditions enable a simulation to use a relatively small number of particles, but allow the particles to experience forces as if they were in a bulk fluid. A two-dimensional example is shown in Figure 2.5, where the coordinates of the particles in the image boxes are calculated by adding or subtracting integral multiples of the box sides.

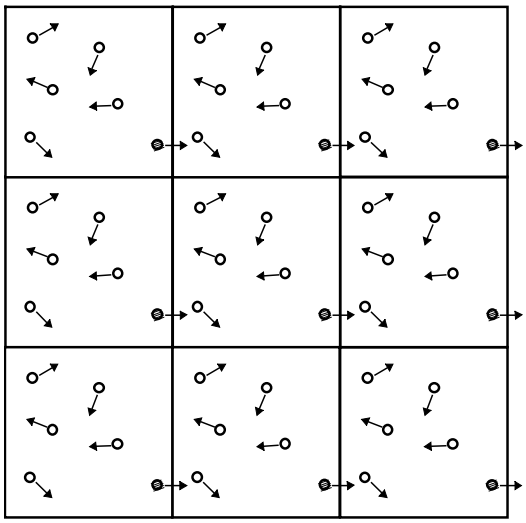

Figure 2.5. *2-D Periodic boundary conditions.*

It is not necessary to store the coordinates of all images in a simulation (this would be an very large number), just those of the molecules in the central box. If a particle leaves the boundary of the box during simulation, it is replaced by an image particle that enters from the opposite side, hence the number of particle remains constant.

Periodic conditions are widely used for simulations, but they do have some limitations.[1] It is not possible to achieve fluctuations that have a wavelength greater than the length of the cell. The range of interactions present in the system is also important. If the box size is large compared to the range over which the interactions act, then there should be no problems. The effects of imposing a periodic boundary condition can be

evaluated empirically by comparing the results of the simulations performed using a variety of box sizes.

2.6.5 Long-Range Electrostatics: Ewald Summation

Long-range electrostatic interactions have been shown to be important when simulating charged species such as molten salts.[63] A possible workaround for this problem would be to construct a much larger simulation box, but this may be too computationally intensive. A variety of methods have been developed to handle long-range forces, but the method used in this thesis is the Ewald summation.

The Ewald sum was developed by Ewald as a method to study the energetics of ionic crystals.[64] In the simulation, a particle interacts with all the other particles and with all the other images in an infinite array of periodic cells. The charge-charge contribution to the potential energy due to all pairs of charges in the central simulation box is:

$$V = \frac{1}{2}\sum_{i=1}^{N}\sum_{j=1}^{N}\frac{q_i q_j}{4\pi\varepsilon_0 r_{ij}} \tag{2.53}$$

where r_{ij} is the minimum distance between the charges i and j.

The problem with the summation is that convergence is extremely slow and is actually conditionally convergent. A conditionally convergent series contains a mixture of positive and negative terms, where the positive and negative terms, when taken alone, form a divergent series (i.e., does not have a finite sum). The Coulomb interaction can also vary rapidly at small distances, which lead to additional problems. The solution to the problem lies in the method for calculating the Ewald sum, separating the summation into two series that converge much faster, seen in the form:

$$\frac{1}{r} = \frac{f(r)}{r} + \frac{1 - f(r)}{r} \tag{2.54}$$

Choosing an appropriate function *f(r)*, which address the rapid variation of *1/r* at small *r* and slows the decay at long *r* is the goal. The sum over point charges is now converted to a sum of the interactions between the charges plus a neutralizing distribution. In the Ewald method, each charge is considered to be surrounded by a neutralizing charge distribution of equal magnitude, but opposite sign. A Gaussian charge distribution is commonly used:

$$\rho_i(r) = \frac{q_i \alpha^3}{\pi^{3/2}} \exp(-\alpha^2 r^2) \tag{2.55}$$

The dual summation can now be given by:

$$V = \frac{1}{2} \sum_{i=1}^{N} \sum_{j=1}^{N} \sum_{|n|=0} \frac{q_i q_j}{4\pi\varepsilon_0} \frac{erfc(\alpha |r_{ij} + n|)}{|r_{ij} + n|} \tag{2.56}$$

The term *erfc* is the complementary error function, which allows rapid converges, while beyond some cutoff distance its value is negligible.

$$erfc(x) = \frac{2}{\sqrt{\pi}} \int_{x}^{\infty} \exp(-t^2) dt \tag{2.57}$$

The rate of convergence depends upon the width of canceling Gaussian distributions, so the wider the Gaussian, the faster the series converges. Hence, α should be chosen so that the only terms in the series are those for which $|n| = 0$ (i.e., only pairwise interactions involving charges in the central box).[1] A second term for charge distribution are added to the system to counteract the first neutralizing distribution and a third term is subtracted to account for the interact of each Gaussian with itself. A fourth

correction term may be required, depending on the medium that surrounds the simulation boxes.

The Ewald sum accurately includes all the effects of the long-range forces in a simulation. It has been used in simulations involving highly charged systems and is being applied to other systems where electrostatic effects are necessary. Ewald have some limitations, in that the summation tends to reinforce artifacts that arise from imposing periodic boundary conditions. The Ewald summation is also computationally expensive, this is where the unfavorable $O(N^2)$ scaling in molecular mechanics come from. Alternative algorithms are being investigated by several research groups that involve fast Fourier transform (FFT), which scales as $O(NlnN)$.[65]

2.7 References

(1) Leach, A. R. *Molecular modelling: principles and applications*; 2nd Edition ed.; Prentice Hall: England, 2001.

(2) Szabo, A.; Ostlund, N. S. *Modern Quantum Chemistry*; Dover Publications, Inc.: New York, 1996.

(3) Born, M.; Oppenheimer, J. R. *Ann. Physik* **1927**, *84*, 457.

(4) Hehre, W. J.; Radom, L.; Schleyer, P. v. R.; Pople, J. A. *Ab initio molecular orbital theory*; John Wiley & Sons, Inc.: New York, 1986.

(5) Houk, K. N.; Li, Y.; Evanseck, J. D. *Angew. Chem. Int. Ed. Engl.* **1992**, *31*, 682.

(6) Foresman, J. B.; Frisch, A. *Exploring Chemistry with Electronic Structure Methods*; Second Edition ed.; Gaussian, Inc.: Pittsburgh, PA, 1996.

(7) Froese, R. D. J.; Humbel, S.; Svensson, M.; Morokuma, K. *J. Phys. Chem. A.* **1997**, *101*, 227.

(8) Wiest, O.; Montiel, D. C.; Houk, K. N. *J. Phys. Chem. A.* **1997**, *101*, 8378.

(9) Wiest, O. In *Encyclopedia of Computational Chemistry*; Schleyer , P. V. R., Ed.; John Wiley & Son Ltd: New York, 1998, pp 3104.

(10) Liu, J.; Niwayama, S.; You, Y.; Houk, K. N. *J. Org. Chem.* **1998**, *63*, 1064; Barone, V.; Arnaud, R. *J. Chem. Phys.* **1997**, *106*, 8727; Barone, V.; Arnaud, R. *Chem. Phys. Lett.* **1996**, *251*, 393; Bernardi, F.; Bottoni, A.; Field, M. J.; Guest, M. F.; Hillier, I. H.; Robb, M. A.; Venturini, A. *J. Am. Chem. Soc.* **1988**, *110*, 3050; Bernardi, F.; Bottoni, A.; Olivucci, M.; McDouall, J. J. W.; Robb, M. A.; Tonachini, G. *J. Mol. Struct. (Theochem)* **1988**, *165*, 341.

(11) Houk, K. N.; Beno, B. R.; Nendel, M.; Black, K.; Yoo, H. Y.; Wilsey, S.; Lee, J. K. *J. Mol. Struct. (Theochem)* **1997**, *398-399*, 169.

(12) Goldstein, E.; Beno, B.; Houk, K. N. *J. Am. Chem. Soc.* **1996**, *118*, 6036.

(13) Cramer, C. J. *Essentials of computational chemistry: theories & models*; Wiley: New York, NY, 2002; Jensen, F. *Introduction to computational chemistry*; Wiley: New York, NY, 1999.

(14) Singleton, D. A.; Merrigan, S. R.; Beno, B. R.; Houk, K. N. *Tetrahedron Lett.* **1999**, *40*, 5817.

(15) Houk, K. N.; Gonzalez, J.; Li, Y. *Acc. Chem. Res.* **1995**, *28*, 81.

(16) Eksterowicz, J. E.; Houk, K. N. *Chem. Rev.* **1993**, *93*, 2439.

(17) Storer, J. W.; Raimondi, L.; Houk, K. N. *J. Am. Chem. Soc.* **1994**, *116*, 9675.

(18) Houk, K. N.; Lin, Y. T.; Brown, F. K. *J. Am. Chem. Soc.* **1986**, *108*, 554.

(19) Herges, R.; Jiao, H.; Schleyer , P. V. R. *Angew. Chem. Int. Ed.* **1994**, *33*, 1376.

(20) Wiest, O.; Houk, K. N.; Black, K. A.; Thomas IV, B. *J. Am. Chem. Soc.* **1995**, *117*, 8594.

(21) Li, Y.; Houk, K. N. *J. Am. Chem. Soc.* **1993**, *115*, 7478.

(22) Uchiyama, M.; Tomioka, T.; Amano, A. *J. Phys. Chem.* **1964**, *68*, 1878.

(23) Schmidt, M. W.; Gordon, M. S. *Annu. Rev. Phys. Chem.* **1998**, *49*, 233.

(24) Becke, A. D. *J. Chem. Phys.* **1993**, *98*, 5648.

(25) Lee, C.; Yang, W.; Parr, R. G. *Phys. Rev.* **1988**, *37*, 785.

(26) Hohenberg, P.; Kohn, W. *Phys. Rev.* **1964**, B864.

(27) Labanowski, J. K.; Andzelm, J. W. *Density Functional Methods in Chemistry*; Springer-Verlag: New York, 1991; García, J. I.; Martínez-Merino, J. A.; Mayoral, J. A.; Salvatella, L. *J. Am. Chem. Soc.* **1998**, *120*, 2415; Houk, K. N.; Wiest, O. *Top. Curr. Chem.* **1996**, *183*, 1; Kong, S.; Evanseck, J. D. *J. Am. Chem. Soc.* **2000**, *122*, 10418.

(28) Kohn, W.; Becke, A. D.; Parr, R. G. *J. Phys. Chem.* **1996**, *100*, 12974.

(29) Kohn, W.; Sham, L. *Phys. Rev.* **1965**, *140*, A1133.

(30) Head-Gordon, M. *J. Phys. Chem.* **1996**, *100*, 13213.

(31) Ziegler, T. *Chem. Rev.* **1991**, *91*, 651.

(32) Becke, A. D. *Phys. Rev.* **1986**, *33*, 2786.

(33) Johnson, B. G.; Gill, P. M. W.; Pople, J. A. *J. Chem. Phys.* **1993**, *98*, 5612.

(34) Becke, A. D. *Phys. Rev. A* **1988**, *37*, 785.

(35) Perdew, J. P.; Wang, Y. *Phys. Rev. B* **1986**, *33*, 8800.

(36) Perdew, J. P.; Wang, Y. *Phys. Rev. B* **1992**, *45*, 13244.

(37) Kristyan, S.; Pulay, P. *Chem. Phys. Lett.* **1994**, *229*, 175; Perez-Jorda, J. M.; Becke, A. D. *Chem. Phys. Lett.* **1995**, *233*, 134.

(38) Becke, A. D. *J. Chem. Phys.* **1996**, *104*, 1040.

(39) Acevedo, O.; Evanseck, J. D. *Org. Lett.* **2003**, *5*, 649.

(40) *Gaussian 98* (Revision A.9), Frisch, M. J.; Trucks, G. W.; Schlegel, H. B.; Scuseria, G. E.; Robb, M. A.; Cheeseman, J. R.; Zakrzewski, V. G.; Montgomery, J. A.; Stratmann, R. E.; Burant, J. C.; Dapprich, S.; Millam, J. M.; Daniels, A. D.; Kudin, K. N.; Strain, M. C.; Farkas, O.; Tomasi, J.; Barone, V.; Cossi, M.; Cammi, R.; Mennucci, B.; Pomelli, C.; Adamo, C.; Clifford, S.; Ochterski, J.; Peterson, G. A.; Ayala, P. Y.; Cui, Q.; Morokuma, K.; Malick, D. K.; Rabuck, A. D.; Raghavachari, K.; Foresman, J. B.; Cioslowski, J.; Ortiz, J. V.; Stefanov, B. B.; Liu, G.; Liashenko, A.; Piskorz, P.; Komaromi, I.; Gomperts, R.; Martin, R. L.; Fox, D. J.; Keith, T.; Al-Laham, M. A.; Peng, C. Y.; Nanayakkara, A.; Gonzalez, C.; Challacombe, M.; Gill, P. M. W.; Johnson, B. G.; Chen, W.; Wong, M. W.; Andres, J. L.; Head-Gordon, M.; Replogle, E. S.; Pople, J. A., Gaussian, Inc., Pittsburgh, PA, 1998.

(41) Ochterski, J. W. *www.gaussian.com* **2000**, 1.

(42) Del Bene, J. E.; Mettee, H. D.; Frisch, M. J.; Luke, B. T.; Pople, J. A. *J. Phys. Chem.* **1983**, *87*, 3279.

(43) Pople, J. A.; Head-Gordon, M.; Fox, D. J.; Raghavachari, K.; Curtiss, L. A. *J. Chem. Phys.* **1989**, *90*, 5622; Curtiss, L. A.; Raghavachari, K.; Trucks, G. W.; Pople, J. A. *J. Chem. Phys.* **1991**, *94*, 7221; Curtiss, L. A.; Carpenter, J. E.; Raghavachari, K.; Pople, J. A. *J. Chem. Phys.* **1992**, *96*, 9030; Curtiss, L. A.; Raghavachari, K.; Pople, J. A. *J. Chem. Phys.* **1993**, *98*, 1293.

(44) Saettel, N. J.; Wiest, O.; Singleton, D. A.; Meyer, M. P. *J. Am. Chem. Soc.* **2002**, *124*, 11552.

(45) Beno, B. R.; Houk, K. N.; Singleton, D. A. *J. Am. Chem. Soc.* **1996**, *118*, 9984.

(46) Carroll, F. A. *Perspectives on Structure and Mechanism in Organic Chemistry*; Brooks/Cole Publishing Co.: Pacific Grove, CA, 1998.

(47) Saunders, W.; Laidig, K. E.; Wolfsberg, M. *J. Am. Chem. Soc.* **1989**, *111*, 8989.

(48) Glassstone, S.; Laidler, K. J.; Eyring, H. *The Theory of Rate Processes*; McGraw-Hill: New York, 1941.

(49) Bigeleisen, J.; Mayer, M. G. *J. Chem. Phys.* **1947**, *15*, 261; Wolfsberg, M.; Hout, R. F.; Hehre, W. *J. Am. Chem. Soc.* **1980**, *102*, 3296.

(50) Scott, A. P.; Radom, L. *J. Phys. Chem.* **1996**, *100*, 16502.

(51) Goedecker, S. *Rev. Mod. Phys.* **1999**, *71*, 1085.

(52) Friesner, R. A.; Dunietz, B. D. *Acc. Chem. Res.* **2001**, *34*, 351.

(53) MacKerell Jr., A. D. In *Computational Biochemistry and Biophysics*; Becker, O. M., MacKerell Jr., A. D., Roux, B., Watanabe, M., Eds.; Marcel Dekker, Inc.: New York, 2001.

(54) Allen, F. H.; Bellard, S.; Brice, M. D.; Cartwright, B. A.; Doubleday, A.; Higgs, H.; Hummelink, T.; Hummelink-Peters, B. G.; Kennard, O.; Motherwell, W. D. S.; Rodgers, J. R.; Watson, D. G. *Acta. Cryst.* **1979**, *B35*, 2331.

(55) Breneman, C. M.; Wiberg, K. B. *J. Comput. Chem.* **1990**, *11*, 361.

(56) MacKerell Jr., A. D.; Bashford, D.; Bellott, M.; Dunbrack, R. L.; Evanseck, J. D.; Field, M. J.; Fisher, S.; Gao, J.; Guo, H.; Ha, S.; Joseph-McCarthy, S.; Kuchnir, L.; Kuczera, K.; Lau, F. T. K.; Mattos, C.; Michnick, S.; Ngo, T.; Nguyen, D. T.; Prodhom,

B.; Reiher III, W. E.; Roux, B.; Schlenkrich, M.; Smith, J. C.; Stote, R.; Straub, J.; Watanabe, M.; Wiorkiewicz-Kuczera, J.; Yin, D.; Karplus, M. *J. Phys. Chem. B* **1998**, *102*, 3586.

(57) Waligorski, A. M.; Thorpe, I. F.; Nelson, A.; MacKerell Jr., A. D.; Evanseck, J. D. *J. Comp. Chem.* **2003**, (Submitted).

(58) Durig, J. R.; Bucy, W. E.; Cole, A. R. H. *Can. J. Phys.* **1975**, *33*, 1832.

(59) van Gunsteren, W. F.; Berendsen, H. J. C. *Angew. Chem. Int. Ed.* **1990**, *29*, 992.

(60) Verlet, L. *Phys. Rev.* **1967**, *159*, 98.

(61) Chandrasekhar, J.; Shariffskul, S.; Jorgensen, W. L. *J. Phys. Chem. B* **2002**, *106*, 8078.

(62) Jorgensen, W. L.; Binning Jr, R. C.; Bigot, B. *J. Am. Chem. Soc.* **1981**, *103*, 4393; Jorgensen, W. L.; Gao, J.; Ravimohan, C. *J. Phys. Chem.* **1985**, *89*, 3470; Jorgensen, W. L.; Buckner, J. K. *J. Phys. Chem.* **1987**, *91*, 6083; Tirado-Rives, J.; Maxwell, D. S.; Jorgensen, W. L. *J. Am. Chem. Soc.* **1993**, *115*, 11590.

(63) Adams, D. J. *J. Chem. Phys.* **1983**, *78*, 2585; Gartrell-Mills, P. R.; McGreevy, R. L. *Phys. Chem. Liq.* **1987**, *17*, 201; Dos Santos, D. J. V. A.; Fernandes, F. M. S. S. *J. Mol. Struc. (Theochem)* **1999**, *463*, 191.

(64) Ewald, P. *Ann. Physik* **1921**, *64*, 253.

(65) Darden, T. A.; York, D.; Pedersen, L. *J. Chem. Phys.* **1993**, *98*, 10089; Hockney, R. W.; Eastwood, J. W. *Computer Simulation using Particles*; Adam Higler: Bristol, 1988; Luty, B. A.; David, M. E.; Tironi, I. G.; van Gunsteren, W. F. *Mol. Sim.* **1994**, *14*, 11; Luty, B. A.; Tironi, I. G.; van Gunsteren, W. F. *J. Chem. Phys.* **1995**, *103*, 3014.

Chapter 3

Kinetic isotope effects on the Diels-Alder reaction

A new transition structure for the Diels-Alder reaction between isoprene and acrolein catalyzed by Et_2AlCl is found to reconcile the original discrepancies between computed and observed secondary kinetic isotope effects (KIEs). Including the effect of solvent realigns the computed results with experiment demonstrating the importance of nonbond interactions at transition structures. Comparison of experimental and newly predicted KIE data reaffirms the ability of theory and experiment to probe the mechanism and transition structure geometry of organic reactions.

Reprinted in part from Org. Lett., **2003**, *5*, 649-652.

Comparison of high-precision experimental kinetic isotope effects (KIEs) with high-level transition structure/KIE calculations is an extremely powerful tool for defining the mechanism and transition state geometry of organic reactions.[1-3] When predicted and observed KIEs match, then the computed transition structure can be used to support a specific reaction mechanism. A number of research groups have produced reasonable agreement between predicted and observed KIEs for pericyclic reactions that have controversial mechanisms ranging from concerted to stepwise processes.[1,4] Even though it is now well established that Diels-Alder cycloadditions proceed through a concerted reaction mechanism,[5] how Lewis acid activation impacts the mechanism of pericyclic reactions continues to be an active area of on-going research.

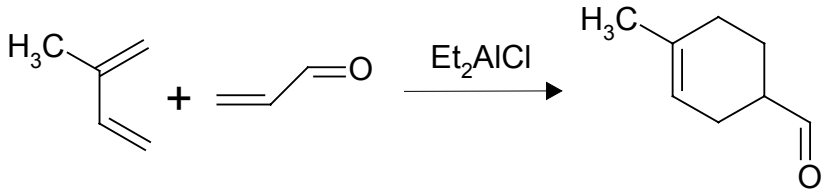

Scheme 3.1. *Diels-Alder reaction between isoprene and acrolein in the presence of a Lewis acid, Et_2AlCl.*

The method of determining kinetic isotope effects experimentally was developed by Singleton through the use of NMR techniques, which is inherently suited for measuring KIEs at natural abundance.[6] It was necessary before to use isotopically labeled and unlabeled material in a competitive reaction, which had restrictions due to the complications involved in the synthesis of the specific atoms for each KIE of interest. The current method allows for simultaneous KIE quantification in natural abundance. There are some limitations, in that the reaction must be sufficiently scalable, the starting material must be isolable from a large amount of product and the reaction cannot be

reversible.[6] Despite these limitations, this method has allowed KIEs to be determined routinely for transition structures.[1,4,6,7]

3.1 Isoprene and Acrolein

Singleton and Houk have recently provided direct experimental support for a highly asynchronous but concerted mechanism for the reaction of isoprene and acrolein with an $AlMe_2Cl$ Lewis acid catalyst. The *endo-cis* transition structure was located in the presence of the Lewis acid catalyst using the Becke three parameter exchange functional[8] and the nonlocal correlation functional of Lee, Yang, and Parr[9] (B3LYP) with the 6-31G(d) basis set.[10] The computed transition structure, seen in Figure 3.1, shows that the chlorine atom is only 2.87 Å from the nearest butadiene proton, suggesting a nontrivial energy of interaction. The calculations predict a large inverse KIE at H3 (see Table 3.1). However, the specific experimental H3 kinetic isotope effect is not as strong as predicted by theory. It was reasoned from the gas phase computations that substantial partial negative charge on the Cl atom (-0.44 e^- from a Mulliken analysis) is drawn towards the partial positive charge in isoprene (+0.29 e^-) which leads to a crowding effect increasing the out-of-plane bending force constant giving the large inverse KIE.[11] Consequently, the results were discounted as an artifact of gas phase computations, which should not occur in solution.

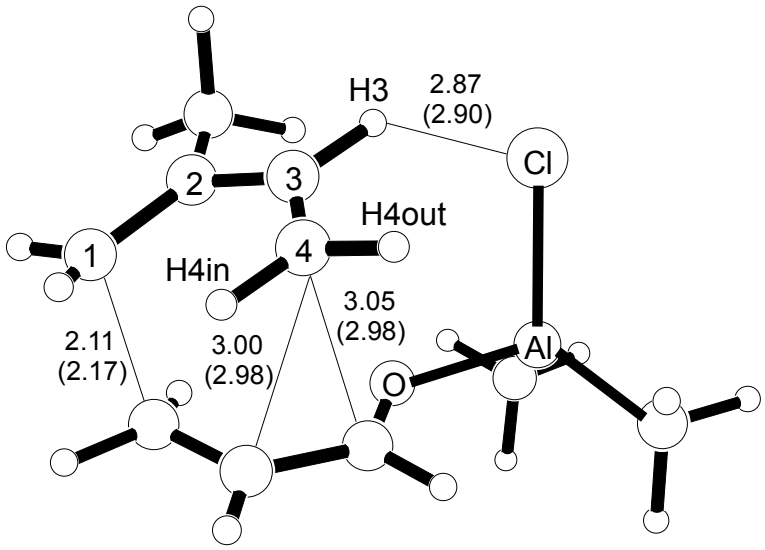

Figure 3.1. *First endo s-cis transition structure*[1] *for the isoprene and acrolein reaction with $AlMe_2Cl$ at B3LYP/6-31G(d). Computed PCM values in parenthesis. Distances in Å.*

Table 3. 1. *The experimental and calculated KIEs (k_H/k_D or k_{12C}/k_{13C}) for the Lewis acid catalyzed Diels-Alder reaction of isoprene and acrolein.*

	exp.1[1]	exp.2[1]	calculated
C1	1.030(3)	1.026(10)	1.031
C2	1.004(3)	1.006(9)	1.004
C3	1.001(2)	1.001(10)	1.000
C4	1.000(3)	1.001(10)	1.002
H1in+H1out	0.915(6)	0.916(7)	0.910
H3	0.965(5)	0.967(13)	0.934
H4out	0.978(6)	0.979(18)	0.986
H4in	0.951(4)	0.947(8)	0.968

Inspired by Corey's findings on unusually strong aldehyde proton interactions with Lewis acids, we investigated a second transition structure to exploit this possible interaction.[12,13] In X-ray crystallographic studies of α, β-unsaturated aldehyde complexes with fluorine and alkyl ether containing boron Lewis acids, Corey and coworkers found a ground state conformational preference in which the formyl group and the B–F or B–O

bond are coplanar.[13-15] It has been proposed that this conformational preference is due to an electrostatic interaction, known as nontraditional (O=C–H···X) hydrogen bonding.[14,16] Previous theoretical investigations have considered the electronic reasons for such stabilization.[17]

Figure 3.2 shows the second transition structure calculated at the B3LYP/6-31G(d) level of theory which takes advantage of nontraditional hydrogen bonding. Frequency analyses of both transition structures were computed to confirm that the stationary points are true transition structures. Crowding of the H3 atom in the new transition structure is computed to be reduced, with the Cl atom at a distance of 3.63 Å away from the H3 hydrogen. In vacuum, we do not find the perfectly eclipsed ground state situation described by Corey, where the transition structure dihedral angle ∠OCHCl = 30.4˚. The observed deviation from planarity is likely due to bad steric interactions that develop between the methyl substituent on aluminum and the diene moiety, where the closest hydrogen-hydrogen distance is 2.51 Å. Alternatively, different nontraditional hydrogen bonding behavior for transition structures as compared to the ground state, or discrepancy between chloro and fluoro substituents, as originally defined by Corey are possible explanations to rationalize the nonplanarity. The new transition structure is different that that reported earlier and should result with modified kinetic isotope effects particularly at H3.

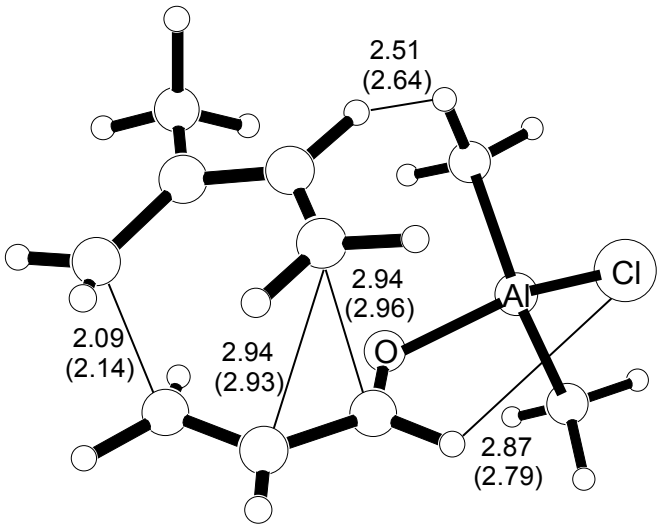

Figure 3.2. *Second endo s-cis transition structure for the Diels-Alder reaction between isoprene and acrolein in the presence of $AlMe_2Cl$ using B3LYP/6-31G(d). Computed PCM values in parenthesis. Distances in Å.*

Using the QUIVER program,[18] the KIEs were calculated for the new transition structure and scaled to the B3LYP/6-31G(d) level of theory using the same procedure described by Singleton and Houk.[1,2] The QUIVER program employs the Bigeleisen and Meyer formulation,[19] based on statistical mechanics and classical transition state theory.[20] The transition structures were calculated using the Gaussian 98 program.[21] The H3 discrepancy between the experimental and calculated KIE is now resolved from the newly computed transition structure. The computed KIE value of 0.964 for the H3 atom nearest the Cl atom is within the experimental accuracy of 0.965(5) and 0.967(13) (see Table 3.2). However, the vacuum electronic energy of the Singleton-Houk transition structure is favored by 0.33 kcal/mol ($\Delta\Delta H^{\ddagger}$ = 0.38 kcal/mol). In essence, the new transition structure explains the experimental KIE data, but is slightly disfavored energetically as compared to the Houk and Singleton transition structure in the gas phase.

Table 3.2. *Calculated KIEs (k_H/k_D or k_{12C}/k_{13C}) for the two TSs of the Lewis acid catalyzed Diels-Alder reaction of isoprene and acrolein at B3LYP/6-31G(d). KIEs from the B3LYP/6-311G(3df) computations are given in brackets.*

	Singleton/Houk TS	Our TS	exp.1[1]	exp.2[1]
C1	1.032 [1.033]	1.032 [1.033]	1.030(3)	1.026(10)
C2	1.003 [1.002]	1.003 [1.002]	1.004(3)	1.006(9)
C3	0.999 [0.999]	0.999 [0.999]	1.001(2)	1.001(10)
C4	1.003 [1.003]	1.004 [1.003]	1.000(3)	1.001(10)
H3	0.943 [0.946]	0.964 [0.962]	0.965(5)	0.967(13)
H4out	0.985 [0.987]	0.975 [0.980]	0.978(6)	0.979(18)
H4in	0.963 [0.961]	0.968 [0.957]	0.951(4)	0.947(8)

Density functional theory (DFT) methods give comparable energetic and structural accuracy compared to more sophisticated and resource demanding computational methods. Specifically, the Becke three parameter exchange functional and the nonlocal correlation functional of Lee, Yang, and Parr[9] with the 6-31G(d) basis set[10] has been shown to produce realistic structures and energies for pericyclic reactions.[22] In order to confirm that this level of theory is accurate for atoms used in the Lewis acid, such as Al and Cl, a larger basis set, 6-311G(3df) was used for comparison. When the Lewis acid catalyzed reaction between isoprene and acrolein was carried out using B3LYP/6-311G(3df), the vacuum electronic energy was very similar to the results seen with the smaller basis set. The Singleton-Houk transition structure is favored by 0.37 kcal/mol ($\Delta\Delta H^{\ddagger}$ = 0.34 kcal/mol) using the larger basis set. The KIEs were also computed using the larger basis set (Table 3.2), and found to be similar to the values from the smaller basis set and experiment. This gives confidence that the B3LYP/6-31G(d)

level of theory accurately represents the transition structures for this particular pericyclic reaction.

Consequently, the effect of solvent upon both transition structures was approximated by using the polarizable continuum model (PCM)[23] with the B3LYP/6-31G(d) level of theory, as we have reported before for other Diels-Alder reactions.[24] The solvent and dielectric constant used was diethyl ether (ε = 4.335). Full geometry optimizations were carried out for both transition structures as shown in Figures 3.1 and 3.2. In solution, the Singleton-Houk transition structure geometry was altered slightly, where the distance between the Cl and the H3 atoms increased from 2.87 Å (vacuum) to 2.90 Å (solution). In the second transition structure, Corey's interaction strengthens by reducing the distance between the Cl atom and the formyl hydrogen from 2.87 Å (vacuum) to 2.79 Å (solution). In addition, when solvent is included the dihedral angle is reduced to $\angle$OCHCl = 9.2˚ at the transition structure which is more in line with Corey's description. The strengthening of the unusual aldehyde nonbond interaction explains why the second transition structure becomes slightly favored, with a computed electronic energy difference of 0.18 kcal/mol ($\Delta\Delta H^{\ddagger}$ = 0.27 kcal/mol). The computed energy differences are small and should not be over interpreted, yet the trend is to favor the transition structure that takes advantage of nontraditional hydrogen bonding as solvent is included in the model. If the energies are correct, then both transition structures would contribute to the observed KIEs. The influence of solvent suggests a switch in the preference to the newly computed transition structure, which is in agreement with experimental KIE values.

3.2 Isoprene and Methyl Vinyl Ketone

Despite a fuller understanding of transition structure nonbond interactions for α, β- unsaturated aldehyde Diels-Alder reactions, Singleton and Houk have observed the same inverse KIE at the H3 position for similar Diels-Alder reactions by experiment, which do not have the ability to exploit nontraditional hydrogen bonding. To investigate the origin of the inverse KIEs for these closely related systems, the reaction between isoprene and methyl vinyl ketone has been computed at the B3LYP/6-31G(d) level of theory and compared to experiment.

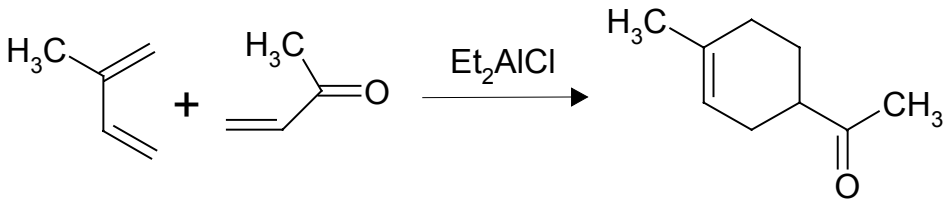

Scheme 3.2. *Diels-Alder reaction between isoprene and methyl vinyl ketone in the presence of Et_2AlCl.*

Even though the nontraditional hydrogen bond is not possible for the isoprene and methyl vinyl ketone reaction, other forces determine the transition structure with moderate KIE effects at H3. Steric repulsions produce a staggering between the methyl group of the dienophile and other subtituents on the catalyst, as shown by the inset in Figure 3.3 (dihedrals = 50.6˚ and 62.3˚). The result eases the crowding effect seen in Singleton and Houk's acrolein system not allowing the Cl group to crowd fully the H3 atom. Three transition structures were found with the Cl rotated about the aluminum-oxygen (carbonyl) axis approximately 120˚ each time. The interdigitation relieves the crowding at H3, thus the inverse effect is reduced. However, the inverse effect observed is due to the through space interaction occurring in Conformation **2**, which can be seen in

Table 3.3. Conformation **1** in Figure 3.3 shows the lowest energy structure. The other two transition structures have less than a 2 kcal/mol relative deviation ($\Delta\Delta H^{\ddagger}$ = 0.58 and 1.64 kcal/mol). Kinetic isotope effects calculated for all three transition structures give an average KIE value of 0.967 ± 0.005 for the H3 atom. This is in very good agreement with the experimental values, as shown in Table 3.4. A competition between transition structures may explain the experimentally observed values.

Table 3.3. *Calculated KIEs (k_H/k_D or k_{12C}/k_{13C}) for the TSs shown in Figure 3.3 of the Lewis acid catalyzed Diels-Alder reaction of isoprene and methyl vinyl ketone at B3LYP/6-31G(d).*

	1	**2**	**3**
C1	1.033	1.033	1.033
C2	1.002	1.002	1.003
C3	1.000	0.999	1.000
C4	1.004	1.004	1.003
H3	0.973	0.957	0.972
H4out	0.986	0.979	0.987
H4in	0.954	0.955	0.956

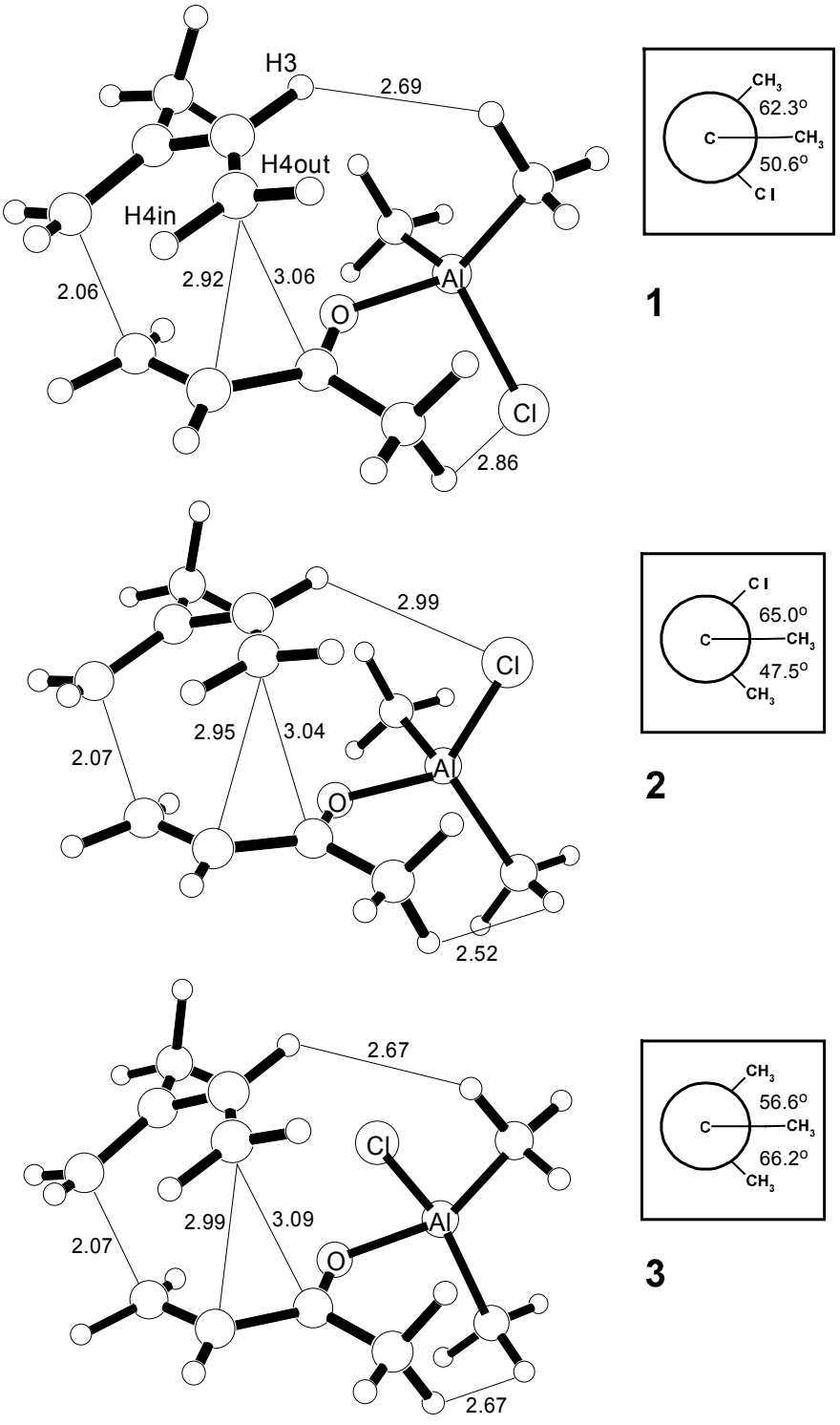

Figure 3.3. *Three calculated endo s-cis transition structures for the isoprene and methyl vinyl ketone reaction with $AlMe_2Cl$ at B3LYP/6-31G(d). Structure **1** is the lowest energy conformation. The insets show a Newman projection along the carbonyl carbon and aluminum atom axis.*

Table 3.4. *Calculated KIEs (k_H/k_D or k_{12C}/k_{13C}) for the lowest energy TS shown in Figure 3.3 and an average of all three possible TSs of the Lewis acid catalyzed Diels-Alder reaction of isoprene and methyl vinyl ketone at B3LYP/6-31G(d).*

	1	ave. calc	exp.1[1]	exp.2[1]
C1	1.033	1.033	1.028(3)	1.030(6)
C2	1.002	1.002	1.007(4)	1.002(6)
C3	1.000	1.000	1.003(4)	1.003(5)
C4	1.004	1.004	1.006(4)	1.005(5)
H3	0.973	0.967	0.970(7)	0.964(3)
H4out	0.986	0.984	0.979(9)	0.983(4)
H4in	0.954	0.955	0.972(5)	0.963(6)

3.3 Isoprene and Methyl Acrylate

The reaction between isoprene and methyl acrylate has been computed at the B3LYP/6-31G(d) level of theory and compared to experiment, as well.

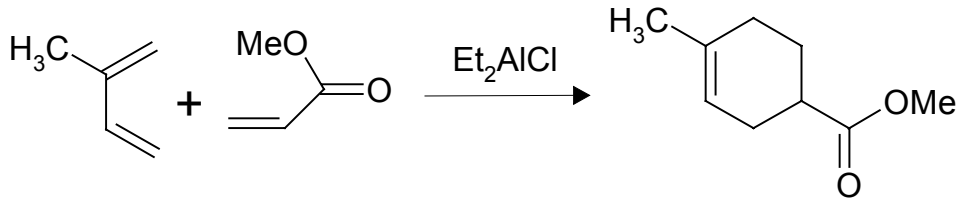

Scheme 3.3. *Diels-Alder reaction between isoprene and methyl acrylate in the presence of Et_2AlCl.*

As with the isoprene and methyl vinyl ketone Diels-Alder reaction, this reaction between isoprene and methyl acrylate does not have the ability to exploit nontraditional hydrogen bonding. The KIEs observed experimentally also have a similar inverse KIE at the H3 position. The transition structure for one of the possible orientations has been computed at the B3LYP/6-31G(d) level of theory.

Similar to the methyl vinyl ketone system, methyl acrylate has steric repulsions the produce a staggering between the methoxy group of the dienophile and other substituents on the catalyst, seen in Figure 3.4.

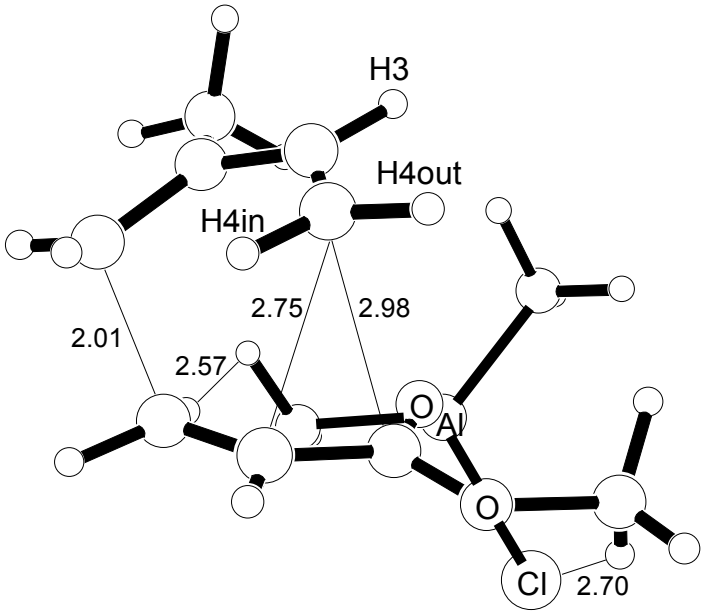

Figure 3.4. *Endo s-cis transition structure for the isoprene and methyl acrylate reaction with $AlMe_2Cl$ at B3LYP/6-31G(d).Distances in Å.*

This results in an easing of the crowding effect at the H3 atom. Kinetic isotope effects have been calculated (Table 3.5) for the transition structure determined in Figure 3.4 and a competition may once again explain the experimental results. The other two possible orientations are found when the Cl is rotated about the aluminum-oxygen (carbonyl) axis. Those transition structures are currently under investigation.

Table 3.5. *Calculated KIEs (k_H/k_D or k_{12C}/k_{13C}) for the lowest energy TS shown in Figure 3.4 of the Lewis acid catalyzed Diels-Alder reaction of isoprene and methyl acrylate at B3LYP/6-31G(d).*

	Fig. 3.4	exp.1[1]	exp.2[1]
C1	1.032	1.026(4)	1.029(4)
C2	1.002	0.999(3)	1.002(4)
C3	1.000	1.002(4)	1.001(5)
C4	1.007	1.003(3)	1.005(4)
H3	0.983	0.970(6)	0.973(3)
H4out	0.988	0.978(9)	0.993(4)
H4in	0.949	0.950(6)	0.958(3)

In conclusion, comparison of the earlier kinetic isotope effect data with our new transition structure data reaffirms the ability of theory and experiment to probe the mechanism and transition structure geometry of organic reactions. Specifically, a new transition structure for the Diels-Alder reaction between isoprene and acrolein catalyzed by Me_2AlCl is found to reconcile the original discrepancies between computed and observed secondary kinetic isotope effects. Two transition structures are possible, and are close in energy. Including the effect of solvent realigns the computational results with experiment, switching the preferred reaction path from that computed in vacuum. For the Diels-Alder reactions between isoprene and methyl vinyl ketone or methyl acrylate, calculations show that the preferred transition structure geometry is a competition between several orientations. The through-space interaction is responsible for the KIE inverse effect seen at the H3 position for all three Diels-Alder reactions. Such detailed investigations allow for the determination of experimentally supported transition structures in the investigation of concerted or stepwise Lewis acid catalyzed reactions.

3.4 References

(1) Singleton, D. A.; Merrigan, S. R.; Beno, B. R.; Houk, K. N. *Tetrahedron Lett.* **1999**, *40*, 5817.

(2) Storer, J. W.; Raimondi, L.; Houk, K. N. *J. Am. Chem. Soc.* **1994**, *116*, 9675; Wiest, O.; Houk, K. N.; Black, K. A.; Thomas IV, B. *J. Am. Chem. Soc.* **1995**, *117*, 8594.

(3) Saettel, N. J.; Wiest, O.; Singleton, D. A.; Meyer, M. P. *J. Am. Chem. Soc.* **2002**, *124*, 11552.

(4) Beno, B. R.; Houk, K. N.; Singleton, D. A. *J. Am. Chem. Soc.* **1996**, *118*, 9984.

(5) Houk, K. N.; Gonzalez, J.; Li, Y. *Acc. Chem. Res.* **1995**, *28*, 81; Houk, K. N.; Beno, B. R.; Nendel, M.; Black, K.; Yoo, H. Y.; Wilsey, S.; Lee, J. K. *J. Mol. Struct. (Theochem)* **1997**, *398-399*, 169.

(6) Singleton, D. A.; Thomas, A. A. *J. Am. Chem. Soc.* **1995**, *117*, 9357.

(7) Singleton, D. A.; Merrigan, S. R.; Liu, J.; Houk, K. N. *J. Am. Chem. Soc.* **1997**, *119*, 3385; Singleton, D. A.; Hang, C. *Tetra. Lett.* **1999**, *40*, 8939.

(8) Becke, A. D. *J. Chem. Phys.* **1993**, *98*, 5648.

(9) Lee, C.; Yang, W.; Parr, R. G. *Phys. Rev.* **1988**, *37*, 785.

(10) Petersson, G. A.; Al-Laham, M. A. *J. Chem. Phys.* **1991**, *94*, 6081.

(11) Streitwieser Jr., A.; Jagow, R. H.; Fahey, R. C.; Suzuki, S. *J. Am. Chem. Soc.* **1958**, *80*, 2326.

(12) Corey, E. J. *Angew. Chem. Int. Ed.* **2002**, *41*, 1650; Corey, E. J.; Lee, T. W. *Chem. Commun.* **2001**, *15*, 1321.

(13) Corey, E. J.; Barnes-Seeman, D.; Lee, T. W. *Tetrahedron Lett.* **1997**, *38*, 4351; Corey, E. J.; Barnes-Seeman, D.; Lee, T. W. *Tetrahedron Lett.* **1997**, *38*, 1699.

(14) Corey, E. J.; Rohde, J. J.; Fischer, A.; Azimioara, M. D. *Tetrahedron Lett.* **1997**, *38*, 33.

(15) Corey, E. J.; Rohde, J. J. *Tetrahedron Lett.* **1997**, *38*, 37.

(16) Alkorta, I.; Rozas, I.; Elguero, J. *Chem. Soc. Rev.* **1998**, *27*, 163.

(17) Mackey, M. D.; Goodman, J. M. *Chem. Commun.* **1997**, *24*, 2388; Goodman, J. M. *Tetrahedron Lett.* **1992**, *33*, 7219; Gung, B. W. *Tetrahedron Lett.* **1991**, *32*, 2867; Gung, B. W.; Wolf, M. A. *J. Org. Chem.* **1992**, *57*, 1370; Gung, B. W.; Xue, X.; Roush, W. R. *J. Am. Chem. Soc.* **2002**, *124*, 10692.

(18) Saunders, W.; Laidig, K. E.; Wolfsberg, M. *J. Am. Chem. Soc.* **1989**, *111*, 8989.

(19) Bigeleisen, J.; Mayer, M. G. *J. Chem. Phys.* **1947**, *15*, 261; Wolfsberg, M.; Hout, R. F.; Hehre, W. *J. Am. Chem. Soc.* **1980**, *102*, 3296.

(20) Glassstone, S.; Laidler, K. J.; Eyring, H. *The Theory of Rate Processes*; McGraw-Hill: New York, 1941.

(21) *Gaussian 98* (Revision A.9), Frisch, M. J.; Trucks, G. W.; Schlegel, H. B.; Scuseria, G. E.; Robb, M. A.; Cheeseman, J. R.; Zakrzewski, V. G.; Montgomery, J. A.; Stratmann, R. E.; Burant, J. C.; Dapprich, S.; Millam, J. M.; Daniels, A. D.; Kudin, K. N.; Strain, M. C.; Farkas, O.; Tomasi, J.; Barone, V.; Cossi, M.; Cammi, R.; Mennucci, B.; Pomelli, C.; Adamo, C.; Clifford, S.; Ochterski, J.; Peterson, G. A.; Ayala, P. Y.; Cui, Q.; Morokuma, K.; Malick, D. K.; Rabuck, A. D.; Raghavachari, K.; Foresman, J. B.; Cioslowski, J.; Ortiz, J. V.; Stefanov, B. B.; Liu, G.; Liashenko, A.; Piskorz, P.; Komaromi, I.; Gomperts, R.; Martin, R. L.; Fox, D. J.; Keith, T.; Al-Laham, M. A.; Peng, C. Y.;

Nanayakkara, A.; Gonzalez, C.; Challacombe, M.; Gill, P. M. W.; Johnson, B. G.; Chen, W.; Wong, M. W.; Andres, J. L.; Head-Gordon, M.; Replogle, E. S.; Pople, J. A., Gaussian, Inc., Pittsburgh, PA, 1998.

(22) Wiest, O.; Montiel, D. C.; Houk, K. N. *J. Phys. Chem. A.* **1997**, *101*, 8378.

(23) Tomasi, J.; Persico, M. *Chem. Rev.* **1994**, *94*, 2027.

(24) Kong, S.; Evanseck, J. D. *J. Am. Chem. Soc.* **2000**, *122*, 10418.

Chapter 4

Novel transition structure interactions in boron Lewis acid catalyzed Diels-Alder reactions

A novel combination of two specific intermolecular interactions between boron Lewis acids and Diels-Alder transition structures is found to amplify *endo/exo* selectivities and accelerate the rates of reaction. The four-stereospecific transition structures of acrolein and butadiene with each of the three possible Lewis acid (BF_2OCH_3) conformers have been computed using the Becke three-parameter density functional theory with the 6-31G(d) basis set. The effect of solvent is included by explicit, continuum and discrete-continuum treatments. The first transition structure interaction is referred to as *nontraditional hydrogen bonding* (O=C–H$\cdots$X), where the Lewis acid B–OMe bond is computed to have an approximately coplanar conformational preference with the formyl group of acrolein. The distance between the formyl hydrogen and the Lewis acid oxygen

ranges from 2.27 to 2.35 Å across the stereospecific transition structures. Simultaneously, a second transition structure *through-space electrostatic interaction* between the Lewis acid and the diene is found to be important, where the Lewis acid fluorine substituent is 2.27-2.67 Å away from the nearest diene proton. To probe the strength of the two interactions, the fluorine substituents on the Lewis acid have been systematically changed to hydrogen one at a time. Without nontraditional hydrogen bonding, the activation enthalpies increase by 0.6-3.0 kcal/mol. Without the through space electrostatic interaction, the activation enthalpies increase by 1.9-2.8 kcal/mol. The two intermolecular interactions account for approximately 30% of the total activation energy reduction. In the *endo-cis* and *endo-trans* conformation, explicit complexation of the Lewis acid accounts for 6.3 and 5.1 kcal/mol drop in the gas phase activation barrier, respectively. The bulk phase effect from the solvent for *endo-cis* and *endo-trans* lowers the activation barrier an additional 3.9 and 7.2 kcal/mol, respectively. In good agreement with experiment, where an activation barrier drop of 7.6 kcal/mol is observed when $AlCl_3$ is used as the Lewis acid in benzene, an 8.6 kcal/mol activation barrier decrease is computed between the presence and absence of the BF_2OCH_3 Lewis acid catalyst in dimethyl ether. In terms of the *endo/exo* selectivity, the *endo-trans* and *endo-cis* activation enthalpies are computed to be 3.3 and 1.6 kcal/mol lower than *exo-trans* and *exo-cis* with both interactions present, respectively. Secondary kinetic isotope effects, which are used routinely to study the geometry and mechanism of organic reactions, were calculated to confirm the presence of the two novel interactions. This study emphasizes the enhanced coordination between the Lewis acid and reactants at the transition structure, which results due to the stabilizing forces resulting from nontraditional

hydrogen bonding and through-space electrostatic interactions. These results provide further insight into how Lewis acids influence chemical reactions, and should establish opportunities in the design of future asymmetric catalytic systems.

Lewis acids are known to influence strongly the rate, regio, *endo/exo*, diastereofacial and enantio selectivities of the Diels-Alder reaction.[1,2 3-5] Specifically, asymmetric catalysis using chiral Lewis acids provides a crucial tool in the enantioselective synthesis of chiral organic compounds.[5] With its well-known and powerful effects, the mechanism of enantioselective catalysis by chiral Lewis acids continues to be an actively studied area of on-going research.[4] Uncovering the differential forces between the ground and transition structures with chiral Lewis acids is a perquisite step towards the creation of more effective enantioselective catalysts. Our efforts focus upon a novel combination of two specific intermolecular interactions between boron Lewis acids and Diels-Alder transition structures. The interactions are referred to as nontraditional hydrogen bonding (O=C–H···X) and the through-space electrostatic interaction, as illustrated below.

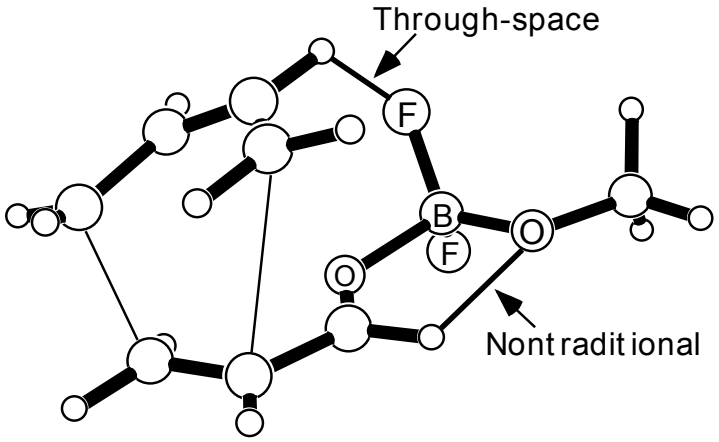

Figure 4.1. *Illustration of two enhanced transition structure interactions between the Lewis acid and reacting organic partners.*

An understanding of the origin of Diels-Alder selectivities and stereochemical preferences has been recently reported by preferred ground state conformations of the Lewis acid-carbonyl complexes and their relative energies and steric requirements in the transition structure.[1,6-8] In X-ray crystallographic studies of α, β-unsaturated aldehyde

complexes with fluorine and alkyl ether containing boron Lewis acids, E. J. Corey and coworkers found a conformational preference in which the formyl group and the B–F or B–O bond are coplanar.[7,8] It has been proposed that this conformational preference is due to an electrostatic interaction, known as nontraditional (O=C–H···X) hydrogen bonding.[7,9] Although the hydrogen atom in the formyl group usually lacks the electrophilicity required for hydrogen bonding, it is greatly enhanced when coordinated to the boron Lewis acid. In addition, the coordination enhances the nucleophilicity of the heteroatom, which acts as the hydrogen bond acceptor. This working hypothesis, based solely upon the ground state conformation, has been used to rationalize the enantioselectivity of some important chiral Lewis acid-catalyzed reactions of aldehydes.[8,10]

The widespread interest in the determination of structures of Lewis acid-carbonyl compound complexes have been studied theoretically as well.[11,12] Those studies confirm a generalized anomeric effect between the uncomplexed lone pair of the carbonyl and the σ* B-F bond and confirm an interaction between F and the hydrogen off the alkyl group nearest to it.[11] Although the formyl proton of an uncomplexed substrate normally lacks the electrophilicity required for hydrogen bonding, coordination to a Lewis acid greatly enhances the positive charge at the formyl hydrogen while increasing the electron density at the oxygen or fluorine atoms attached to boron.[6] Despite its predictive power, originating from ground state conformations, the hypothesis neglects the impact of significant interactions between the Lewis acid and organic partners that could develop at the transition structure.

Compared to the huge amount of experimental work available on Lewis acid catalyzed Diels-Alder reactions, only a few theoretical assessments have been made to

understand the origin of the catalytic effect.[13-17] The theoretical and computational efforts have been recently reviewed.[14] The predominant frontier orbital interaction in Diels-Alder reactions involves reactions of electron-rich dienes and electron-deficient dienophiles. Controlled by the diene HOMO and dienophile LUMO, increased regioselectivity and rate accelerations are facilitated by Lewis acid complexation, which lowers the dienophile LUMO energy to a large extent.[17] García and coworkers reproduced the normal one-step reaction using second-order Møller-Plesset theory with the 6-31G(d) basis set, demonstrating the importance of electron correlation in describing the Diels-Alder reaction.[18] In addition, the BF_3 catalyzed Diels-Alder reaction has been studied by García using density functional theory.[15] Specifically, the B3LYP was used with the 6-31G(d) basis set to compute the activation parameters of butadiene plus acrolein.[14,15] The computed activation energies were close to those found experimentally.[19]

Yamabe has recently demonstrated that a solvent molecule must be considered explicitly to reduce the overestimated catalytic strength a Lewis acid, such as BF_3 or $AlCl_3$ in the gas phase.[20] In their study, an explicit ether molecule was included in the calculations to take into account the $BF_3 \cdot OEt_2$ interaction imposed by the ether solvent. Solvent has also been looked at with QM/MM simulations of Diels-Alder reactions in water.[21] In our recent report on the cycloaddition of acrolein and butadiene in water, the effect of solvent on the activation energies and *endo/exo* selectivity observed by experiment was computed accurately only when the discrete-continuum model approximated solvation forces.[14] We found that the inclusion of two explicit water molecules accounted for roughly 50% of the rate and *endo/exo* selectivity enhancements

observed by experiment. Consequently, we have adopted the strategy of using the polarizable continuum model (PCM), explicit definition of a single ether molecule, and the combined strategy of the discrete-continuum model to understand how solvent and Lewis acids impact chemical reactivity.

Given the synthetic importance and limited understanding of Lewis acid effects on Diels-Alder reactions, it is important to further investigate the transition structure interactions, which impact its rate and selectivity. Density functional theory is used to include the effects of electron correlation in determining the transition structures, while the local and bulk influence of solvent is simultaneously included by continuum, explicit, and combined discrete-continuum models to describe accurately the effect of solvent and the Lewis acid on the Diels-Alder reaction. As a result of the greatly enhanced Lewis acid coordination at the transition state, new insight into the Lewis acid intermolecular interactions that influence the reaction path, energetics and selectivities are directly computed by a combined density functional theory and PCM treatment.

4.1 Geometries of the Ground States

The three possible ground state conformations of the BF_2OCH_3 Lewis acid with *trans*-acrolein are shown in Scheme 4.1. The conformations are determined by the boron atom coordination to the carbonyl oxygen lone pair *syn* to the formyl proton, and an eclipsing B–X bond (X = F or OMe) directed in-plane towards the formyl proton.

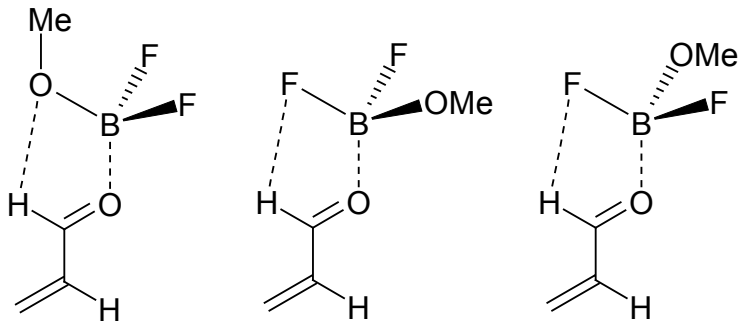

1 **2** **3**

Scheme 4.1. *Three ground state conformations the BF_2OCH_3 Lewis acid with trans-acrolein.*

Conformations **2** and **3** have a fluoro atom coplanar with the formyl proton, and are computed to be local minima. Consistent with the proposed formyl C–H···X nontraditional hydrogen bonds in the complexes of Lewis acids and aldehydes,[6-9] our calculations show that the formyl group and the B–F bond are coplanar, and the distance between F and formyl hydrogen is 2.41 Å, considerably shorter than the sum of the van der Waals radii, 2.67 Å. A stationary point for conformation **1**, where the Lewis acid oxygen is coplanar with the formyl hydrogen, could not be located. Symmetry constrained systems resulted with imaginary frequencies after vibrational analysis. The coordination of BF_2OCH_3 to acrolein is weak, indicated by the distance B···O of 2.36 Å, and an energy of interaction of 4.5 kcal/mol.

The change of F to OCH_3, from BF_3 to BF_2OCH_3, significantly lengthens the distance of B—O, since the calculated B—O distance in BF_3 and *trans*-acrolein complex is 1.61 Å. The strengthening of the bond can be rationalized by the fact that O is less electronegative, and as a result, the boro atom in BF_2OCH_3 is less positively charged than in BF_3, which may be one reason why it results in a weaker interaction with the partially negatively charged acrolein carbonyl oxygen. It is interesting that the conformer which

B—O is coplanar with C—H is not a local minimum. This geometry changes to the B—F coplanar with C—H conformer during optimization process.

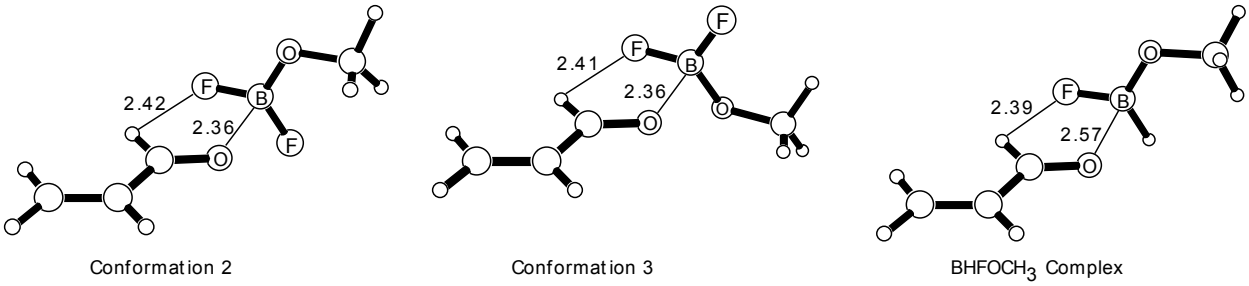

Figure 4.2. *Structures of trans-acrolein complexed with BF_2OCH_3 and $BHFOCH_3$*

The lowest energy *trans*-acrolein and $BHFOCH_3$ complex has been located as shown in Figure 4.2. As expected, the distance between B—O 2.57 Å is 0.21 Å longer than that in the BF_2OCH_3 complex. Interestingly, the hydrogen bond distance is 2.39 Å, 0.02 Å shorter than in the BF_2OCH_3 complex.

To confirm the validity of B3LYP/6-31G(d) theory we have used in the computations, we have reproduced the same results by adding defusing function at B3LYP/6-31+G(d) level of theory, and using MP2/6-31G(d) level of theory. In both cases, conformer 1 does not exist, and only conformers with B—F and C—H coplanar can be located. The distances of B—O are so long (2.43 Å for B3LYP/6-31+G(d) and 2.31 Å MP2/6-31G(d)) that the B has nearly planar configuration. It is consistent with Corey's unusual hydrogen bonding theory between formyl hydrogen and F on Lewis acid.[7] Since F is a better electron donor than O, when both are present, only the conformers with C—H···F hydrogen bonding are true energy minimum.

4.2 Geometries of the Transition Structures

A greatly enhanced coordination of BF_2OCH_3 to its organic partners is computed as the reaction path is advanced, where the B···O=C distance decreases from 2.36 Å in the ground state complex to *ca.* 1.60 Å in the transition structures. The significant change in the boron atom's hybridization, geometry and interaction strength at the transition structure allows for the unique creation of the two additional interaction sites. Four possible reaction pathways are possible for the Diels-Alder reaction between acrolein and *s-cis* butadiene. Consistent with previous conventions,[15,22] the transition structures are denoted as NC (*endo*, *s-cis* acrolein), XC (*exo*, *s-cis* acrolein), NT (*endo*, *s-trans* acrolein) and XT (*exo*, *s-trans* acrolein).[15,22] Corresponding to the three conformation of Lewis acid complexation, there are totally twelve transition structures that have been studied.

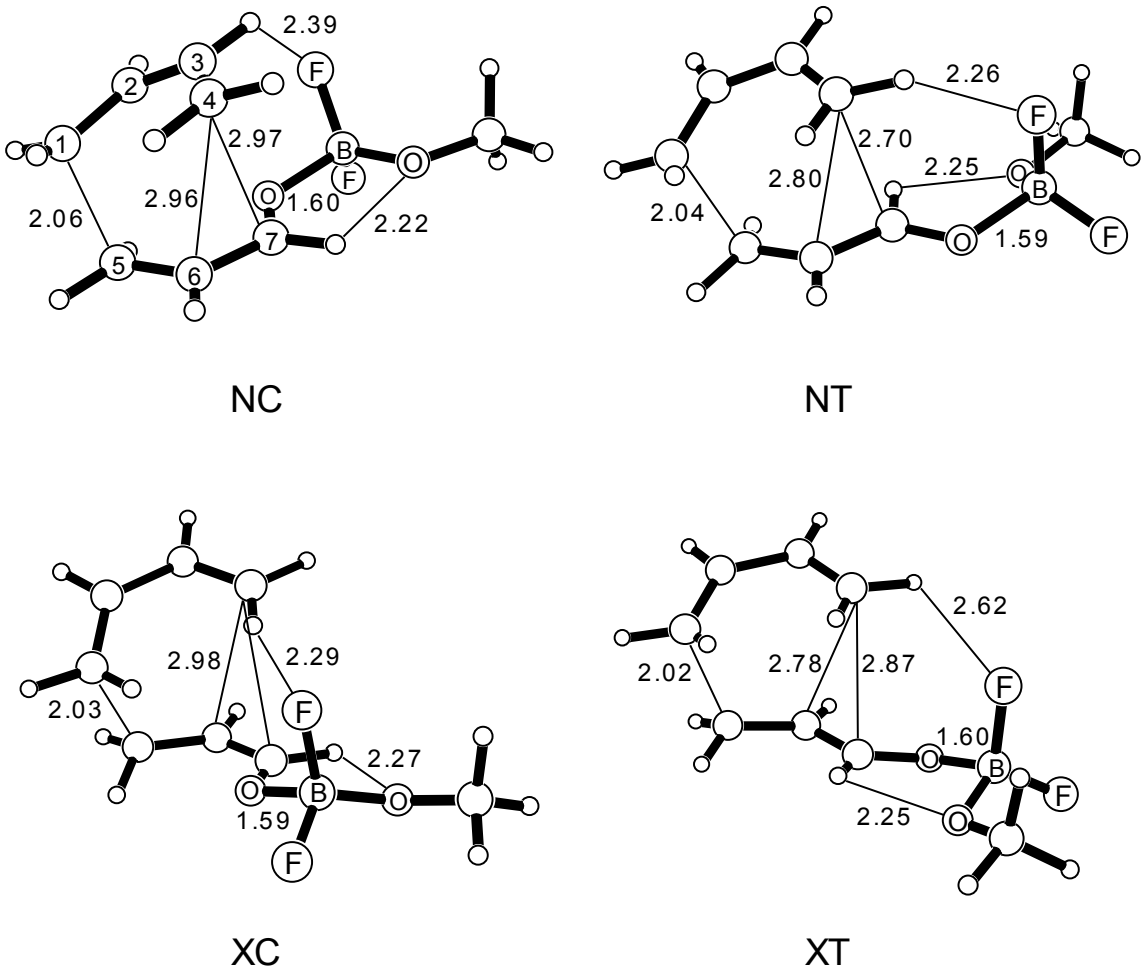

Figure 4.3. *Transition structures of BF_2OCH_3 catalyzed Diels-Alder reaction between butadiene and acrolein (conformation 1).*

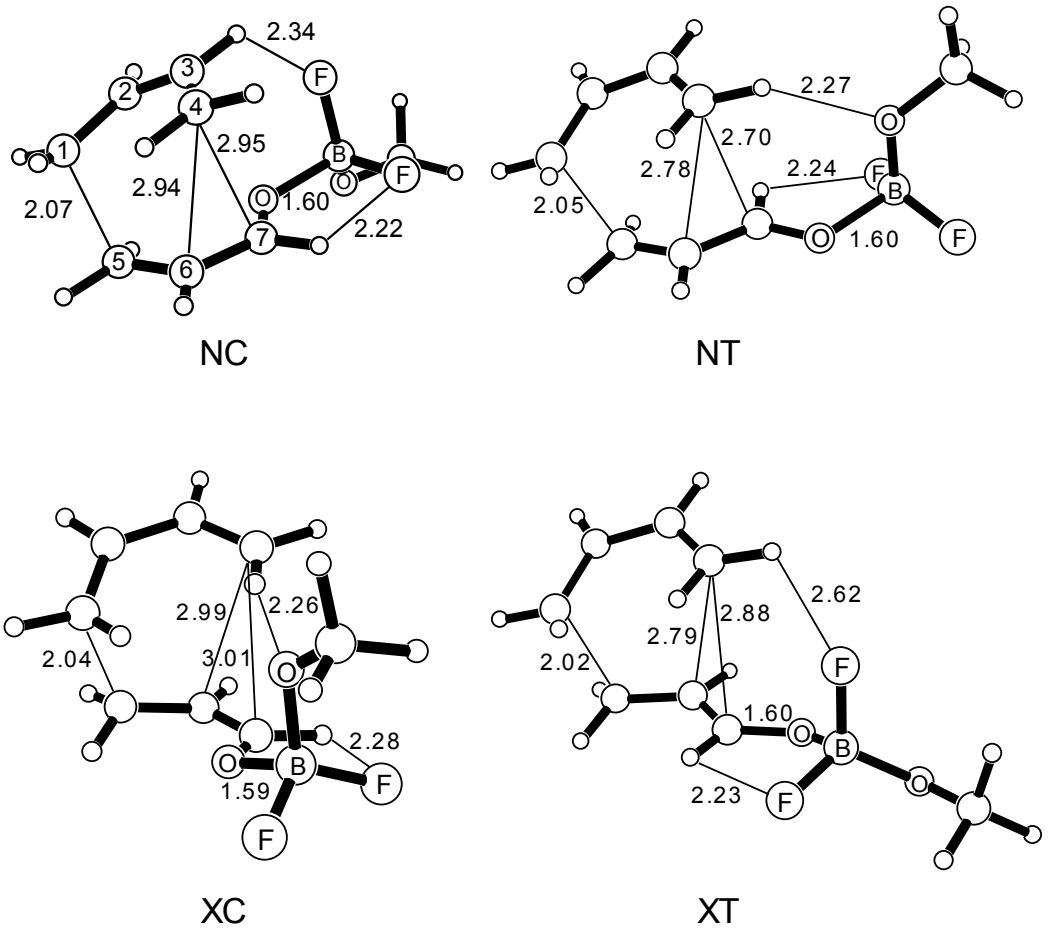

Figure 4.4. *Transition structures of BF_2OCH_3 catalyzed Diels-Alder reaction between butadiene and acrolein (conformation 2).*

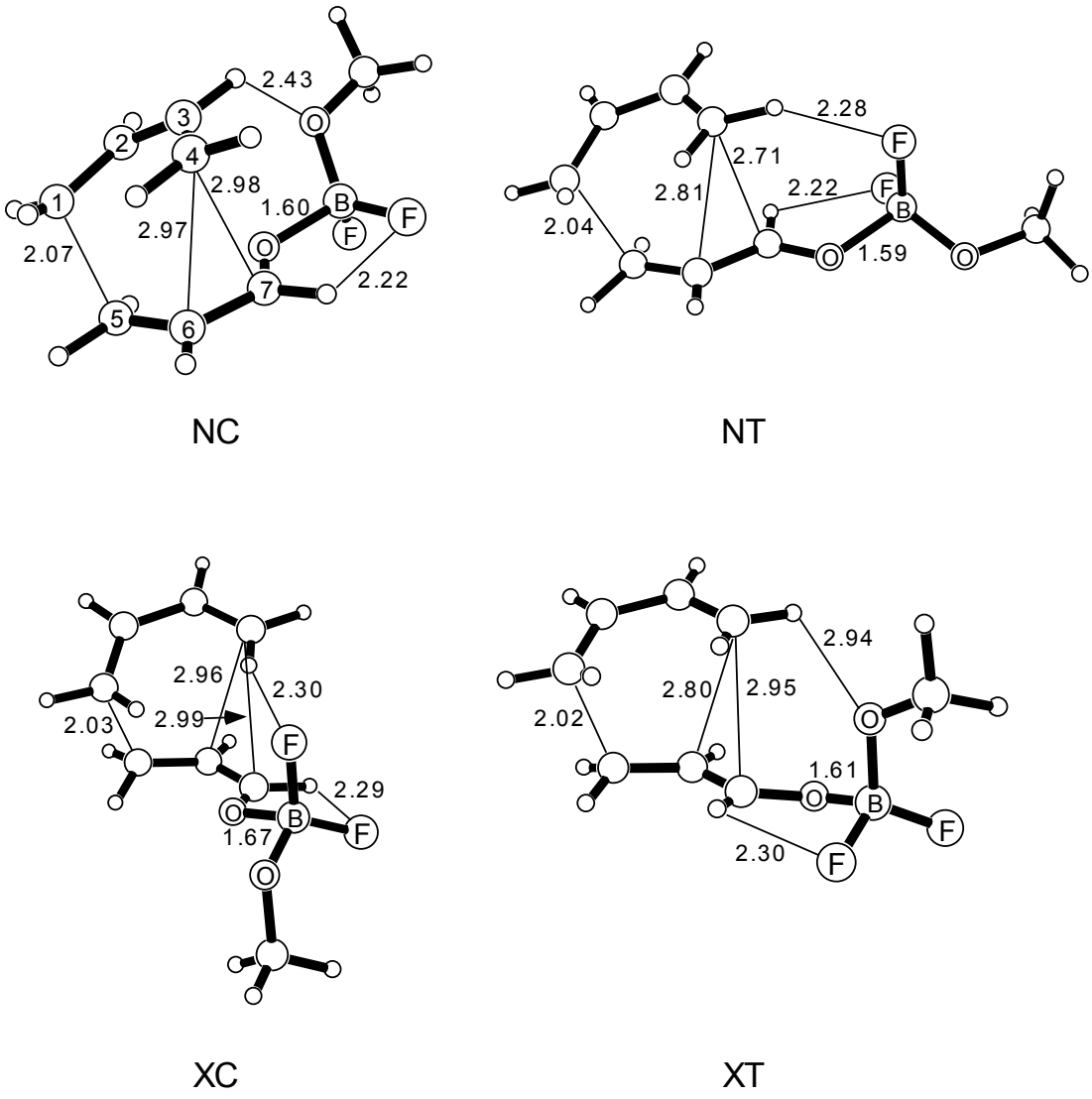

Figure 4.5. *Transition structures of BF_2OCH_3 catalyzed Diels-Alder reaction between butadiene and acrolein (conformation 3).*

To study the interactions that the F's may participate in, and their effect on the enhancement of rate and *endo* selectivity, it was necessary to probe the strength of the nontraditional hydrogen bonding and the through-space interaction. This was accomplished by systematically changing the fluorine substituents on the Lewis acid, BF_2OCH_3, to hydrogen one at a time. We have located the four stereospecific transition structures for conformation 1 with a change of one fluorine in the Lewis acid to a hydrogen. Three different conformations were obtained for each TS, where 1) The F changed to H does not participate in either the nontraditional hydrogen bond or the through space interaction, denoted H_{back}. This determines the strength of a F atom in its ability to lower the energy of the system. 2) The F changed to H participated in the through space interaction. This is denoted as H_{up}. 3) The F changed to H is now located where the O participated in the nontraditional hydrogen bond. This conformation is denoted as H_{down}.

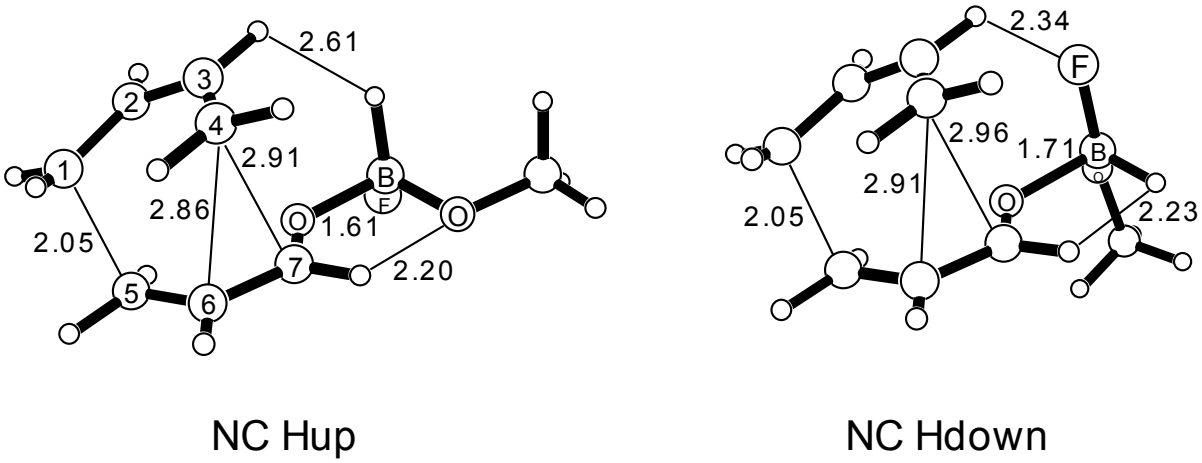

Figure 4.6. *Endo-cis transition structures of BHFOCH3 catalyzed Diels-Alder reaction between butadiene and acrolein (conformation 1).*

The important bond lengths of the calculated TS's with BF_2OCH_3 as catalyst are shown in Figures 4.3, 4.4 and 4.5. Although conformation 1 of the ground state structure does not exist, its corresponding four TS have been located, and give the lowest activation energy of all. The distances of B—O in TS are substantially shorter than in the GS, which are in the order of 1.59-1.61 Å with the exception of 1.67 Å in XC conformation 3, compared to 2.36 Å in the GS. The stronger complexation results in shorter C—H···X distances, which are *ca.* 2.2-2.3 Å, indicating stronger hydrogen bonding in the TS. The properties in the TS has made the Lewis acid combine stronger and thus is attributed the rate acceleration and stereoselectivity enhancement. In particular, an induced charge separation across the dienophile double bond could possibly cause significant stronger stabilization of the transition structure by the Lewis acid. As shown in Scheme 4.2, the CHELPG charges of the uncatalyzed TS show an enhanced charge distribution, particularly the increased positive charge on the C_2 of the diene, and the negative charge build-up on C_6 and O_8 of the dienophile fragments are consistent with earlier comparisons of the charges from the allyl cation with butadiene, and the enolate anion with acrolein.[22] The negative charge increase on carbonyl oxygen from –0.44 in *trans*-acrolein to –0.48 in the TS may contribute to the greater complexation with the Lewis acid.

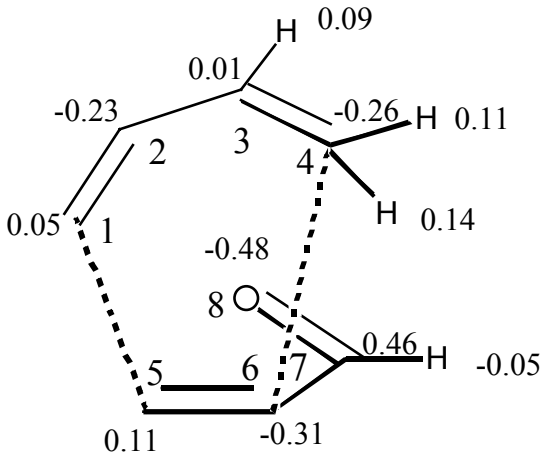

Scheme 4.2. *Atomic charges in the NC transition structure given from the vacuum.*

Apart from the increase charge separation in the TS, we have discovered another nontraditional C—H···X (X = F, O) interaction in the TS between the X atom in the Lewis acid and the butadiene hydrogens which contribute to the stronger complexation of Lewis acid and the TS. Although the C—H protons of butadiene lacks the electrophilicity required for hydrogen bonding to oxygen, the positive charge at these protons are greatly enhanced in the TS. As shown in Scheme 4.2, the butadiene protons involved in the newly discovered unusual hydrogen bonding has much high acidity (0.09-0.14) than the formyl proton (-0.05) which is the hydrogen donor in Corey's hydrogen bonding. The distances of F and H involved in the interactions are shown in Figures 4.3, 4.4 and 4.5, most of which are significantly shorter than the sum of van de Waals radii.

The geometry and important parameters are shown in Figures 4.3-4.5. B—O distances are 1.61 to 1.70 Å in the TS compared to the 2.57 Å in the GS. The distances between F and butadiene H indicate the existence of an electrostatic through space H bonding interaction and the distance between the ester oxygen and the acrolein H shows the nontraditional hydrogen bonding. To support this idea, the CHELPG charges are

compared between the corresponding H_{up} and H_{down} transition structures using the BF_2OCH_3 and $BHFOCH_3$ catalysts. Specifically, the charges on the carbonyl oxygen, the B atom, the acrolein H and the H substituted for the ester oxygen in the $BHFOCH_3$ catalyst in the NC structure for H_{down} are –0.27, 0.58, 0.02 and –0.23. This weakens the nontraditional hydrogen bond when compared to values of the acrolein H and ester oxygen in the BF_2OCH_3 , of 0.19 and –0.52. For the H_{up} transition structure, the charges on the carbonyl oxygen, the B atom, the butadiene H and the H substituted for the F atom are –0.29, 0.54, 0.18 and –0.22. Comparing them to the full catalyst, BF_2OCH_3, the through space electrostatic interaction is also weakened from the values of 0.19 and –0.33, which gives a stronger attraction. In both cases of H_{up} and H_{down}, the B—O distance lengthen in the BF_2OCH_3 catalyzed transition structure, which is in accordance to a weaker charges on the atoms, where the carbonyl oxygen and F atom have values of –0.31 and 0.65 in the full BF_2OCH_3 catalyst.

4.3 Kinetic Isotope Effects

In a recent combined experimental and computational study of isotope effects for Lewis acid catalyzed Diels-Alder reactions, Singleton and Houk demonstrated that the reaction of isoprene with acrolein with a $AlMe_2Cl$ Lewis acid catalyst follows a normal electron demand concerted [4 + 2] cycloaddition with increased asynchronicity.[16] In addition, the *endo-cis* transition structure for this reaction with the Lewis acid catalyst was located using B3LYP with the 6-31G(d) basis set. In the computed transition structure, the chlorine atom was only 2.87 Å from the nearest butadiene proton, suggesting nontrivial energy of interaction. However, the experimental kinetic isotope

effects did not show the specific interaction, and was discounted as an artifact of gas phase computations, which did not occur in solution. There are significant differences between the $AlMe_2Cl$ catalyst and the one employed here, which underscores the importance of bidentate binding at the transition structure. Foremost, the $AlMe_2Cl$ catalyst can acquire only one of the two postulated positions to stabilize the transition structure. We have computed both transition structures for this system in a recent publication, and found that the through space interaction transition structure is favored by 0.38 kcal/mol in vacuum.[13] Including the effect of solvent realigns the computational results with experiment, switching the preferred reaction path from that computed in vacuum. Comparison of the earlier kinetic isotope effect data with our new transition structure data reaffirms the ability of theory and experiment to probe the mechanism and transition structure geometry of organic reactions.[13]

Secondary kinetic isotope effects were calculated for the four stereospecific transition structures catalyzed with BF_2OCH_3 and $BHFOCH_3$ for conformation 1. In each case, the KIEs confirmed the presence of the through space and nontraditional electrostatic bonds. For the NC transition structure catalyzed with BF_2OCH_3, a strong inverse effect of 0.929 was calculated at H3, which is consistent with crowding of the butadiene hydrogen with the F atom or the through space interaction. When the KIEs were calculated with the $BHFOCH_3$ catalyst in the H_{up} position, which should diminish the through space interaction by replacing the F atom with a hydrogen, the value at H3 increased to 0.967 confirming a weakened interaction. A strong inverse effect of 0.843 was also seen at H7, which is consistent with the crowding of the acrolein hydrogen with the methoxy group or the nontraditional hydrogen bond. Similar results are seen for the

other transition structure conformations, NT, XC and XT in Tables 4.1 and 4.2, confirming the existence of the through space and nontraditional interactions in each system.

Table 4.1a. *Calculated KIEs (k_H/k_D or k_{12C}/k_{13C}) for the BF_2OCH_3 catalyzed reaction between 1,3-butadiene and acrolein, conformation 1, computed and scaled at the B3LYP/6-31G(d) level of theory.*

	NC	NT	XC	XT
C1	1.034	1.032	1.032	1.032
C2	1.001	1.001	1.001	1.001
C3	0.999	1.001	1.001	1.001
C4	1.004	1.006	1.005	1.006
H3	0.929	0.982	0.990	0.991
H4out	0.990	0.925	0.987	0.947
H4in	0.965	0.951	0.892	0.961

Table 4.1b. *Calculated KIEs (k_H/k_D or k_{12C}/k_{13C}) for the $BFHOCH_3$ catalyzed reaction between 1,3-butadiene and acrolein, conformation 1, computed and scaled at the B3LYP/6-31G(d) level of theory.*

	NC	NT	XC	XT
C1	1.033	1.032	1.032	1.032
C2	1.001	1.001	1.001	1.001
C3	0.999	1.000	1.001	1.000
C4	1.006	1.007	1.007	1.008
H3	0.967	0.981	0.989	0.992
H4out	0.989	0.952	0.988	0.987
H4in	0.962	0.958	0.912	0.946

Table 4.2a. *Calculated KIEs (k_H/k_D or k_{12C}/k_{13C}) for the BF_2OCH_3 catalyzed reaction between 1,3-butadiene and acrolein, conformation 1, computed and scaled at the B3LYP/6-31G(d) level of theory.*

	NC	NT	XC	XT
C5	1.034	1.034	1.034	1.035
C6	1.001	1.003	1.002	1.004
C7	1.000	1.000	0.999	0.999
H7	0.843	0.840	0.841	0.862
H6	0.998	1.004	0.986	0.990
H5out	0.908	0.885	0.899	0.908
H5in	0.870	0.921	0.894	0.890

Table 4.2b. *Calculated KIEs (k_H/k_D or k_{12C}/k_{13C}) for the $BFHOCH_3$ catalyzed reaction between 1,3-butadiene and acrolein, conformation 1, computed and scaled at the B3LYP/6-31G(d) level of theory.*

	NC	NT	XC	XT
C5	1.034	1.034	1.035	1.035
C6	1.003	1.003	1.003	1.004
C7	1.000	1.000	0.999	0.999
H7	0.840	0.871	0.886	0.886
H6	1.004	1.001	0.992	0.987
H5out	0.919	0.921	0.900	0.907
H5in	0.887	0.890	0.894	0.887

4.4 Energies

The computed activation energy in vacuum at the level of B3LYP/6-31G(d) level of theory has been reported[15] to be in excellent agreement with the experimental value,[19] and the use of B3LYP/6-31G(d) level of theory has been suggested to be accurate for the study of BF_3 catalyzed Diels-Alder reactions.[15] The absolute energies and thermodynamic corrections from frequency analyses at 298.15 K and 1 atm for acrolein, butadiene, BF_2OCH_3 and transition structures have been computed. The activation energies are calculated by subtracting the isolated butadiene and the coordinated acrolein and BF_2OCH_3 complex energies from the total transition structure energy. The computed activation energies, enthalpies and Gibbs energies in vacuum are presented in Table 4.3, 4.4 and 4.5 for conformation 1, 2 and 3 respectively.

Table 4.3. *Activation energies, enthalpies, and free energies (in kcal/mol) of the reaction between 1,3-butadiene and acrolein, conformation 1, in Vacuum, Lewis acid (BF_2OCH_3) and PCM.*[a]

TS	$\Delta E^{\ddagger}_{0}$[b]	$\Delta E^{\ddagger}_{298}$	$\Delta H^{\ddagger}_{298}$	$\Delta G^{\ddagger}_{298}$
		Vacuum		
NC	20.1	19.6	19.1	32.2
NT	21.4	20.9	20.3	33.5
XC	20.2	19.7	19.2	32.2
XT	22.0	21.6	21.0	34.1
		LA		
NC	14.5	13.5	12.9	28.7
NT	16.9	15.8	15.2	31.5
XC	16.3	15.2	14.6	30.4
XT	20.0	19.1	18.5	34.0
		PCM[c]		
NCP	10.61	9.59	8.99	24.73
NTP	9.74	8.63	8.04	24.35
XCP	12.17	11.16	10.56	26.33
XTP	12.89	11.92	11.33	26.85

[a] Using the B3LYP/6-31G(d) level of theory. [b] Zero-point energy included. [c] The dielectric constant of ether, 4.335, was used.

Table 4.4. *Activation energies, enthalpies, and free energies (in kcal/mol) of the reaction between 1,3-butadiene and acrolein, conformation 2, in Vacuum, Lewis acid (BF_2OCH_3) and PCM.*[a]

TS	$\Delta E^{\ddagger}_{0}$[b]	$\Delta E^{\ddagger}_{298}$	$\Delta H^{\ddagger}_{298}$	$\Delta G^{\ddagger}_{298}$
		Vacuum		
NC	20.1	19.6	19.1	32.2
NT	21.4	20.9	20.3	33.5
XC	20.2	19.7	19.2	32.2
XT	22.0	21.6	21.0	34.1
		LA		
NC	15.2	14.1	13.5	29.6
NT	16.9	15.8	15.2	31.4
XC	16.0	14.9	14.3	30.4
XT	20.8	19.8	19.2	34.9
		PCM[c]		
NCP	10.84	9.78	9.18	25.26
NTP	-	-	-	-
XCP	12.35	11.28	10.69	26.82
XTP	13.10	12.10	11.50	27.24

[a] Using the B3LYP/6-31G(d) level of theory. [b] Zero-point energy included. [c] The dielectric constant of ether, 4.335, was used.

Table 4.5. *Activation energies, enthalpies, and free energies (in kcal/mol) of the reaction between 1,3-butadiene and acrolein, conformation 3, in Vacuum, Lewis acid (BF_2OCH_3) and PCM.*[a]

TS	$\Delta E^{\ddagger}_0$[b]	$\Delta E^{\ddagger}_{298}$	$\Delta H^{\ddagger}_{298}$	$\Delta G^{\ddagger}_{298}$
		Vacuum		
NC	20.1	19.6	19.1	32.2
NT	21.4	20.9	20.3	33.5
XC	20.2	19.7	19.2	32.2
XT	22.0	21.6	21.0	34.1
		LA		
NC	14.8	13.7	13.1	29.5
NT	17.5	16.4	15.8	32.3
XC	15.9	14.9	14.3	30.3
XT	19.8	18.9	18.3	33.9
		PCM[c]		
NCP	11.18	10.09	9.50	25.82
NTP	9.81	8.68	8.09	24.56
XCP	11.71	10.73	10.14	26.11
XTP	14.46	13.49	12.90	28.47

[a] Using the B3LYP/6-31G(d) level of theory. [b] Zero-point energy included. [c] The dielectric constant of ether, 4.335, was used.

Consistent with the shorter B—O distance and thus stronger complexation in the TS, the binding energy of BF_2OCH_3 and the TS is 10.67 kcal/mol at 298.15 K, while that of BF_2OCH_3 and acrolein is 4.54 kcal/mol. The order of activation barrier is NC < XC < NT < XT, the same as uncatalyzed and BF_3 catalyzed reactions.[15] The NC activation enthalpy of 12.9 kcal/mol lies in between of uncatalyzed reaction of 19.1 kcal/mol and BF_3 catalyzed reaction of 8.7 kcal/mol. This can be explained by the less electronegative oxygen in the BF_2OCH_3, which results in its relative weakness of the Lewis acidity.

When solvation is taken into account using PCM, the order of the activation barrier changes to NT < NC < XC < XT. The NT activation enthalpy is lowered to 8.0 kcal/mol and the NC activation barrier is lowered to 9.0 kcal/mol. Whereas the Lewis acid alone accounted for about 50% of the activation barrier lowering, the inclusion of bulk phase effects plus Lewis acid now account for about 90%. The Lewis acid is necessary to induce a charge polarization of the transition structure, which the solvent can

further stabilize. The lowest energy transition structures are now NT and NC, which helps to explain the *endo* selectivity.

Compared to the calculated uncatalyzed reaction, The BF_2OCH_3 catalyzed gas phase NC activation enthalpies decrease by 6.2, 5.6 and 6.0 kcal /mol in conformation 1, 2 and 3 respectively. Conformation 1, with the B—O eclipsed with formyl C—H in the acrolein, gives the lowest energy NC. The Mulliken overlap populations from the density functional computations are given in Tables 4.6, 4.7 and 4.8 which are used to explain the relative energies of these conformations and the *endo* selectivities and the reaction as shown later.

Table 4.6. *Mulliken overlap of the 1,3-butadiene and acrolein transition structure with BF_2OCH_3 computed at the B3LYP/6-31G* level of theory in vacuum and ether PCM (Conformation 1).*

TS	NC1	NT1	XC1	XT1
		Vacuum		
3-7	.004221	.000072	-.000129	-.001262
4-7	.013166	.019910	.015462	.012590
2-8	.016517	.000072	.000367	.000043
F-H[a]	.017168	.030549	.033481	.007361
O-H[b]	.025320	.026979	.025161	.027396
		PCM		
3-7	.004181	.000848	-.000147	-.000913
4-7	.014887	.020639	.015926	.011168
2-8	.009343	.000068	.000289	.000044
F-H[a]	.020211	.029348	.029954	.005911
O-H[b]	.025652	.024743	.023590	.024107

[a] Not always the same atoms, represents through-space interaction [b]Nontraditional hydrogen bond

Table 4.7. Mulliken overlap of the 1,3-butadiene and acrolein transition structure with BF_2OCH_3 computed at the B3LYP/6-31G* level of theory in vacuum and ether PCM (Conformation 2).

TS	NC2	NT2	XC2	XT2
		Vacuum		
3-7	.004303	.000199	.000272	-.000793
4-7	.013805	.019710	.013240	.012052
2-8	.014477	.000068	.000373	.000042
Through space[a]	.020566	.036932	.038990	.007313
F-H[b]	.020364	.020342	.018285	.021656
		PCM		
3-7	.004750	-	.000317	-.000520
4-7	.014690	-	.013770	.011147
2-8	.010122	-	.000308	.000046
Through space[a]	.020658	-	.033924	.007164
F-H[b]	.020883	-	.017928	.020224

[a]Through-space interaction [b]Nontraditional hydrogen bond

Table 4.8. *Mulliken overlap of the 1,3-butadiene and acrolein transition structure with BF_2OCH_3 computed at the B3LYP/6-31G* level of theory in vacuum and ether PCM (Conformation 3).*

TS	NC4	NT4	XC4	XT4
		Vacuum		
3-7	.004375	.000304	.000004	-.000758
4-7	.013445	.020019	.014163	.009980
2-8	.015866	.000072	.000348	.000036
Through space[a]	.023083	.029894	.031981	.003217
F-H[b]	.020297	.021754	.017963	.017280
		PCM		
3-7	.004985	.001119	.000151	-.000741
4-7	.014946	.020268	.014867	.010798
2-8	.010608	.000067	.000289	.000040
Through space[a]	.022571	.028257	.030903	.005828
F-H[b]	.021089	.020717	.018961	.016764

[a]Through-space interaction [b]Nontraditional hydrogen bond

Frontier molecular orbital (FMO) theory[23,24] and the Woodward-Hoffmann rules[25] provide a theoretical framework to analyze the unusual reactivity, selectivity and asynchronicity of Diels-Alder reactions. Briefly, secondary orbital interactions are the transition structure terms that do not involve covalent bond making or breaking. From FMO theory, the diene HOMO and dienophile LUMO coefficients allow for a number of positive overlaps, or stabilizing interactions, where three of the individual secondary orbital interactions are considered. The classical secondary orbital interactions defined by Woodward and Hoffmann (C_3C_7) resulted from the FMO treatment of butadiene dimerization, denoted WH.[25] The interaction defined from independent theoretical studies of the butadiene and acrolein reaction by Salem,[24] Houk,[26] and Alston[27] (C_2O_8), is given by SAH in the discussion. Finally, Singleton proposed the [4+3] secondary orbital interactions (C_4C_7) involving bond making/breaking centers.[28]

All three terms contribute to the stability of the NC transition structures, with SAH > S43 > WH, and the former two significantly stronger than WH. Among Conformation 1, 2, and 3, the WH interaction remains essentially the same (0.0042,

0.0043, 0.0044), S43 of conformation 1 slightly weaker than the other two (0.0132, 0.0138, 0.0134), but SAH stronger than conformation 2 and 3 (0.0165, 0.0145, 0.0159), which results in a total stronger secondary orbital interactions for this particular conformation (0.0339, 0.0326, 0.0337). This subtle secondary interaction change in the transition structure correlates with the order of activation barrier of 12.9, 13.5 and 13.1 for the three NC transition structures.

The computed activation energies, enthalpies and Gibbs energies when one F atom is changed to a H, or $BHFOCH_3$ as catalyst are presented in Table 4.9. The NC activation enthalpies increased by 2.7 kcal/mol in H_{back} (value of a F atom in the catalyst), 2.3 kcal/mol in H_{up} (through space interaction) and 0.6 kcal/mol in H_{down} (nontraditional hydrogen bond).

Table 4.9. *Activation energies, enthalpies, and free energies (in kcal/mol) of the BF_2OCH_3 and $BFHOCH_3$ catalyzed reaction between 1,3-butadiene and acrolein, conformation 1, computed in vacuum at the B3LYP/6-31G* level of theory.*

TS	$\Delta E^{\ddagger}_0$	$\Delta E^{\ddagger}_{298}$	$\Delta H^{\ddagger}_{298}$	$\Delta G^{\ddagger}_{298}$
BF_2OCH_3				
NC	14.5	13.5	12.9	28.7
NT	16.9	15.8	15.2	31.5
XC	16.3	15.2	14.6	30.4
XT	20.0	19.1	18.5	34.0
H_{back}				
NC	17.4	16.2	15.6	31.8
NT	20.0	18.9	18.3	34.5
XC	18.4	17.3	16.7	32.8
XT	21.6	20.6	20.1	35.8
H_{up}				
NC	19.6	18.5	17.9	33.7
NT	21.8	20.7	20.1	36.0
XC	21.1	20.1	19.5	34.8
XT	23.6	22.6	22.0	37.2
H_{down}				
NC	17.8	16.8	16.2	32.2
NT	21.7	20.5	19.9	36.2
XC	19.1	18.1	17.5	33.2
XT	24.6	23.6	23.0	38.2

The difference in activation energies, which shows the strength of the nontraditional hydrogen bond and the through space interaction, between each of the four stereospecific conformations is shown in Table 4.10. The calculations show that in terms of activation enthalpy at 298.15 K ($\Delta\Delta H^{\ddagger}_{298}$), a F is worth 2-3 kcal/mol, the nontraditional hydrogen bond is worth 1-3 kcal/mol and the through space interaction is worth 2-3 kcal/mol in the catalyst. The increase of activation enthalpy can be rationalized by the specific interactions utilized between the different catalytic effect of BF_2OCH_3 and $BFHOCH_3$.

Table 4.10. *Difference in activation energies, enthalpies, and free energies (in kcal/mol) of the BF_2OCH_3 and $BFHOCH_3$ catalyzed reaction between 1,3-butadiene and acrolein, conformation 1, computed in vacuum at the B3LYP/6-31G* level of theory.*

TS	$\Delta\Delta E^{\ddagger}_{0}$	$\Delta\Delta E^{\ddagger}_{298}$	$\Delta\Delta H^{\ddagger}_{298}$	$\Delta\Delta G^{\ddagger}_{298}$
F interaction				
NC	2.89	2.74	2.74	3.07
NT	3.15	3.06	3.07	3.05
XC	2.08	2.12	2.13	2.40
XT	1.62	1.54	1.55	1.82
Through-space				
NC	2.20	2.27	2.27	1.97
NT	1.78	1.86	1.86	1.49
XC	2.76	2.82	2.82	1.99
XT	1.94	1.93	1.93	1.42
Nontraditional				
NC	0.45	0.56	0.56	0.39
NT	1.61	1.62	1.62	1.67
XC	0.68	0.75	0.75	0.44
XT	3.00	2.99	2.99	2.35

4.5 Asynchronicity

All the TSs correspond to a concerted, but asynchronous reaction pathway. The degree of asynchronicity promoted by solvent effects is measured by the difference in the forming bond distances, $\Delta d = (C_4C_6 - C_1C_5)$, and by the pyramidalization[29] of the four reacting carbon centers, i.e., $\Delta p_5 = (\angle C_6C_5HH - 180°)$, as summarized in Table 4.11.

Table 4.11. *Asynchronicity, Δd in Å, of the reaction between 1,3-butadiene and acrolein, conformation 1, in vacuum, Lewis acid (BF_2OCH_3) and PCM computed at the B3LYP/6-31G* level of theory.*

TS	Vacuum	LA	PCM
	Δd	Δd	Δd
NC	0.61	0.90	0.78
NT	0.44	0.76	0.81
XC	0.62	0.95	0.91
XT	0.39	0.76	0.82

It is generally accepted that asynchronicity increases in Diels-Alder transition structures result in a corresponding activation energy barrier lowering.[30] As described in our previous study,[14] the vacuum *s-trans* transition structures are computed to be more synchronous than the corresponding *s-cis* structures. The Δd are calculated as 0.61, 0.44, 0.62 and 0.39 Å in the order of NC, NT, XC and XT. Consistent with the hypothesis, NT is 1.2 kcal/mol greater in energy than NC, XT is 1.8 kcal/mol greater than XC, and XT is 0.7 greater than NT. The gas phase results follow the general guidelines and a strong relationship between gas phase activation enthalpy and asynchronicity is found in vacuum. In the case of the BF_3 catalyzed process,[15] the s-*trans* TS's are still more synchronous than their *s-cis* counterparts. The Δd has been reported as 0.89, 0.76, 0.97 and 0.78 Å in the order of NC, NT, XC, and XT TS's, and the corresponding activation

enthalpies in the same order are 8.7, 11.0, 10.4 and 14.3 kcal/mol.[15] The general rule is questioned in the presence of Lewis acid.

For BF_2OCH_3 catalyzed reaction, the trend keeps that *s-trans* TS's are more synchronous than their *s-cis* counterparts, but multiple discrepancies are observed in the relationship between asynchronicity and activation barrier. For conformation 1, Δd = 0.90, 0.76, 0.95, 0.76 for the NC, NT, XC and XT TS's, and the corresponding activation enthalpies are 12.9, 15.2, 14.6 and 18.5 kcal/mol. While XC is 0.50 Å more asynchronous than NC, it is 1.7 kcal/mol higher in energy. The empirical rule that relates the degree of synchronicity with the relative energies of the TS's is not valid in this case of BF_2OCH_3 catalyzed Diels-Alder reactions. Nevertheless, among the NC transition structures of the three conformations, the lowest energy conformation 1 corresponds to the most asynchronous TS. This trend is no longer consistent when solvent from PCM is included. The asynchronicity seen for conformation 1 is Δd = 0.78, 0.81, 0.91, 0.82 for NC, NT, XC and XT TS's respectively. The corresponding activation enthalpies are 9.0, 8.0, 10.6 and 11.3 kcal/mol. The drop in the activation barriers do not correspond to the degree of asynchronicity, since NC and NT have a higher synchronicity than their XC and XT counterparts but still have lower activation enthalpies. However, this is consistent with the Δd trend seen for the BF_3 catalyzed process, where the XC has a much larger degree of asynchronicity than NC and XT has a slightly larger value than NT.

In general, greater asynchronicity is observed in Lewis acid catalyzed reactions. Despite the fact that BF_2OCH_3 is a weaker Lewis acid than BF_3, and the activation barriers of BF_2OCH_3 catalyzed reaction are higher than those of BF_3 in gas phase, the asynchronicity of the TS in both catalyzed reactions have shown great similarity.

Frontier molecular orbital (FMO) theory has been used to rationalize the asynchronicity of Diels-Alder transition structures.[22] Briefly, the acrolein LUMO has a large coefficient on the β carbon (C_5 in this case), which makes it more electrophilic than the α carbon (C_6). Consequently, greater overlap between the β carbon and the diene HOMO leads to a stronger and shorter C_1C_5 bond at the transition structure. The computations produce a ratio of 1.7 of *s-cis* acrolein LUMO β and α carbon coefficients. When complexed with BF_2OCH_3, the ratio increases to 2.1 which explains the enhanced asynchronicity of the Lewis acid catalyzed TS. Despite the enhanced asynchronicity, extensive searches have not produced lower energy intermediates that would indicate a change from a concerted mechanism.

Table 4.12. *Asynchronicity, Δd in Å, of the reaction between 1,3-butadiene and acrolein, conformation 1, with the Lewis acid, $BHFOCH_3$, at the B3LYP/6-31G* level of theory.*

TS	H_{up}	H_{down}	H_{back}
	Δd	Δd	Δd
NC	0.82	0.87	0.94
NT	0.72	0.75	0.75
XC	0.84	0.93	0.91
XT	0.66	0.78	0.71

In the transition structures of $BHFOCH_3$ catalyzed reaction, the computed Δd's for the H_{up} TS's are 0.82, 0.72, 0.84 and 0.66 and for H_{down} are 0.87, 0.75, 0.93 and 0.78 Å for the NC, NT, XC and XT (conformation 1), are shown in Table 4.12. The results once again confirmed that the general rule of more asynchronicity of the TS corresponds to lower energy does not work for Lewis acid catalyzed reactions.

4.6 *Endo/Exo* Selectivity

The *s-trans* transition structure is known to be more *endo* selective than the *s-cis* transition structures for acrolein and butadiene[15] and other Diels-Alder reactions[31,32] The calculated gas phase *endo* selectivities based upon the activation enthalpies are 0.1 kcal/mol (*s-cis*) and 0.7 kcal/mol (*s-trans*). In the case of BF_3 catalyzed reaction, the *endo* selectivities increased to 1.7 kcal/mol (*s-cis*) and 3.3 kcal/mol (*s-trans*). In our BF_2OCH_3 catalyzed system, we have observed *endo* selectivities of 1.7 kcal/mol (*s-cis*), 3.3 kcal/mol (*s-trans*) for conformation 1, which are identical to the BF_3 catalyzed reaction. When PCM solvent is included for our BF_2OCH_3 catalyzed system, the *endo* selectivities are 1.6 kcal/mol (*s-cis*) and 3.3 kcal/mol (*s-trans*) for conformation 1, once again similar to the BF_3 system. For conformations 2 and 3, the results are 0.8 kcal/mol (*s-cis*), 4.0 kcal/mol (*s-trans*) and 1.2 kcal/mol (*s-cis*), 2.5 kcal/mol (*s-trans*), respectively.

With a F changed to a H in the Lewis acid, $BHFOCH_3$ catalyzed *s-cis* reaction pathway, an *endo* selectivity of 1.6 kcal/mol and 1.3 kcal/mol are observed in H_{up} and H_{down} conformations, which is respectively 0.1 kcal/mol and 0.1 kcal/mol lower than the BF_2OCH_3 catalyzed reaction. The data suggests that with a change of bottom F to H, the *endo* selectivity decreases, but by keeping the F which interact with the butadiene proton, the *endo* selectivity keeps about the same. The *s-trans* reaction pathway *endo* selectivity of 1.9 kcal/mol and 3.1 kcal/mol observed for the H_{up} and H_{down} conformations are 0.2 kcal/mol and 0.2 kcal/mol lower than the BF_2OCH_3 catalyzed reaction.

The more *endo* selectivity of *s-trans* TS's has generally been explained by the particular instability of the XT TS.[31] The XT's in all of the three conformations have particularly higher energies than other TS's. Compared to the lowest energy NC's, the

XT's in conformation 1, 2, and 3 have energies which are higher by 5.6, 5.7, and 5.2 kcal/mol.

The Mulliken overlap populations in Tables 4.6-4.8 have been used to understand the *endo* selectivities of this reaction. In our previous calculations for the uncatalyzed reaction, it is clear that all three secondary orbital interactions contribute to the NC enhanced stability. The SAH term is found to dominate the secondary orbital interactions (0.009), as compared to S43 (0.003) and WH (0.002). Summed together, the total secondary overlap from the gas phase Mulliken population is 0.014 for NC. For each of the other transition structures, the Mulliken overlap terms become insignificant or repulsive, except for the S43 interaction. The XC, NT and XT transition structures have 0.002, 0.006 and 0.002 S43 Mulliken population overlaps, respectively, which are roughly an order of magnitude less than the combined terms of NC. Consequently, all three possible secondary orbital interactions contribute to the total Mulliken population overlap of the NC transition structure, while only the S43 impacts the other transition structures. Therefore, this explanation of *endo* selectivity is consistent with the original rule[33] of "maximum accumulation of unsaturation."

In the BF_2OCH_3 catalyzed reaction, consistent with the uncatalyzed reaction, the NC is the only one that benefits from all three terms of secondary orbital interaction, with SAH and S43 significant higher than WH. For NT, XC and XT, except for the S43 interaction, the other two Mulliken overlap terms become insignificant or repulsive. The contrasting of the results from uncatalyzed and catalyzed reaction provides interesting insights. WH increases by 0.0022 in NC while remains insignificant in XC. While WH moves from slightly repulsive (-0.002) to zero in NT, it changes from slightly positive

(0.001) to repulsive (-0.001) in XT. Only in NC there is a significant increase of 0.008 for SAH, and others remain insignificant. In all the transition structures, there is significant increase of S43 term. It increases by 0.010, 0.017, 0.012 and 0.010 for NC, NT, XC and XT, respectively. In conclusion, the increase of S43 contributes to the lowering of activation barriers and the change of WH and SAH secondary orbital interactions contributes to the enhanced *endo* selectivity in the Lewis acid catalyzed Diels-Alder reaction.

4.7 Conclusion

The effect of Lewis acid on the activation energies and *endo/exo* selectivity on the four transition structures of the butadiene and acrolein Diels-Alder has been studied with density functional theory. Consistent with the proposed hydrogen bonding between formyl C—H and the heteroatom in the catalyst, all possible conformers with eclipsed B—F or B—O and formyl C—H have been located for the GS as well as the TS. A total of twelve TS have been located for all three possible conformers. A greatly enhanced coordination of BF_2OCH_3 to acrolein has been observed in the TS. The B—O distance is shorter by *ca.* 0.76 Å in the TS-BF_2OCH_3 complexes. While the conformation where B—O is coplanar with the C—H can not be located as a local minimum in the GS, the corresponding NC transition structure gives the lowest activation energy. The specific TS properties and a new unusual C—H···X (X=F, O) hydrogen bond between X in the Lewis acid and the butadiene protons has been discovered to contribute to greater complexation and the resulting rate enhancement and stereoselectivities of the Diels-Alder reaction.

4.8 References

(1) Corey, E. J. *Angew. Chem. Int. Ed.* **2002**, *41*, 1650.

(2) Ryu, D. H.; Lee, T. W.; Corey, E. J. *J. Am. Chem. Soc.* **2002**, *124*, 9992.

(3) Matthias, B.; Corey, E. J. *Org. Lett.* **2001**, *3*, 1559; Otto, S.; Engberts, J. *Pure and Applied Chemistry* **2000**, *72*, 1365; Fringuelli, F.; Piermatti, O.; Pizzo, F.; Vaccaro, L. *Euro. J. Org. Chem.* **2001**, *3*, 439; Dalko, P. I.; Moisan, L. *Angew. Chem. Int. Ed.* **2001**, *40*, 3726; Ishihara, K.; Yamamoto, H. *Cattech* **1997**, *1*, 51; Ghosez, L. *Pure Appl. Chem.* **1996**, *68*, 15; Oh, T.; Reilly, M. *Org. Prep. Proced. Int.* **1994**, *26*, 129; Oppolzer, W. In *Comprehensive Organic Synthesis*; Trost, B. M., Ed.; Pergamon Press: Oxford, 1991; Vol. 5, p 315; Weinreb, S. M. In *Comprehensive Organic Synthesis*; Trost, B. M., Ed.; Pergamon Press: Oxford, 1991; Vol. 5, p 401; Boger, D. L. In *Comprehensive Organic Synthesis*; Trost, B. M., Ed.; Pergamon Press: Oxford, 1991; Vol. 5, p 451; Roush, W. R. In *Comprehensive Organic Synthesis*; Trost, B. M., Ed.; Pergamon Press: Oxford, 1991; Vol. 5, p 513; Sweger, R. W.; Czarnik, A. W. In *Comprehensive Organic Synthesis*; Trost, B. M., Ed.; Pergamon Press: Oxford, 1991; Vol. 5, p 551; Carruthers, W. *Cycloaddition Reactions in Organic Synthesis*; Pergamon Press: New York, 1990; Fringuelli, F.; Tatichi, A. *Dienes in the Diels-Alder reaction*; Wiley: New York, 1990.

(4) Evans, D. A.; Johnson, J. S. *Compr. Asymmetric Catal. I-III* **1999**, *3*, 1177.

(5) Dias, L. C. *Journal of the Brazilian Chemical Society* **1997**, *8*, 289.

(6) Corey, E. J.; Lee, T. W. *Chem. Commun.* **2001**, *15*, 1321.

(7) Corey, E. J.; Rohde, J. J.; Fischer, A.; Azimioara, M. D. *Tetrahedron Lett.* **1997**, *38*, 33.

(8) Corey, E. J.; Rohde, J. J. *Tetrahedron Lett.* **1997**, *38*, 37; Corey, E. J.; Barnes-Seeman, D.; Lee, T. W. *Tetrahedron Lett.* **1997**, *38*, 1699; Corey, E. J.; Barnes-Seeman, D.; Lee, T. W. *Tetrahedron Lett.* **1997**, *38*, 4351.

(9) Alkorta, I.; Elguero, J. *Chem. Soc. Rev.* **1998**, *27*, 163.

(10) Ishihara, K.; Gao, Q.; Yamamoto, H. *J. Am. Chem. Soc.* **1993**, *115*, 10412.

(11) Mackey, M. D.; Goodman, J. M. *Chem. Commun.* **1997**, *24*, 2388; Goodman, J. M. *Tetrahedron Lett.* **1992**, *33*, 7219.

(12) Gung, B. W. *Tetrahedron Lett.* **1991**, *32*, 2867; Gung, B. W.; Wolf, M. A. *J. Org. Chem.* **1992**, *57*, 1370.

(13) Acevedo, O.; Evanseck, J. D. *Org. Lett.* **2003**, *(in press)*.

(14) Kong, S.; Evanseck, J. D. *J. Am. Chem. Soc.* **2000**, *122*, 10418.

(15) García, J. I.; Martinez-Merino, V.; Mayoral, J. A.; Salvatella, L. *J. Am. Chem. Soc.* **1998**, *120*, 2415.

(16) Singleton, D. A.; Merrigan, S. R.; Beno, B. R.; Houk, K. N. *Tetrahedron Lett.* **1999**, *40*, 5817.

(17) Houk, K. N.; Strozier, R. W. *J. Am. Chem. Soc.* **1973**, *95*, 4094.

(18) García, J. I.; Mayoral, J. A.; Salvatella, L. *J. Am. Chem. Soc.* **1996**, *118*, 11680.

(19) Kistiakowaki, G. B.; Lacher, J. R. *J. Am. Chem. Soc.* **1936**, *58*, 123.

(20) Yamabe, S.; Minato, T. *J. Org. Chem.* **2000**, *65*, 1830.

(21) Chandrasekhar, J.; Shariffskul, S.; Jorgensen, W. L. *J. Phys. Chem. B* **2002**, *106*, 8078.

(22) Birney, D. M.; Houk, K. N. *J. Am. Chem. Soc.* **1990**, *112*, 4127.

(23) Fukui, K. *Acc. Chem. Res.* **1971**, *4*, 57; Salem, L. *J. Am. Chem. Soc.* **1968**, *90*, 543.

(24) Salem, L. *J. Am. Chem. Soc.* **1968**, *90*, 553.

(25) Woodward, R. B. H., R. *The Conservation of Orbital Symmetry*; VCH: Weinheim, 1985.

(26) Houk, K. N. *Tetrahedron Lett.* **1970**, 2621.

(27) Alston, P. V.; Ottenbrite, R. M.; Cohen, T. *J. Org. Chem.* **1978**, *43*, 1864.

(28) Singleton, D. A. *J. Am. Chem. Soc.* **1992**, *114*, 6563.

(29) Haddon, R. C. *Acc. Chem. Res.* **1988**, *21*, 243.

(30) Jorgensen, W. L.; Lim, D.; Blake, J. F. *J. Am. Chem. Soc.* **1993**, *115*, 2936; Sodupe, M.; Rios, R.; Branchadell, B.; Nicholas, T.; Oliva, A.; Dannenberg, J. J. *J. Am. Chem. Soc.* **1997**, *119*, 4232.

(31) Ruiz-López, M. F.; Assfeld, X.; García, J. I.; Mayoral, J. A.; Salvatella, L. *J. Am. Chem. Soc.* **1993**, *115*, 8780; Jorgensen, W. L.; Blake, J. F.; Lim, D.; Severance, D. L. *J. Chem. Soc., Farady Trans.* **1994**, *90*, 1727.

(32) García, J. I.; Mayoral, J. A.; Salvatella, L. *Tetrahedron* **1997**, *53*, 6057.

(33) Alder, K. *Annalen* **1951**, *571*, 87.

Chapter 5

Ionic Liquids

The observed effects of ionic liquids on chemical reactions range from weak to powerful.[1] Unfortunately, only a few systematic studies addressing the microscopic details on how ionic liquids influence chemical reactivity and selectivity have been reported.[2,3] Consequently, the molecular factors that endow room temperature ionic liquids with the ability to rate enhance and control a vast range of organic, inorganic, and enzymatic reactions in an environmentally safe manner are largely unknown. Experimental evidence suggests that the ionic interactions resulting from cation-to-anion ratios are crucial to understanding the physical and chemical properties of the ionic melts. This chapter focuses upon efforts to understand the local microscopic interactions of ion pairs at the transition structure that give ionic liquids the ability to impact the rates and

endo/exo selectivities of organic reactions. The focus is to examine the possibility that 1-ethyl-3-methylimidazolium cation (EMI^+) and N-1-butylpyridinium chloride (BPC) act as Lewis acids, and how they are modulated by the surrounding chloroaluminate counterions. The local effects of different cation-to-anion ratios upon chemical reactivity are being investigated using density functional theory. The four-stereospecific Diels-Alder transition structures for the cyclopentadiene and methyl acrylate cycloaddition have been computed using the Becke three-parameter density functional theory with the 6-31G(d) basis set within basic and acidic ionic melt approximations. The computational model includes EMI^+ and chloroaluminates ($AlCl_4^-$ and $Al_2Cl_7^-$) in a stacked configuration, which exploits lessons learned from other Lewis acid, catalyzed Diels-Alder reactions. The isolated ions that form in the melts ($AlCl_4^-$, $Al_2Cl_7^-$ and EMI^+) along with their 1:1 complexes ($AlCl_4^{-}\cdots EMI^+$ and $Al_2Cl_7^{-}\cdots EMI^+$) and 2:1 anion-cation complexes ($Cl^-\cdots EMI^+\cdots AlCl_4^-$, $AlCl_4^-\cdots EMI^+\cdots AlCl_4^-$, $Al_2Cl_7^-\cdots EMI^+\cdots AlCl_4^-$ and $Al_2Cl_7^-\cdots EMI^+\cdots Al_2Cl_7^-$) have been computed. Several orientations and possible interactions have been located. The computed activation energies, structures and vibrations partially explain the experimental data. However, additional ions are needed to describe the physical and chemical properties of ionic liquids. Consequently, further large-scale computations are necessary to probe larger models including several anion and cation layers, and the inclusion of bulk phase effects.

Reprinted in part from ACS Symposium Series (**2003**), (Ionic Liquids as Green Solvents: Progress and Prospects),(in Press).

Osteryoung, Wilkes and Hussey have developed ionic liquids that are fluid at room temperature.[4-6] The most commonly used salts are those with alkylammonium, alkylphosphonium, N-alkylpyridinium, and N,N'-dialkylimidazolium cations. Our interest is in 1-ethyl-3-methylimidazolium chloride (EMIC), and N-1-butylpyridinium chloride (BPC), shown in Scheme 5.1.

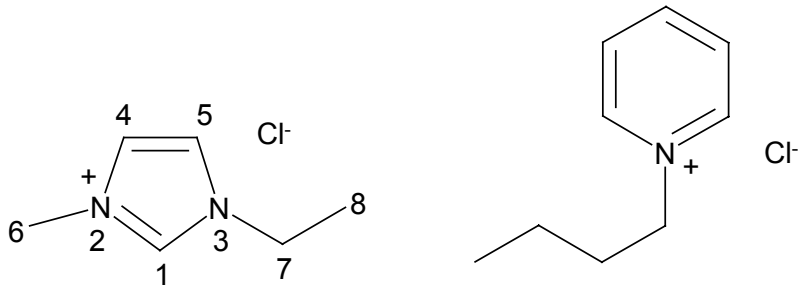

1 **2**

Scheme 5.1. *Common ionic liquids 1-ethyl-3-methylimidazolium chloride (EMIC),* ***1****, and N-1-butylpyridinium chloride (BPC),* ***2****.*

Several anions are typically used when forming an ionic liquid, such as BF_4^-, PF_6^-, ClO_4^- and of particular interest are the chloroaluminates from $AlCl_3$. An attractive property of using $AlCl_3$ is that the Lewis acidity of the melt can be varied with the composition of the liquid.[5] Raman,[6] ^{27}Al NMR[7] and mass spectra[8] all indicate that when $AlCl_3$ comprises <50% by mol of the melt in a pure ionic liquid, $AlCl_4^-$ is the only chloroaluminate(III) species present. These are known as "basic melts" because they contain $AlCl_4^-$ along with chloride ions that are not bound to aluminum. When an excess of >50% ratio of $AlCl_3$ to cation exists, this is referred to as an "acidic melt". ^{27}Al NMR[9] and negative-ion FAB mass spectra[10] have shown that $AlCl_4^-$ and $Al_2Cl_7^-$ are the principal constituents of the system.

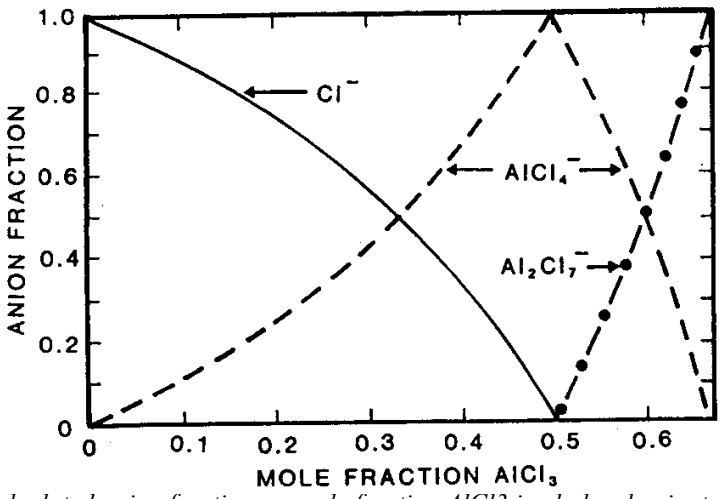

Figure 5.1. *Calculated anion fraction vs. mole fraction AlCl3 in choloraluminate melts.*[11,12]

Our approach in understanding how ionic liquids influence chemical reactions is to build upon the extensive body of recent experimental[13-18] and computational[19-24] data that yields insight into the microscopic factors at the origin of increased rate and *endo/exo* selectivities of aqueous phase Diels-Alder reactions. "Enhanced hydrogen bonding" between solvent and the transition structure relative to the initial state,[15,16] and "enforced hydrophobic interactions" as the reactant hydrophobic surface area decreases during the activation process are two major effects.[14,17,18] Several efforts have been aimed at separating and quantifying the relative contribution of each interaction type to aqueous acceleration.[13-22,24] Jorgensen and coworkers have probed enhanced hydrogen bonding effects by employing an explicit treatment of solvent using the OPLS force-field and Monte Carlo simulations.[19,24] The Gibbs energy of solvation (ΔG_{sol}) for the cyclopentadiene and methyl vinyl ketone Diels-Alder reaction has been computed.[19,22,24] Analysis revealed *ca.* 2-2.5 hydrogen bonds with the dienophile along the reaction coordinate. The polarized carbonyl group produced stronger hydrogen bonds (1-2

kcal/mol per hydrogen bond) at the transition structure. *Ab initio* calculations support the idea that the observed rate enhancements for Diels-Alder reactions arise from the hydrogen bonding effect in addition to a relatively constant hydrophobic contribution (estimated to be ca. 1 kcal/mol).[19] However, the special effect of water on Diels-Alder reactions beyond hydrogen bonding has been shown by the reduced rate constants in fluorinated alcohol solvents, which have stronger hydrogen bond donor capacity than water.[14,15] Therefore, factors other than hydrogen bonding are in operation. We have recently shown that local hydrogen bonding effects account for roughly one-half of the observed rate and *endo/exo* selectivity enhancements, while the remaining contributions are derived from the bulk phase.[20] In addition, we have found that novel interactions at the transition structure impact the rate and selectivity of some Diels-Alder reactions.[25]

Breslow first suggested that hydrophobic packing of the diene and dienophile is responsible for observed rate accelerations.[17,26] Subsequently, Engberts has articulated the difference between hydrophobic packing and enforced hydrophobic interactions. The term "enforced" is used to stress that hydrophobic interactions are an integral part of the activation process.[14,17,18] As with enhanced hydrogen bonding, the focus is on the relative stabilization between the initial state and the transition structure, which manifests in the available hydrophobic surface area along the reaction coordinate. In mixed solvent systems, Breslow has recently reported antihydrophobic cosolvent effects, which is a relationship between reaction rate and inaccessible hydrophobic surface area of the transition structure.[27,28] Briefly, an alcohol cosolvent does not interfere with water's ability to stabilize polarizable transition structures, rather it enhances transition structure solvation by stabilizing hydrophobic regions.[27]

Since the inception of aqueous rate accelerations and enhanced stereoselectivities of organic reactions,[29] many interpretations beyond enhanced hydrogen bonding and enforced hydrophobic effects have been advanced and recently discussed.[14] Most notably are internal pressure,[30] cohesive energy density of water,[31] micellar,[32] and medium polarity and solvophobic effects.[18,33] Even though electrostatic effects through enhanced hydrogen bonding between water and the transition structure account for an important part of the Diels-Alder rate acceleration, the remainder of enhancements by hydrophobic and other effects continue to be controversial and an active area of research.

5.1 Ionic Liquid Complexes

In the same spirit as considering water as a weak Lewis acid, the plan is to examine the potential of the 1-ethyl-3-methylimidazolium cation (EMI^+) as a Lewis acid as it is modulated by the surrounding chloroaluminate counterions. This chapter focuses upon efforts to understand the local microscopic interactions of ion pairs at the transition structure that give ionic liquids the ability to impact the rates and *endo/exo* selectivities of organic reactions.

5.1.1 1:1 Ionic Liquid Complexes

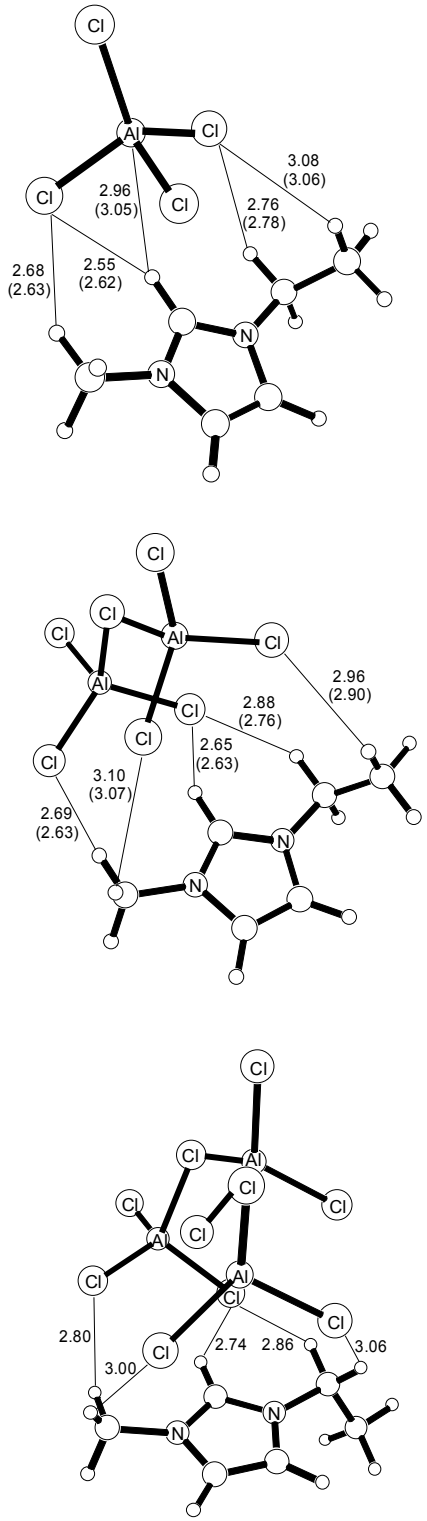

Figure 5.2. *B3LYP/6-31G(d) (MP2/6-31G(d) values in parenthesis) optimized structures of 1:1 basic and acidic ionic liquid complexes.*

5.1.2 Binding Energies for 1:1 Complexes

The B3LYP/6-31G(d) level of theory has been employed to compute the isolated ions which form in the acidic and basic melts ($AlCl_4^-$, $Al_2Cl_7^-$ and EMI^+) along with their 1:1 complexes ($AlCl_4^{-}\cdots EMI^+$ and $Al_2Cl_7^{-}\cdots EMI^+$). It has been determined that the binding energy for the $AlCl_4^{-}\cdots EMI^+$ complex is 69.9 kcal/mol, while the binding energy of the acidic melt, $Al_2Cl_7^{-}\cdots EMI^+$ is 63.9 kcal/mol, as shown in Table 5.1. The computed B3LYP/6-31G(d) energetics compare well to results previously reported using the HF method and the 6-31G(d) basis set[3] and MP2/6-31G(d) calculated here, as well. We have also determined the $Al_3Cl_{10}^{-}\cdots EMI^+$complex, found in highly acidic melts.

Table 5.1. *Binding enthalpies of ionic liquid complexes using the HF/ 6-31G(d), B3LYP/6-31G(d) and MP2/6-31G(d) levels of theory (binding enthalpies in kcal/mol).*

HF	*Binding Enthalpy*
$AlCl_4^{-}\cdots EMI^+$	68.0[a]
$Al_2Cl_7^{-}\cdots EMI^+$	63.2[a]
$Al_3Cl_{10}^{-}\cdots EMI^+$	57.7
B3LYP	
$AlCl_4^{-}\cdots EMI^+$	69.9
$Al_2Cl_7^{-}\cdots EMI^+$	63.9
$Al_3Cl_{10}^{-}\cdots EMI^+$	60.5
MP2	
$AlCl_4^{-}\cdots EMI^+$	73.9
$Al_2Cl_7^{-}\cdots EMI^+$	68.5

[a] Taken from ref. 3.

The B3LYP/6-31G(d) level of theory predicts a slightly greater binding energy for both the $AlCl_4^{-}\cdots EMI^+$ and $Al_2Cl_7^{-}\cdots EMI^+$ complexes as compared to HF/6-31G(d). The trend exists for both levels of theory, where the binding energy decreases significantly as the chloroaluminate ion becomes larger. The results are important, since

as the binding energy decreases between EMI^+ and the chloroaluminate ion, the more likely a Lewis acid adduct with the dienophile will form. The formation of a Lewis acid adduct has been a serious topic of debate, especially for the more acidic forms of the chloroaluminates.[34] In this study, the assumption is that the ion pairs between $AlCl_4^{-}\cdots EMI^+$ (basic melt model) and $Al_2Cl_7^{-}\cdots EMI^+$ (acidic melt model) stay in tact, where adduct formation does not take place. In collaboration with Dan Singleton, on-going research is aimed at addressing the possibility of adduct formation through a combined experimental and computational effort in the determination of secondary kinetic isotope effects.[25,35] Using the force constants from transition structure frequency calculations, KIEs will be determined in a similar fashion to the Diels-Alder reactions in Chapters 3 and 4 of this thesis.

5.1.3 2:1 Ionic Liquid Complexes

Nuclear magnetic resonance (NMR) experiments on mixtures of EMIC and $AlCl_3$ have shown that chemical shifts of protons on the cations are highly dependent on the proportion of the melt.[12] Wilkes et al. have studied the composition dependence for ^1H shifts of the cations in the 1-ethyl-3-methylimidazolium chloride-$AlCl_3$ system and have found that the melts are relatively organized in the liquid state.[12,36,37] This suggests a stack model, where an anion is positioned on top of the EMI^+ ring, with another anion below the ring. A better understanding of the physical and chemical properties of these melts requires the investigation of these ionic interactions and cation-to-anion ratios.

NMR experiments have been reported to elucidate the cation-anion ratio.[12] In order to interpret quantitatively the changes in chemical shifts with composition, some

assumptions about the cation-anion interactions have been made. The fundamental assumptions are that they can affect shifts by modifying the net charge of the cation and that the complexes formed are relatively weak so that fast exchange can be made. Wilkes et al. looked at several models, in Model 1, the melt involves ions that exist as simple ion pairs; each cation is coordinated with a single anion, as calculated in the previous section. We have referred to Model 1 as a 1:1 complex. Using the chemical shift data for the proton at the 1-position in Scheme 5.1 tests the model, because it shows the greatest change. This model is shown in Equation 5.1 is linear, but can only be tested well for the basic compositions because the acidic melts showed little change with different $AlCl_3$ mole fractions.

$$\delta_{obsd} = \delta_1 X_1 + \delta_4 X_4 + \delta_7 X_7 \tag{5.1}$$

The δ terms are the chemical shifts, which are a function of the X_i's, mole fractions of the complexes. The mole fractions are determined by the given melt composition in the range of $0 \leq N \leq 0.67$. The anion fraction (Y_i) relate to the X_i's in the following equations:

Basic compositions

$$Y_{Cl^-} = \frac{1-2N}{1-N} = X_1 \tag{5.2}$$

$$Y_{AlCl_4^-} = \frac{N}{1-N} = X_4 \tag{5.3}$$

Acidic compositions

$$Y_{AlCl_4^-} = \frac{2-3N}{1-N} = X_4 \tag{5.4}$$

$$Y_{Al_2Cl_4^-} = \frac{2N-1}{1-N} = X_7 \tag{5.5}$$

where, X_1 is $Cl^{-}\cdots EMI^{+}$, X_4 is $AlCl_4^{-}\cdots EMI^{+}$ and X_7 is $Al_2Cl_7^{-}\cdots EMI^{+}$. Plotting the data gives a straight line, which shows a systematic deviation from the data points, so one of the assumptions may be incorrect.[12] The anion-cation, one-to-one pair, is the weakest assumption. So assuming the cation may interact with two or more anions is reasonable.

The new assumption, model 2, allows two anions per cation. In this case, Equation 5.6 for the model is quadratic, which fits all of the experimental data very well.[12]

$$\delta_{obsd} = \delta_2 X_2 + \delta_2 X_5 + \delta_8 X_8 + \delta_{11} X_{11} + \delta_{14} X_{14} \tag{5.6}$$

There are five possible complexes when taking a 2:1 anion-cation ratio as seen in Scheme 5.2.

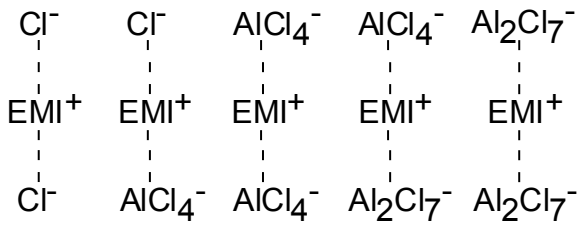

Scheme 5.2. *Five different complexes of the stack model at basic and acidic melts.*

If the five complexes have a random distribution of anions among the cations, then the X_i's may be calculated in a similar fashion to Model 1.

Basic compositions

$$X_2 = Y_{Cl^-}^2 \tag{5.7}$$

$$X_5 = 2Y_{Cl^-}Y_{AlCl_4^-} \tag{5.8}$$

all compositions

$$X_8 = Y_{AlCl_4^-}^2 \tag{5.9}$$

acidic compositions

$$X_{11} = 2Y_{AlCl_4^-}Y_{Al_2Cl_7^-} \tag{5.10}$$

$$X_{14} = Y^2_{Al_2Cl_7^-} \tag{5.11}$$

Assuming that the anions are randomly distributed may be false. It is possible that the anions are distributed so that there are chloride-rich, tetrachloroaluminate-rich or heptachloroaluminate-rich regions. Where the first, third and fifth complexes in Scheme 5.2 are preferred. It is also possible that they may be avoided, maximizing complexes two and four, which have different anion compositions complexed to the EMI^+. Both models were tested, by calculating the shifts, but in both cases the fits to chemical shift data were poor than the random distribution model.[12] Model 2, which we refer to as a 2:1 complex, with a random distribution has excellent agreement with experimental data. This evidence supports the assumption that five different complexes (Scheme 5.2) are present in the ionic liquid, depending on whether the melt is acidic or basic.

A third model (Model 3), where the coordination number of each cation was three anions, was tested. The fit was not improved relative to the two-coordinate system. Further support for the 2:1 anion-cation model comes from the results of experimental densities. The experimental densities of the EMIC-$AlCl_3$ melts were least-square fitted with ten parameters.[36] As was observed with the proton NMR data, the structural model with 2 anions reproduced the data significantly better than did a coordination of 1:1. Limited theoretical work on distinguishing the ratio of anion to cation has been reported.[11,37] Monte Carlo calculations in which the EMI^+ was represented by an oblate spheroid or plate and the anions were taken to be spherical. These calculations predicted that the plates would tend to stack up with their planes parallel in the acidic melt.[11] Each stack is expected to extend indefinitely. Low level quantum calculations were carried out

using AM1, in which a more extensive stack model was constructed by placing two $AlCl_4$ on the outer ends of EMI^+ ions, with a Cl^- in the middle.[37] A similar system with the Cl^- in the middle replaced with $AlCl_4$ was also carried out. In basic melts, IR spectral analysis showed shifts in the frequencies of hydrogen stretches in the 1, 4 and 5 positions in Scheme 5.1. Computed vibrational shifts were in the opposite direction from that observed and lead to the conclusion that AM1 is not capable of reproducing the experimentally observed Cl^- interaction band frequencies.[37]

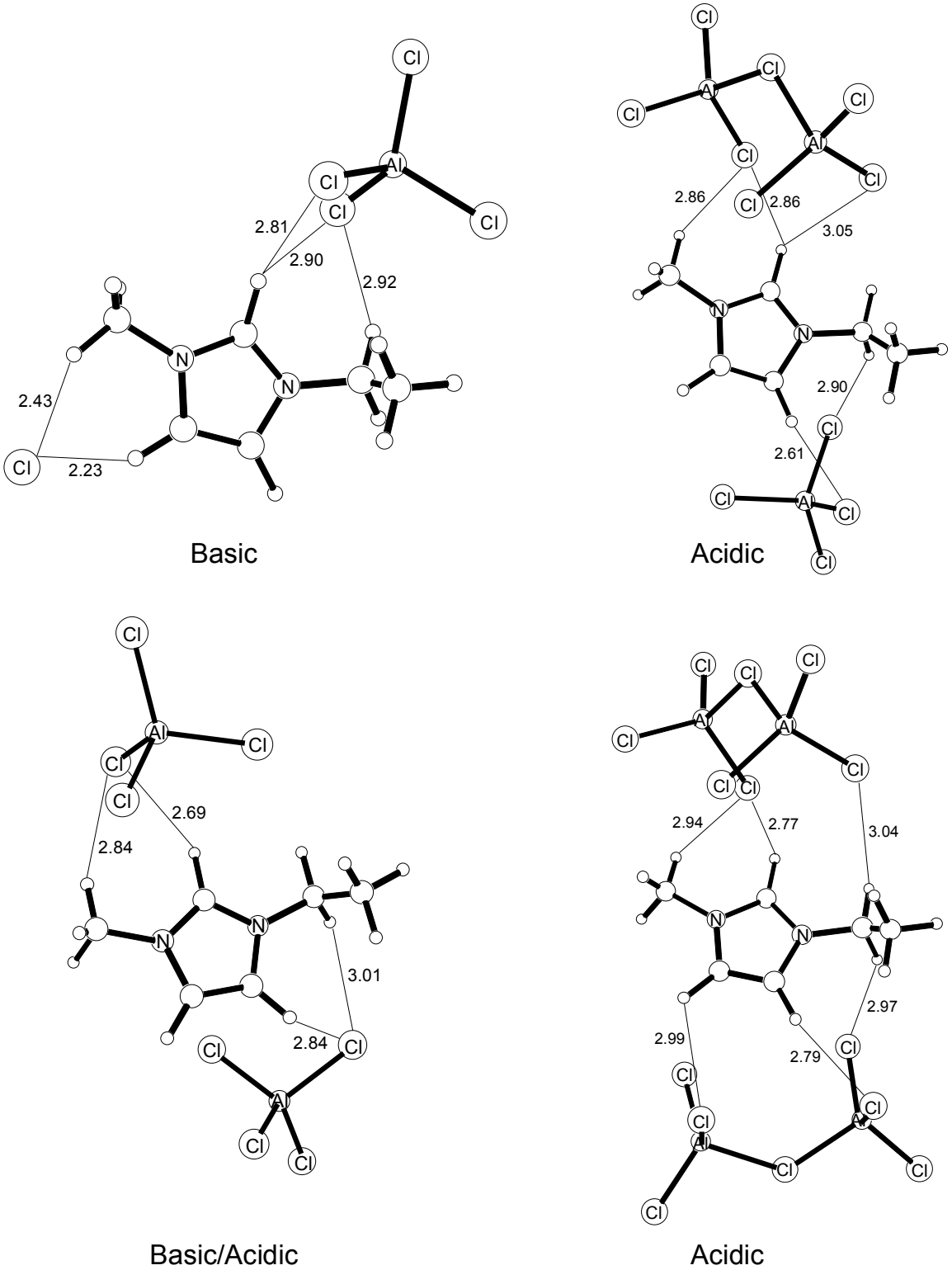

Figure 5.3. *B3LYP/6-31G(d) optimized structures of 2:1 basic and acidic ionic liquid complexes.*

5.1.4 Binding Energies for 2:1 Complexes

The B3LYP/6-31G(d) level of theory was used to compute the binding energies and vibrational analysis for the 2:1 anion-cation complexes. The basic melt and acidic melt were approximated by complexation similar to Scheme 5.2. The basic melt is represented by the $Cl^{-}\cdots EMI^{+}\cdots AlCl_4^{-}$ and $AlCl_4^{-}\cdots EMI^{+}\cdots AlCl_4^{-}$ complexes, while the acidic melt is characterized by the $Al_2Cl_7^{-}\cdots EMI^{+}\cdots AlCl_4^{-}$ and $Al_2Cl_7^{-}\cdots EMI^{+}\cdots Al_2Cl_7^{-}$ complex.

Table 5.2. *Binding enthalpies of ionic liquid complexes using the B3LYP/6-31G(d) level of theory (binding enthalpies in kcal/mol).*

	Binding Enthalpy
$Cl^{-}\cdots EMI^{+}\cdots AlCl_4^{-}$	111.0
$AlCl_4^{-}\cdots EMI^{+}\cdots AlCl_4^{-}$	90.3
$Al_2Cl_7^{-}\cdots EMI^{+}\cdots AlCl_4^{-}$	86.5
$Al_2Cl_7^{-}\cdots EMI^{+}\cdots Al_2Cl_7^{-}$	83.6

The trend where the binding energy decreases significantly as the chloroaluminate ion becomes larger, is once again seen. As in the 1:1 ratio, the results are significant since as the binding energy decreases between EMI^{+} and the larger chloroaluminate ions, the more likely a Lewis acid adduct with the dienophile will form. This adduct however has not been reported in experimental results.

5.1.5 Ionic Liquid Geometries

B3LYP/6-31G(d) calculations have been performed on the anions in the molten chloroaluminate salts to determine their geometry. The geometry of the anion, $AlCl_4^{-}$, is confirmed to be tetrahedral in accordance with x-ray crystallographic results.[38] The geometry of $Al_2Cl_7^{-}$ is found to be C_2 symmetric confirmed by the observed IR

spectrum.[11] The computed structures are consistent with results presented earlier from MNDO calculations.[11]

An x-ray crystal structure of the basic melt involving EMIC and $AlCl_3$, where the mole fraction of $AlCl_3$ compared to EMIC was less that 0.5, has been previously reported.[39] The geometry has been compared to HF/6-31G(d) calculations by Takahashi and coworkers.[40] The bond lengths and angles for EMI^+ are presented in Table 5.3, along with our calculations using the B3LYP/6-31G(d) and second-order MP2/6-31G(d) levels of theory. In general the comparison between experimental and both levels of theory is good. However, there seems to be an unusual distortion at the N_3 ethyl group in the crystal structure. The crystallographic C_7C_8 distance is shorter than that expected for a single bond, the N_3C_7 length is greater than the typical nitrogen-carbon single bond, and the $N_3C_7C_8$ angle is compressed from the usual sp^3 tetrahedral value, as shown in Table 5.3. Crystal packing forces could be in operation.

Table 5.3. *Comparisons of x-ray and theoretical data for EMI^{+a}.*

Geometry	*x-ray*[b]	*HF*	*B3LYP*	*MP2*
C_1N_2	1.30	1.32	1.34	1.34
C_1N_3	1.27	1.31	1.34	1.34
N_2C_4	1.39	1.38	1.38	1.37
N_3C_5	1.41	1.38	1.38	1.37
C_4C_5	1.38	1.34	1.36	1.37
N_2C_6	1.48	1.47	1.47	1.46
N_3C_7	1.55	1.48	1.48	1.47
C_7C_8	1.43	1.52	1.52	1.52
$\angle N_2C_1N_3$	110	110	109	108
$\angle C_1N_2C_4$	111	108	108	109
$\angle C_1N_3C_5$	109	108	108	109
$\angle N_2C_4C_5$	104	107	107	107
$\angle N_3C_5C_4$	106	107	107	107
$\angle C_1N_2C_6$	126	126	126	126
$\angle C_1N_3C_7$	130	126	126	126
$\angle N_3C_7C_8$	104	112	112	111

[a] Bond distances (Å) and bond angles (º) defined in Scheme 5.1. HF/6-31G(d) total energy of EMI^+ is -342.31340 hartrees, B3LYP/6-31G(d) total energy is -344.5497092 hartrees, MP2/6-31G(d) total energy is -343.4048579. [b] Taken from ref. 6.

5.1.6 Vibrational Analysis

An infrared study of two separate ionic liquids (EMIC and BPC) was carried out by Osteryoung, which can be used to compare specific vibrational data with computed values.[41] A frequency analysis has been carried out and reported using the semi-empirical method AM1.[37] The vibrations were later investigated using MNDO and HF/6-31G(d) on the individual ions.[11,42] We carried out the frequency analysis on the EMI^+ ion and the 1:1 and 2:1 acidic and basic melt models at B3LYP/6-31G(d) and compared specific stretches to experimental data in Table 5.4. The scaled vibrational frequencies are within 2% of experimental frequencies of vibration. The B3LYP/6-31G(d) level of theory, in agreement with previous structural, vibrational and energetic ionic melt studies, is an appropriate level of theory to describe chloroaluminate ionic liquids.

Table 5.4. *Comparison of peak frequency (cm^{-1}) changes occurring with melt acidity, calculated at the B3LYP/6-31G(d) level of theory.*

melt	*aromatic C-H str*	*aliphatic C-H str*	*-C=N-str*	*ring str*	*ring i/p b*	*ring o/p b*
EMI^{+} [a]	3183	3039	1550	1139	794	717
acidic						
EMI-Al_2Cl_7 [a]	3176	2970	1547	1140	837	710
EMI-Al_2Cl_7-$AlCl_4$ [b]	3161	2979	1552	1146	808	726
EMI-$2Al_2Cl_7$ [b]	3180	2982	1552	1148	810	730
1.50:1 melt [c]	3161	2992	1595	1169	836	747
basic						
EMI-$AlCl_4$ [a]	3152	2971	1549	1140	867	712
EMI-$AlCl_4$-Cl [b]	3181	2943	1558	1151	793	715
EMI-$2AlCl_4$ [b]	3168	2969	1553	1147	841	725
0.55:1 melt [c]	3154	2983	1590	1175	838	758

All calculations scaled by 0.9614.[43] [a]1:1 ratio [b]2:1 ratio [c]Experimental data taken from ref. 41.

5.2 Transition Structures

The influence of solvent on the *endo/exo* selectivity and reaction rate of the reaction of cyclopentadiene (**3**) and methyl acrylate (**4**) to give the *endo* (**5**) and *exo* (**6**) bicyclic products (Scheme 5.3) has been recently reported in a range of molecular solvents, including different ionic liquids.

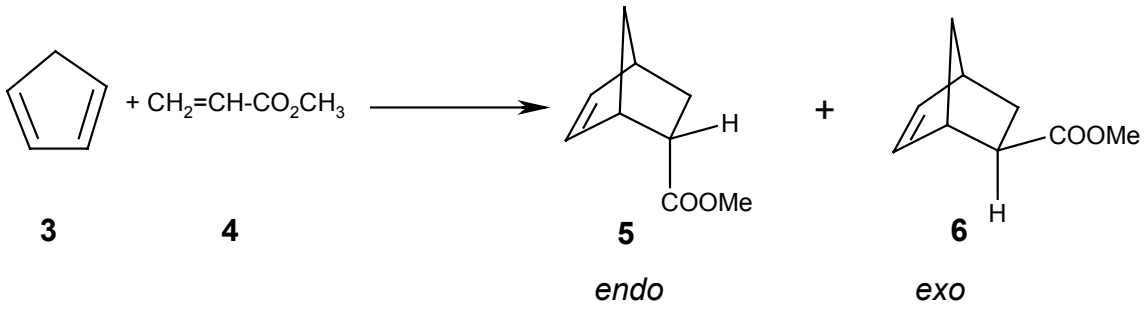

Scheme 5.3. *Diels-Alder reaction between cyclopentadiene (**3**) and methyl acrylate (**4**) to give the endo(**5**) and exo (**6**) bicyclic products.*

As shown by Carlos W. Lee, when an acidic melt (51% $AlCl_3$) of EMIC was used as the solvent for the equimolar reaction of **3** and **4**, the rate of reaction is 10 times faster than in water and 175 faster than in ethyl ammonium nitrate.[44] The results are significant, since the reaction rate is already 20 times faster in water as compared to nonpolar solvents.[45] However, when the basic melt (48% $AlCl_3$) of EMIC was used as the solvent, Lee found that the rate was significantly slower. Water has a reaction rate 2.4 times faster that the basic melt. *Endo* selectivity is enhanced with good yield when using the EMIC ionic liquid. A 6.7:1 *endo* to *exo* ratio is observed for the solvent ethyl ammonium nitrate (EAN), the basic ionic liquid melt has a ratio of 5.25:1, while the acidic melt ionic liquid EMIC has a ratio of 19:1. In nonpolar solvents, *endo/exo* selectivity is 2:1.[44,46]

5.2.1 Parent Reaction

Four possible reaction pathways are possible for the Diels-Alder reaction between cyclopentadiene and methyl acrylate. Consistent with previous conventions, the computed four-stereospecific transition structures are denoted as NC (*endo*, *s-cis* methyl acrylate), XC (*exo*, *s-cis* methyl acrylate), NT (*endo*, *s-trans* methyl acrylate) and XT (*exo*, *s-trans* methyl acrylate), as shown in Figure 5.4.

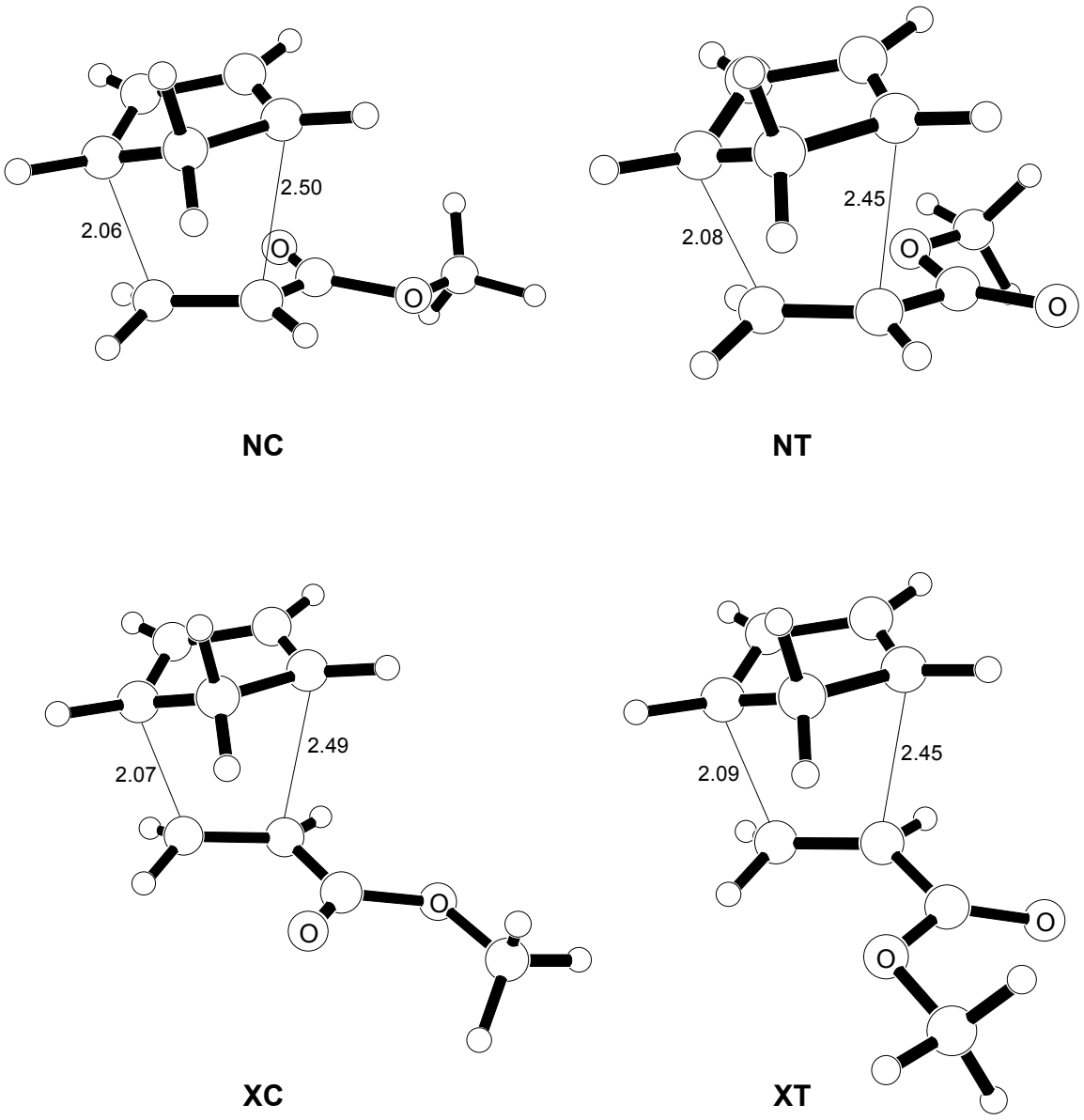

Figure 5.4. *The four stereospecific transition structures optimized using the B3LYP/6-31G(d) level of theory*

5.2.2 Activation Energies

The computed activation energies, enthalpies and Gibbs energies in vacuum are presented in Table 5.5. The computed B3LYP/6-31G(d) activation enthalpy is 16.6 kcal/mol in vacuum at 298 K for the parent reaction. The experimental activation enthalpy and entropy is 15.1 kcal/mol and –29.7 cal/mol-K when determined in toluene.[45] To provide a rough comparison, we have previously computed that the activation enthalpy drops roughly by 1.5 kcal/mol when comparing the barriers from vacuum and in benzene (similar to toluene) for the similar Diels-Alder reaction of acrolein and butadiene.[20] Consequently, our computed activation enthalpy is in excellent agreement (16.6 – 1.5 = 15.1 kcal/mol) with the experimental value of 15.1 kcal/mol. Furthermore, we expect an additional drop of 4.9 kcal/mol in the activation enthalpy when the reaction is carried out in a methanol/water mixture from benzene.[20] The observed activation enthalpy and entropy for the cyclopentadiene and methyl acrylate reaction is 10.2 kcal/mol and –40.9 cal/mol-K, respectively, in a methanol/water mixture, which is in excellent agreement with the B3LYP/6-31G(d) value of (16.6 – 1.5 – 4.9 = 10. 2 kcal/mol).[45]

Table 5.5. *Computed thermodynamic activation parameters for the parent Diels-Alder reaction from the B3LYP/6-31G(d) level of theory.*

TS	$\Delta E^{\ddagger}_{o}$	$\Delta E^{\ddagger}_{298}$	$\Delta H^{\ddagger}_{298}$	$\Delta G^{\ddagger}_{298}$
NC	17.7	17.5	16.9	30.6
NT	19.2	19.0	18.4	32.2
XC	17.3	17.2	16.6	30.3
XT	19.3	19.1	18.5	32.2

$\Delta E^{\ddagger}_{o}$ is the activation energy given by the electronic energy corrected by the zero-point energy at zero K. $\Delta E^{\ddagger}_{298}$, $\Delta H^{\ddagger}_{298}$ and $\Delta G^{\ddagger}_{298}$ are the activation energy, activation enthalpy and activation free energy at 298 K, respectively.

The most recent experimental work by Lee suggests that basic melts suppress the rate and *endo* selectivity of the cyclopentadiene and methyl acrylate Diels-Alder reaction compared to water, while the acidic melt enhances both.[44] Consequently, it is necessary to worry about the principal constituents of the basic system, $[EMI]^+[AlCl_4]^-$ and $[EMI]^+Cl^-$, and of the acidic system, $[EMI]^+[AlCl_4]^-$ and $[EMI]^+[Al_2Cl_7]^-$. A full density functional theory treatment on a box of ionic species is currently beyond the limit of computer resources available. Consequently for this study, three levels of approximation are made to understand how ionic liquids impact chemical reactivity and stereoselectivity. First, only the EMI^+ cation is used to activate the dienophile as a Lewis acid. This represents an unrealistic situation, since the positive charge is not diminished by surrounding counter anions and it does not serve to differentiate between the enhanced and suppressed chemical reactivity observed by the acidic and basic experiments. For both the second and third approximations, the assumption is that the ion pairs between $AlCl_4^{-}\cdots EMI^+$ (basic melt model) and $Al_2Cl_7^{-}\cdots EMI^+$ (acidic melt model) stay in tact, where adduct formation does not take place. However, the proportion of anion to cation is investigated by varying the number of anions in both the acidic and basic melt. These models are still rudimentary, yet form the basis of this current work and future simulations, which require extensively more resources.

5.2.3 Complexation of EMI^+

The four stereospecific (NC, NT, XC and XT) transition structures have been located for the cyclopentadiene and methyl acrylate Diels-Alder reaction in four different configurations with the EMI^+ cation, as shown in Figures 5.5, 5.6, 5.7 and 5.8. The

configurations were selected to orient the acidic imidazolium proton towards the carbonyl oxygen of methyl acrylate (**8** and **9**), or away from methyl acrylate (**7** and **10**). Additionally, the computations resulted with the carbonyl oxygen forming a weaker second interaction with either the methyl proton (**7** and **8**) or the proton from the ethyl group (**9** and **10**).

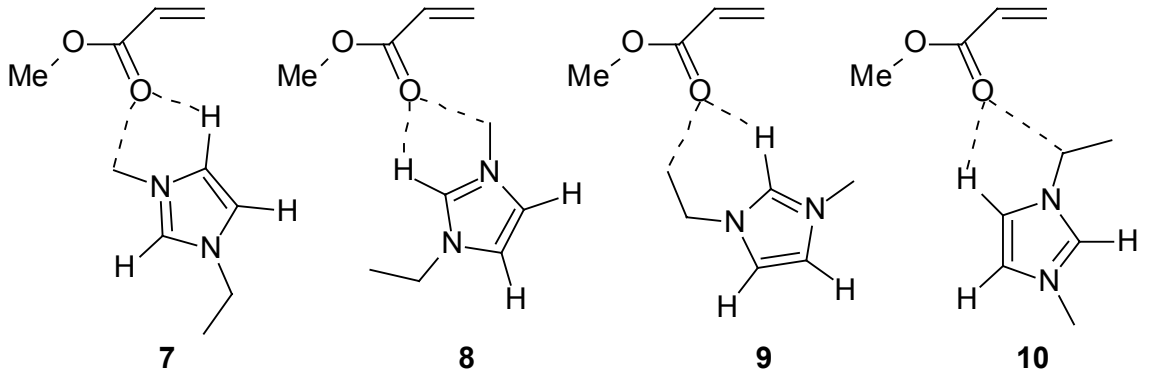

Scheme 5.4. *S-cis methyl acrylate with four different configurations of the EMI$^+$ cation.*

Complexation of EMI$^+$ to each of the four transition structures are concerted and asynchronous, as indicated by the lengths of the breaking and forming bonds (~2.03 and ~2.56 Å). The four transition structures are similar, where the breaking and forming bonds are within 0.03 A. However, the interaction between EMI$^+$ and the transition structure varies. As expected, the orientations with the acidic imidazolium proton towards the carbonyl oxygen of methyl acrylate (**8** and **9**) give a stronger energy of interaction by roughly 2 kcal/mol (see Table 5.6), and result with the key carbonyl oxygen and imidazolium proton interaction distance being about 0.1 Å closer. The favored configuration with this model is to have the acidic imidazolium proton point towards the carbonyl oxygen of methyl acrylate and have a second interaction form with a methyl hydrogen. The results match that expected from chemical intuition, however this analysis is an oversimplification of the environment found in an ionic liquid. In this explicit ionic

liquid cation model, the activation energies in Table 5.6 are computed by subtracting the isolated cyclopentadiene and the hydrogen bonded methyl acrylate and ion complex energies from the total transition structure energy.

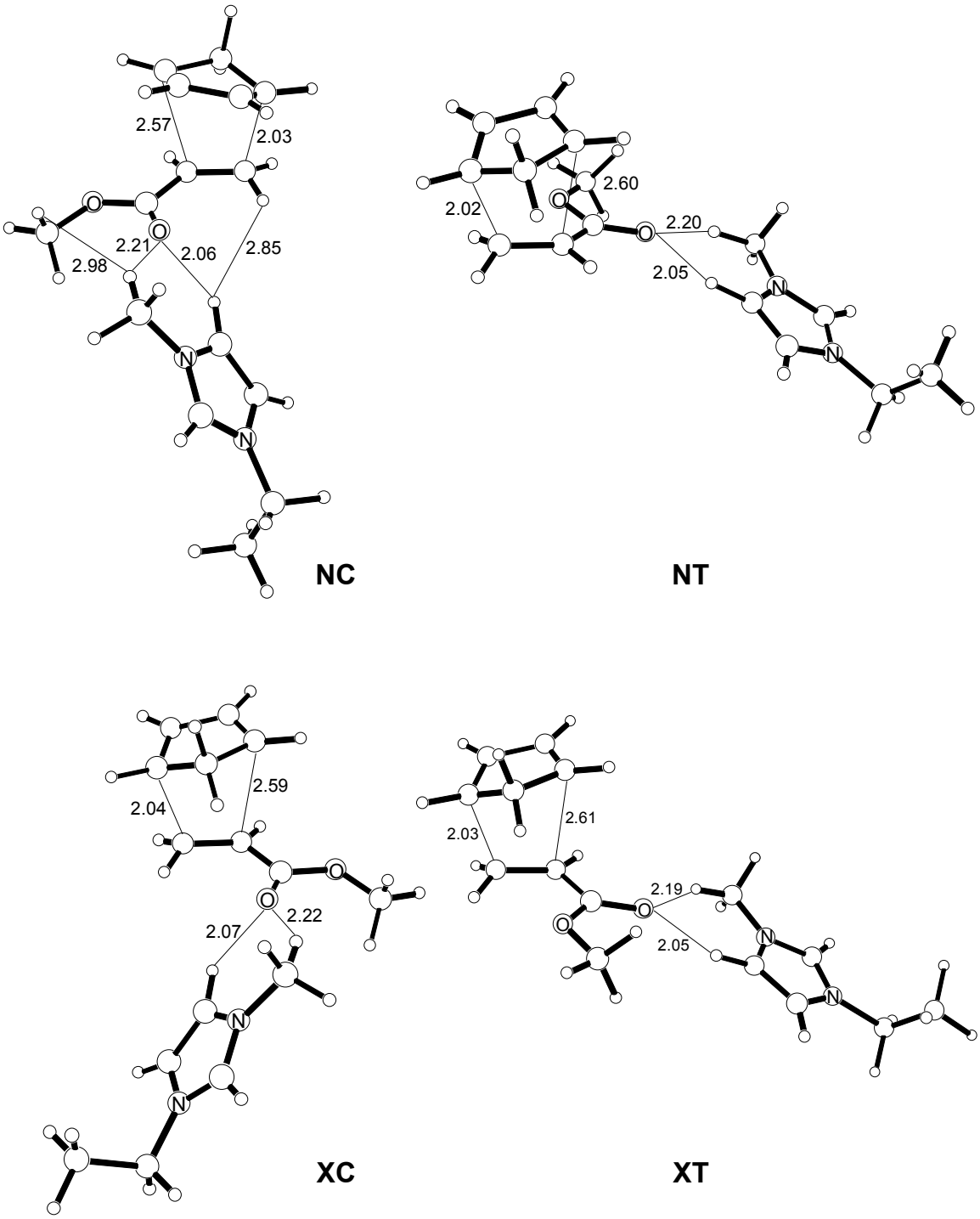

Figure 5.5. *The four stereospecific transition structures with the EMI^+ cation in conformation 1, optimized using the B3LYP/6-31G(d) level of theory.*

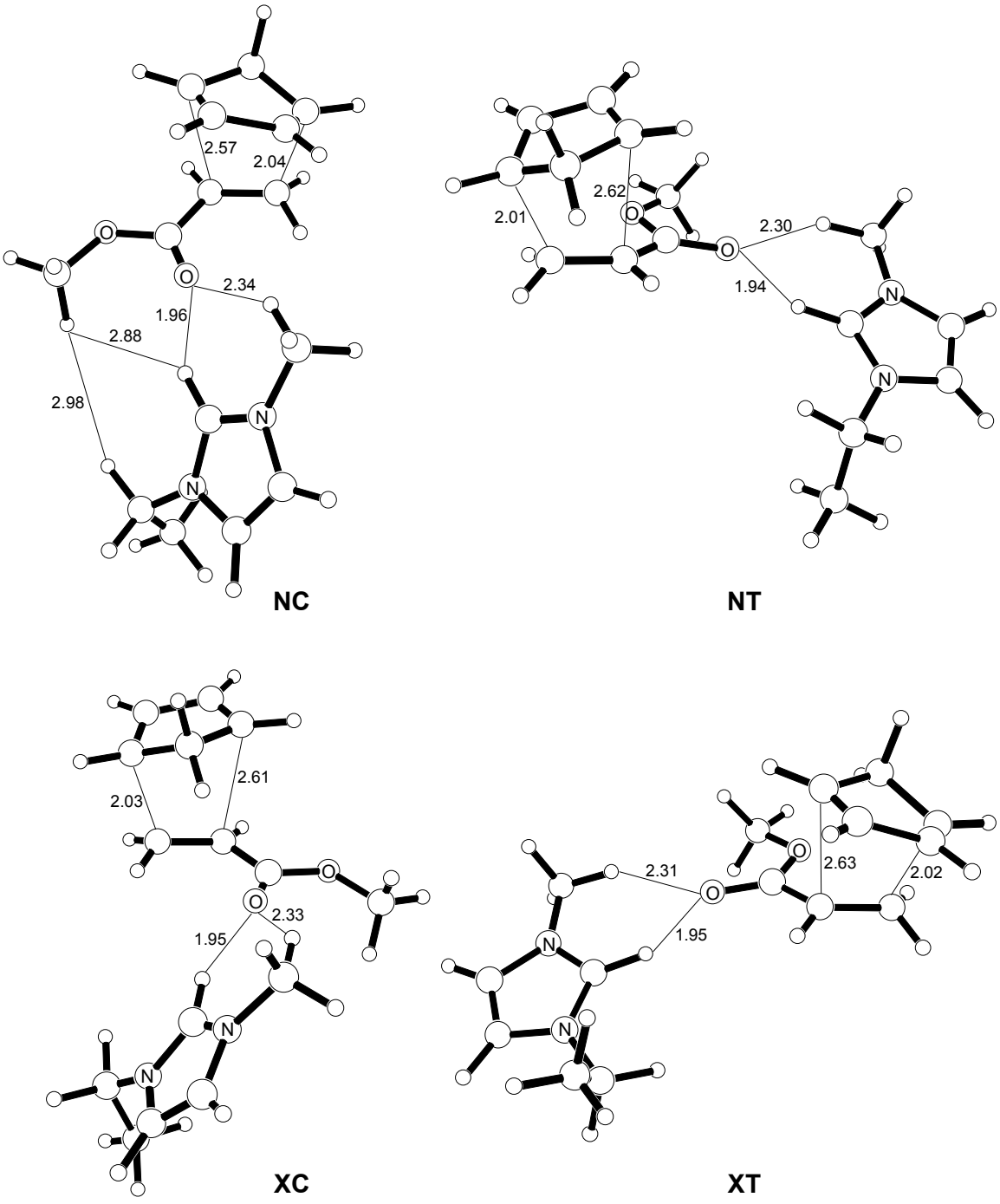

Figure 5.6. *The four stereospecific transition structures with the EMI^+ cation in conformation 2, optimized using the B3LYP/6-31G(d) level of theory.*

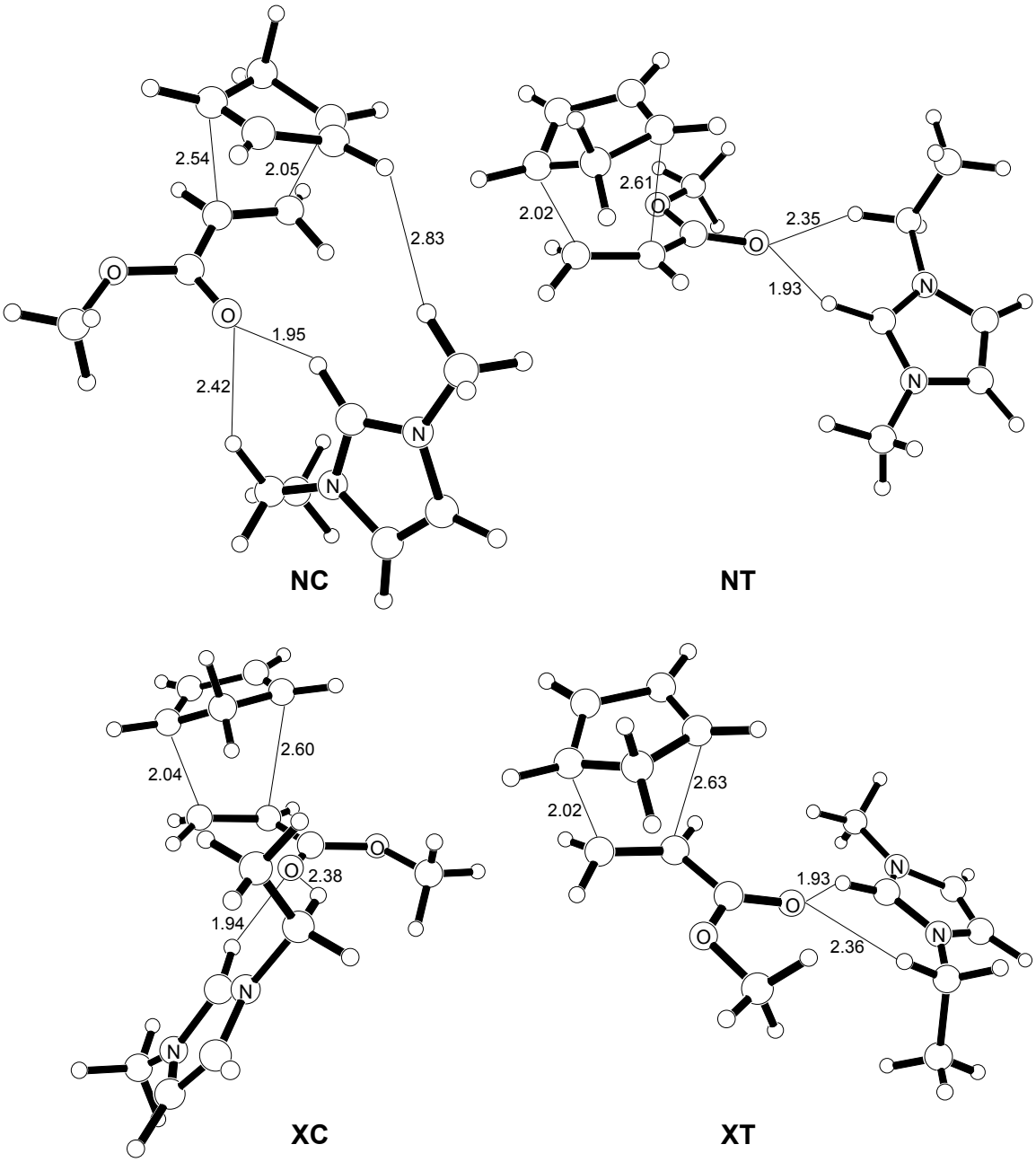

Figure 5.7. *The four stereospecific transition structures with the EMI^+ cation in conformation 3, optimized using the B3LYP/6-31G(d) level of theory.*

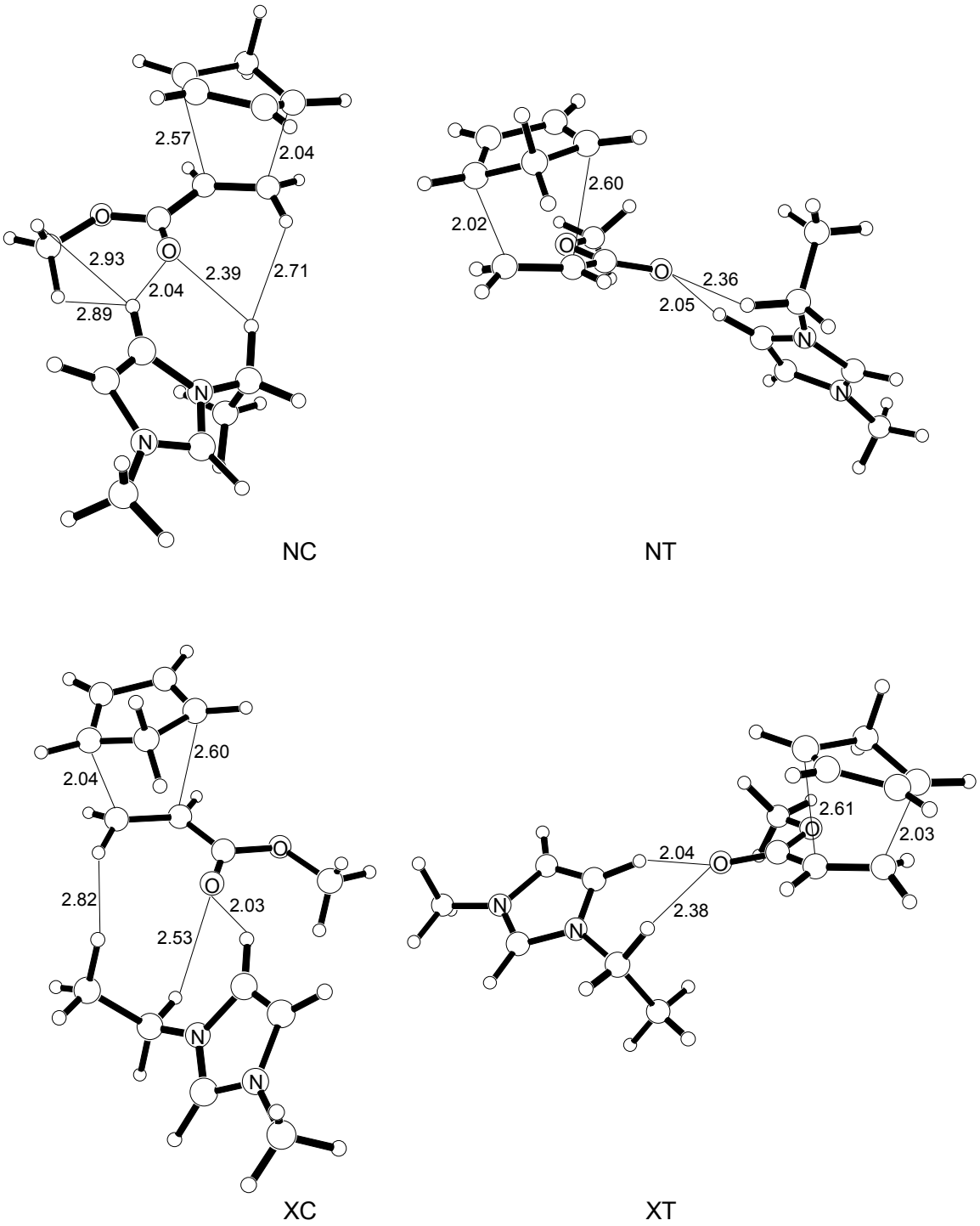

Figure 5.8. *The four stereospecific transition structures with the EMI^+ cation in conformation 4, optimized using the B3LYP/6-31G(d) level of theory.*

Table 5.6. *Computed activation energies for EMI^+ and the four stereospecific transition structures from Scheme 5.4 using the B3LYP/6-31G(d) level of theory (in kcal/mol).*

Structure	$\Delta E^{\ddagger}_{0}$	$\Delta E^{\ddagger}_{298}$	$\Delta H^{\ddagger}_{298}$	$\Delta G^{\ddagger}_{298}$
7				
NC	17.72	17.59	16.96	31.59
NT[a]	17.20	16.42	15.79	33.33
XC	17.89	17.74	17.10	32.25
XT	17.62	16.87	16.23	33.47
8				
NC[a]	15.52	14.72	14.09	31.99
NT	14.61	14.39	13.75	29.25
XC	15.40	15.24	14.61	29.69
XT	15.11	14.90	14.26	29.37
9				
NC	15.98	15.92	15.28	30.21
NT	14.79	14.70	14.07	28.19
XC	15.61	15.54	14.90	29.63
XT	15.39	15.26	14.63	29.68
10				
NC[a]	17.65	16.99	16.35	33.54
NT	17.42	17.38	16.74	31.13
XC	18.08	18.05	17.41	32.10
XT[a]	17.73	17.05	16.41	33.64

[a] 2-imaginary frequencies. $\Delta E^{\ddagger}_{o}$ is the activation energy given by the electronic energy corrected by the zero-point energy at zero K. $\Delta E^{\ddagger}_{298,}$ $\Delta H^{\ddagger}_{298}$ and $\Delta G^{\ddagger}_{298}$ are the activation energy, activation enthalpy and activation free energy at 298 K, respectively.

5.2.4 1:1 Acidic and Basic Melts

In calculating activation energies for the transition structure of cyclopentadiene and methyl acrylate in a basic and acidic environment, as shown in Figure 5.9, two different approaches were used. The first method is identical to reports, where the activation energies are computed by subtracting the isolated cyclopentadiene and the hydrogen bonded methyl acrylate and ion complex energies from the total transition structure energy. The second method is different, where the isolated cyclopentadiene, isolated methyl acrylate, and the ion complex energies are subtracted from the total

transition structure energy. For a weak Lewis acid, such as water, the first method delivers a realistic picture of the energetic behavior.[20] However, using this method in a truncated ionic environment leads to binding energies that are superficially large because the environment does not partially quench the full ionic charges on EMI^+ or the chloroaluminate. This enhanced coordination results in larger activation enthalpies for both the acidic (13.9 kcal/mol) and basic melts (14.7 kcal/mol) than expected. Using the second method, the computed lowering of the activation enthalpies of 9.1 and 8.1 kcal/mol for the basic and acidic melts, respectively, leads to gross overestimations of the impact on the activation barrier lowering.

Table 5.7. *Comparison of computed thermodynamic activation parameters for the 1:1 approximated basic and acidic melt using the B3LYP/6-31G(d) level of theory.*

TS	$\Delta E^{\ddagger}_{o}$	$\Delta E^{\ddagger}_{298}$	$\Delta H^{\ddagger}_{298}$	$\Delta G^{\ddagger}_{298}$
NC				
$TS+EMI^+ + AlCl_4^-$	15.4/9.0	15.3/10.3	14.7/9.1	29.1/32.4
$TS+EMI^+ + Al_2Cl_7^-$	14.6/8.1	14.5/9.3	13.9/8.1	28.9/31.9

$\Delta E^{\ddagger}_{o}$ is the activation energy given by the electronic energy corrected by the zero-point energy at zero K. $\Delta E^{\ddagger}_{298}$, $\Delta H^{\ddagger}_{298}$ and $\Delta G^{\ddagger}_{298}$ are the activation energy, activation enthalpy and activation free energy at 298 K, respectively.

The experimental activation barrier lowering is between the two extremes of 9.1 to 14.7 kcal/mol for the basic melt and 8.1 to 13.9 kcal/mol for the acidic melt activation enthalpies as seen in Table 5.7. The relative difference between basic and acidic melts follows the same general trend as experiment, where the acidic melt has a lower activation barrier than the basic melt by 1 kcal/mol.

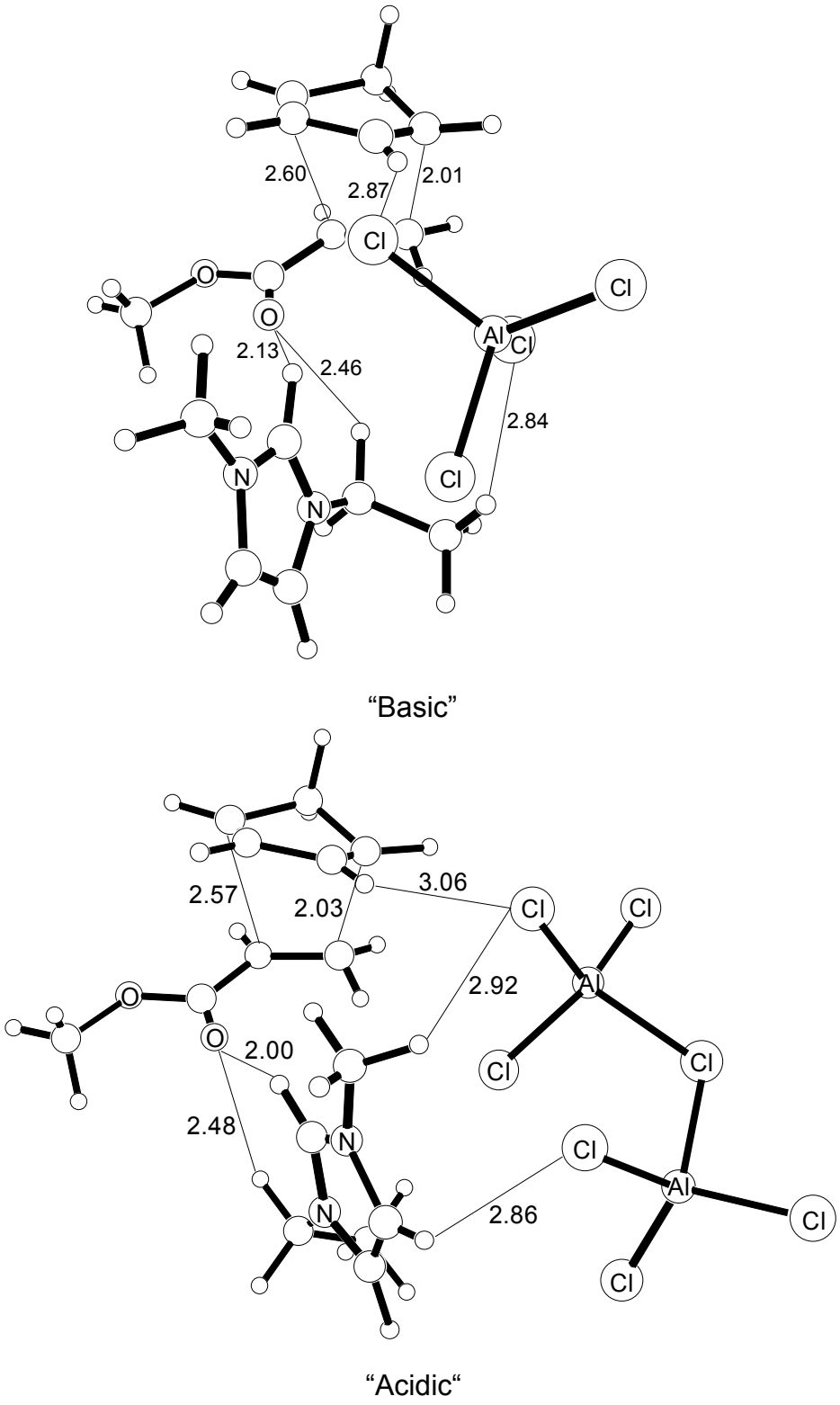

Figure 5.9. *The NC transition structures for the cyclopentadiene and methyl acrylate with a basic and acidic approximated 1:1 ratio anion-cation environment computed using the B3LYP/6-31G(d) level of theory.*

A single kcal/mol is not the energy difference measured experimentally and consequently exhibits a weakness in our model. This suggests that further bulk phase or additional ion participation is necessary to explain the experimental phenomenon.

5.2.5 2:1 Acidic and Basic Melts

A better approximation to the acidic and basic melt environment effecting the transition structure is to use the 2:1 anion-to-cation ratio. This specific complexation is more in line with experimental data.[11,12,36,37] This lends the ability to satisfy more key electrostatic interactions on the diene and dienophile, while further stabilizing the transition structure.

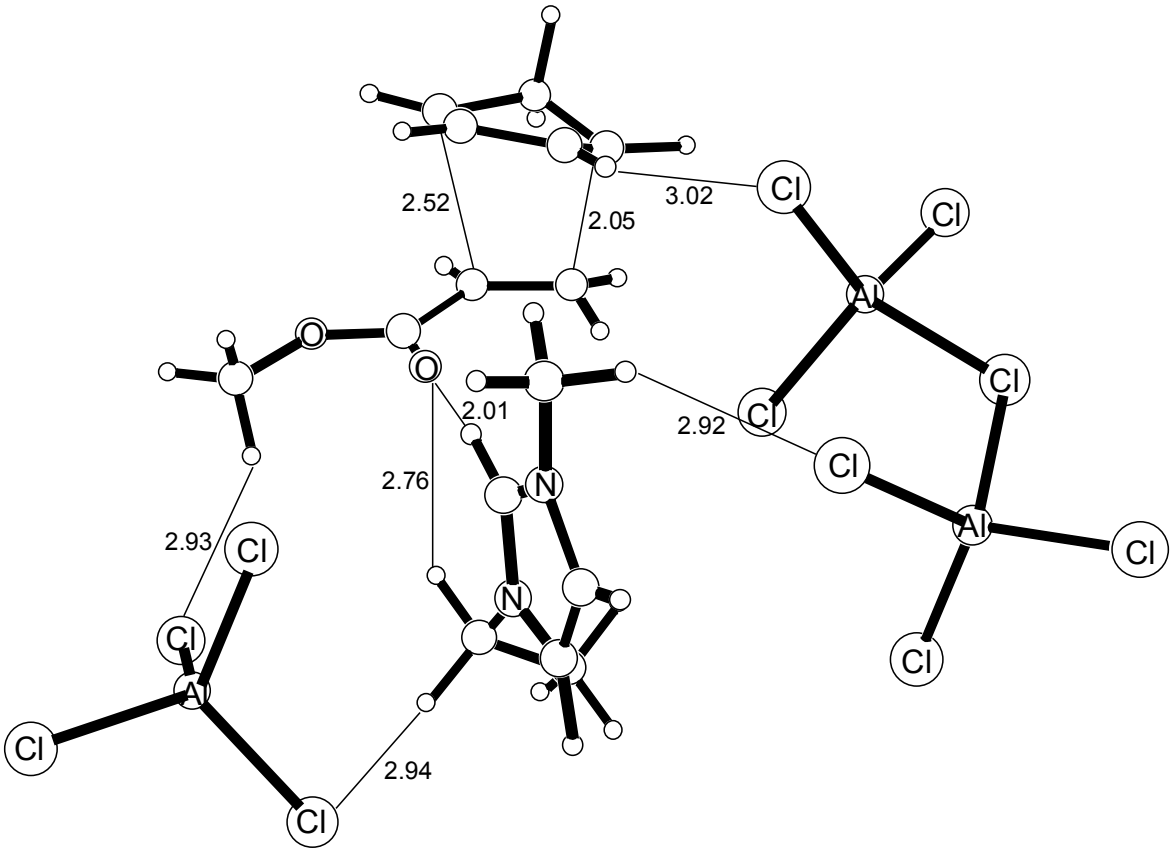

Figure 5.10. *The NC transition structure for the cyclopentadiene and methyl acrylate with an acidic approximated 2:1 ratio anion-cation environment computed using the B3LYP/6-31G(d) level of theory.*

The second method was used to calculate the thermodynamic activation barriers for the 2:1 complex, where the isolated cyclopentadiene, isolated methyl acrylate, and the ion complex energies are subtracted from the total transition structure energy. As shown by Lee, when an acidic melt (51% $AlCl_3$) of EMIC was used as the solvent for the equimolar reaction of **3** and **4** (see Scheme 5.3), the rate of reaction is 10 times faster than in water and 175 faster than in ethyl ammonium nitrate.[44] The results are significant, since the reaction rate is already 20 times faster in water as compared to nonpolar solvents.[45] However, when the basic melt (48% $AlCl_3$) of EMIC was used as the solvent, Lee found that the rate was significantly slower. Water has a reaction rate 2.4 times faster that the basic melt.[44] The value calculated for the 2:1 melt falls in-between the values calculated for the acidic melt approximation using a 1:1 ratio, which is more in-line with experimental observations.

Table 5.8. *Comparison of computed thermodynamic activation parameters for the 2:1 approximated acidic melt using the B3LYP/6-31G(d) level of theory.*

TS	$\Delta E^{\ddagger}_{o}$	$\Delta E^{\ddagger}_{298}$	$\Delta H^{\ddagger}_{298}$	$\Delta G^{\ddagger}_{298}$
NC				
TS+EMI^++$Al_2Cl_7^-$ +$AlCl_4^-$	11.7	12.9	11.8	35.8

$\Delta E^{\ddagger}_{o}$ is the activation energy given by the electronic energy corrected by the zero-point energy at zero K. $\Delta E^{\ddagger}_{298}$, $\Delta H^{\ddagger}_{298}$ and $\Delta G^{\ddagger}_{298}$ are the activation energy, activation enthalpy and activation free energy at 298 K, respectively.

The difference in activation energy between the acidic melt and the basic melt, comparing rate data,[44] is approximately 1.5 kcal/mol, the computed 1:1 complex predicts a difference of about 1 kcal/mol. The difference in activation barrier between acidic melt and water, is about 1.3 kcal/mol experimentally.[44] Since water has an activation barrier of 10.2 kcal/mol[45] and our computed 1:1 acidic melt has an activation barrier of 8.1

kcal/mol, the difference is about 2.1 kcal/mol, overestimating the value by about 1 kcal/mol. The 2:1 acidic melt has an activation barrier of 11.8 kcal/mol, which underestimates the value by 1.6 kcal/mol. However, the transition structure with two $Al_2Cl_7^-$ anions complexed along with the EMI^+ cation is expected to be more in line with experiment. Since we compute the correct experimental trend of the acidic melt having a lower activation barrier than the basic melt, we conclude that local effects impact the rate enhancement of Diels-Alder reactions, but that other unexplored effects can make significant contributions.

5.3 Force Field Development

To explore larger systems in a stacked conformation or to include the effects of the bulk phase, it is necessary to use molecular mechanics due to demands on computational resources. Recent force field parameters have been reported for several different ionic liquid complexes.[47] A new force field was created for the liquid phase of the 1-ethyl-3-methyl-imidazolium (EMI^+) chloroaluminate ionic liquid, which takes advantage of the Lewis acid variability of the acidic or basic melt. Our parameters allow for the first time, the ability to construct boxes of ionic liquids at different acidic and basic melt ratios. The different acidic and basic ionic liquid boxes will allow systems, such as the Diels-Alder reaction we have been investigating (see Scheme 5.3), to be explored using the differing melt ratios. Using experimental data reported and our results with the single and complexed molecule quantum calculations, new parameters were developed to describe the relationship of chemical structure to energy.

5.3.1 Anion Parameter Validation

The $AlCl_4^-$ anion's intramolecular parameters, K_b and K_θ, which are the bond and angle force constants have been obtained by reproducing the experimental vibrational spectra. Adjustment of the bond and angle equilibrium values was generally straightforward, using the values seen experimentally. The Lenard-Jones parameter for the chlorine atoms are those from parameters developed by Kollman,[48] the parameters for the aluminum atoms have been taken from the DREIDING force field.[49] Partial atomic charges were derived using the CHELPG method.[50] All the anion's potential parameters are summarized in Table 5.9.

Table 5.9. *The force field parameters for $AlCl_4^-$.*

Force	Force constant	
Bond	K_b (kcal mol^{-1} Å^{-2})	b_0 (Å)
Al-Cl	126.0	2.1771
Angle	K_θ (kcal mol^{-1} rad^{-2})	Θ_0 (degrees)
Cl-Al-Cl	12.8	109.4712
Urey-Bradley	K_{UB} (kcal mol rad^{-2})	S_0 (Å)
Cl-Al-Cl	15.0	3.500
Lennard-Jones	ε (kcal/mol)	$R_{min}/2$ (Å)
Al	0.265	3.4709
Cl	0.310	3.9111
CHELPG charges	q (units of e)	
Al	0.72	
Cl	-0.43	

Results from these new parameters can be seen in Tables 5.10 and 5.11. Vibrational analysis using the new parameters in CHARMM agree within 2.5% of experimental values and several different methods of quantum mechanical calculations. The

frequencies obtained by QM were scaled by their appropriate factor. The Al-Cl bond distance of 2.17 Å also agreed with experiment and QM treatments.

Table 5.10. *Frequency (cm^{-1}) comparison of $AlCl_4^-$, calculated at the 6-31G(d) basis set.*

Sym	MNDO[42]	HF[42]	B3LYP	MP2	CHARMM	Exp[42]
E	108	121	113	117	124	121
T_2	169	192	176	183	150	186
A_1	362	353	332	352	352	351
T_2	528	510	491	521	493	490

Table 5.11. *Distance (Å) comparison of $AlCl_4$, calculated at the 6-31G(d) basis set.*

MNDO[42]	HF[42]	B3LYP	MP2	CHARMM	Exp[42]
2.15	2.17	2.18	2.16	2.17	2.11-2.16

To model the acidic melt, it was necessary to create a new parameter set for the $Al_2Cl_7^-$ anion. Force constants, bond and angle equilibrium values were developed in a similar fashion to the basic melt anion, $AlCl_4^-$. Partial charges were obtained using the CHELPG treatment,[50] as well.

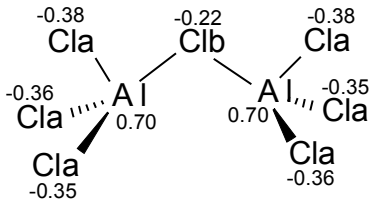

Scheme 5.5. *$Al_2Cl_7^-$ anion with the partial CHELPG charges calculated at B3LYP/6-31G(d).*

Table 5.12. *The force field parameters for $Al_2Cl_7^-$.*

Force	Force constant	
Bond	K_b (kcal mol^{-1} Å^{-2})	b_0 (Å)
Al-Cla	64.0	2.1771
Al-Clb	105.0	2.3248
Angle	K_θ (kcal mol^{-1} rad^{-2})	Θ_0 (degrees)
Cla-Al-Cla	48.0	109.4712
Cla-Al-Clb	15.8	104.93
Al-Clb-Al	35.0	121.9707
Urey-Bradley	K_{UB} (kcal mol rad^{-2})	S_0 (Å)
Cla-Al-Cla	15.0	3.500
Cla-Al-Clb	26.0	3.459
Al-Clb-Al	19.0	4.066
Dihedral	Kφ (kcal/mol) n	δ
Cla-Al-Clb-Al	0.00 1	120.0
Lennard-Jones	ε (kcal/mol)	$R_{min}/2$ (Å)
Al	0.265	3.4709
Cl	0.310	3.9111

Table 5.13. *Frequency (cm^{-1}) comparison of $AlCl_4^-$, calculated at the 6-31G(d) basis set.*

Sym	MNDO[42]	HF[42]	B3LYP	MP2	CHARMM	Exp[42]
Eu	162	146	153	149	152	158
A2u	184	175	177	179	172	179
A1g	315	278	285	302	296	308
A2u	348	297	311	328	332	331
A2u	401	351	363	379	380	381
A1g	447	395	408	425	439	439
Eu	572	512	528	548	526	525

HF scaled by 0.8929, B3LYP scaled by 0.9614, MP2 scaled by 0.9427[43]

5.3.2 Cation Parameter Validation

The force field developed for the cation EMI^+ was based on existing force constants and atom types for histidine and other imidazoles in the CHARMM program in order to make the parameters as transferable as possible.[51] New force constants were created for the missing parameters. Coulombic interactions were modeled using the fixed partial charges, identical to the anions, using the CHELPG method. Bond, angle and Urey-Bradley equilibrium parameters were developed by using DFT calculations and experimental data. All cation intermolecular and Lennard-Jones parameters that are shared with histidine were taken directly from CHARMM 27 force field and used without modification.[51] A detailed potential energy surface plot for the rotation of the dihedral angle about the ethyl side chain was modeled in the parameter set by comparison of QM calculation carried out at the B3LYP/6-31(d) level of theory. This ensures that the energies of all minima and are as accurate as possible when several minima are present. A properly parameterized potential energy surface also ensures that the correct activation barriers between the minima are represented accurately.

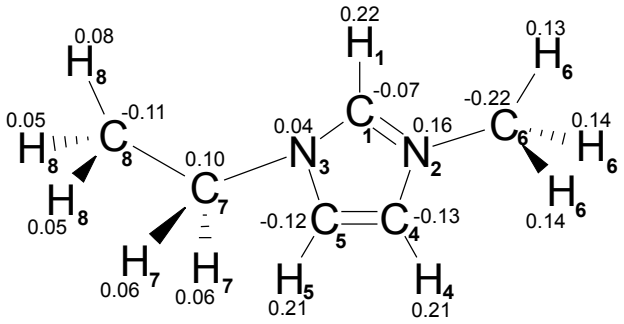

Scheme 5.6. *EMI^+ cation with the partial CHELPG charges calculated at B3LYP/6-31G(d).*

Table 5.14. *The force field parameters for EMI^+.*

Force	Force constant			Force	Force constant		
Bond	K_b (kcal mol^{-1} Å^{-2})	b_0 (Å)		*Bond*	K_b (kcal mol^{-1} Å^{-2})	b_0 (Å)	
C_1-$N_{2,3}$	380.0	1.320		N_2-C_6	240.0	1.455	
C_1-H_1	333.0	1.070		$C_{6,8}$-$H_{6,8}$	322.0	1.111	
$C_{5,4}$-$N_{3,2}$	380.0	1.370		N_3-C_7	261.0	1.490	
$C_{5,4}$-$H_{5,4}$	375.0	1.083		C_7-C_8	222.5	1.528	
C_4-C_5	410.0	1.360		C_7-H_7	309.0	1.111	
Angle	K_θ (kcal mol^{-1} rad^{-2})	Θ_0 (degrees)		*Angle*	K_θ (kcal mol^{-1} rad^{-2})	Θ_0 (degrees)	
$C_{5,4}$-$N_{3,2}$-C_1	145.0	108.0		H_6-C_6-N_2	38.0	109.5	
$N_{2,3}$-$C_{4,5}$-$C_{5,4}$	145.0	108.0		C_7-N_3-C_1	62.3	120.0	
N_2-C_1-N_3	145.0	108.0		C_7-N_3-C_5	62.3	120.0	
H_1-C_1-$N_{2,3}$	32.0	126.0		H_7-C_7-N_3	45.0	107.5	
$H_{5,4}$-$C_{5,4}$-$C_{4,5}$	22.0	130.0		H_7-C_7-C_8	34.6	110.1	
$H_{5,4}$-$C_{5,4}$-$N_{3,2}$	22.0	122.0		C_8-C_7-N_3	67.7	110.0	
C_6-N_2-C_1	62.3	120.0		H_8-C_8-C_7	34.6	110.1	
C_6-N_2-C_4	62.3	120.0					
Urey-Bradley	K_{UB} (kcal mol^{-1} rad^{-2})	S_0 (Å)		*Urey-Bradley*	K_{UB} (kcal mol^{-1} rad^{-2})	S_0 (Å)	
H_1-C_1-$N_{2,3}$	25.00	2.140		H_7-C_7-N_3	35.00	2.101	
$H_{5,4}$-$C_{5,4}$-$C_{4,5}$	15.00	2.215		H_7-C_7-C_8	22.53	2.179	
$H_{5,4}$-$C_{5,4}$-$N_{3,2}$	15.00	2.180		H_8-C_8-C_7	22.53	2.179	
H_6-C_6-N_2	50.00	2.140					
Dihedral	K_Φ (kcal mol^{-1})	n	δ (degree)	*Dihedral*	K_Φ (kcal mol^{-1})	n	δ (degree)
H_1-C_1-$N_{3,2}$-$C_{5,4}$	3.00	2	180.0	C_4-N_2-C_6-H_6	3.00	2	180.0
H_1-C_1-N_3-C_7	3.00	2	180.0	C_4-C_5-N_3-C_7	12.00	2	180.0
H_1-C_1-N_2-C_6	3.00	2	180.0	$C_{5,4}$-$N_{3,2}$-C_1-$N_{2,3}$	12.00	2	180.0
C_1-$N_{3,2}$-$C_{5,4}$-$H_{5,4}$	2.50	2	180.0	C_5-N_3-C_7-H_7	3.00	2	180.0
C_1-$N_{3,2}$-$C_{5,4}$-$C_{4,5}$	12.00	2	180.0	C_5-C_4-N_2-C_6	12.00	2	180.0
C_1-N_3-C_7-C_8	0.255	1	55.0	C_5-N_3-C_7-C_8	0.270	1	0.0
	0.00	2	0.0		4.650	2	180.0
	0.20	3	180.0		0.050	3	180.0
C_1-N_3-C_7-H_7	2.50	2	180.0	N_3-C_7-C_8-H_8	0.160	3	0.0
C_1-N_2-C_6-H_6	2.50	2	180.0	N_3-C_1-N_2-C_6	12.00	2	180.0
N_2-C_4-C_5-N_3	12.00	2	180.0	C_7-N_3-C_5-H_5	2.50	2	180.0
$N_{2,3}$-$C_{4,5}$-$C_{5,4}$-$H_{5,4}$	2.50	2	180.0	C_6-N_2-C_4-H_4	2.50	2	180.0
N_2-C_1-N_3-C_7	12.00	2	180.0	H_5-C_5-C_4-H_4	1.00	2	180.0
				H_7-C_7-C_8-H_8	0.160	3	0.0
Improper	Kφ (kcal mol^{-1} rad^{-2})	Φ_0 (degree)		*Improper*	Kφ (kcal mol^{-1} rad^{-2})	Φ_0 (degree)	
H_1-N_3-N_2-C_1	0.50	0.00		$H_{4,5}$-$C_{5,4}$-$N_{2,3}$-$C_{4,5}$	1.00	0.00	
$H_{5,4}$-$N_{3,2}$-$C_{4,5}$-$C_{5,4}$	0.50	0.00					
Lennard-Jones	ε (kcal/mol)	$R_{min}/2$ (Å)		*Lennard-Jones*	ε (kcal/mol)	$R_{min}/2$ (Å)	
H_1	-0.046	0.700		$C_{4,5}$	-0.050	1.800	
C_1	-0.050	1.800		$H_{4,5}$	-0.046	0.900	
$C_{6,8}$	-0.080	2.060		C_7	-0.055	2.175	
	-0.010	1.900			-0.010	1.900	
$N_{2,3}$	-0.200	1.850		$H_{6,7,8}$	-0.022	1.320	

Table 5.15. *Comparisons of x-ray and theoretical data for EMI^{+a}*

Geometry	*x-ray*[b]	*B3LYP*	*CHARMM*
C_1N_2	1.30	1.34	1.32
C_1N_3	1.27	1.34	1.33
N_2C_4	1.39	1.38	1.37
N_3C_5	1.41	1.38	1.37
C_4C_5	1.38	1.36	1.36
N_2C_6	1.48	1.47	1.46
N_3C_7	1.55	1.48	1.49
C_7C_8	1.43	1.52	1.54
$\angle N_2C_1N_3$	110	109	108
$\angle C_1N_2C_4$	111	108	109
$\angle C_1N_3C_5$	109	108	109
$\angle N_2C_4C_5$	104	107	107
$\angle N_3C_5C_4$	106	107	107
$\angle C_1N_2C_6$	126	126	126
$\angle C_1N_3C_7$	130	126	126
$\angle N_3C_7C_8$	104	112	110

[a] Bond distances (Å) and bond angles (º) defined in Scheme 5.6. B3LYP/6-31G(d) total energy is -344.5497092 hartrees. [b] Taken from ref. 6.

The potential energy surface plot for the rotation about the C1-N3-C7-C8 angle was computed using CHARMM with the new parameters and compared to quantum mechanical data at the B3LYP/6-31G(d) level of theory. The force constants, multiplicities and phase shifts were manipulated until they reproduced the QM energy surface of two maxima and one minima. The minima was found to be 100 degrees for both QM and MM, both maxima calculated using MM were within 0.2 kcal/mol of the QM results.

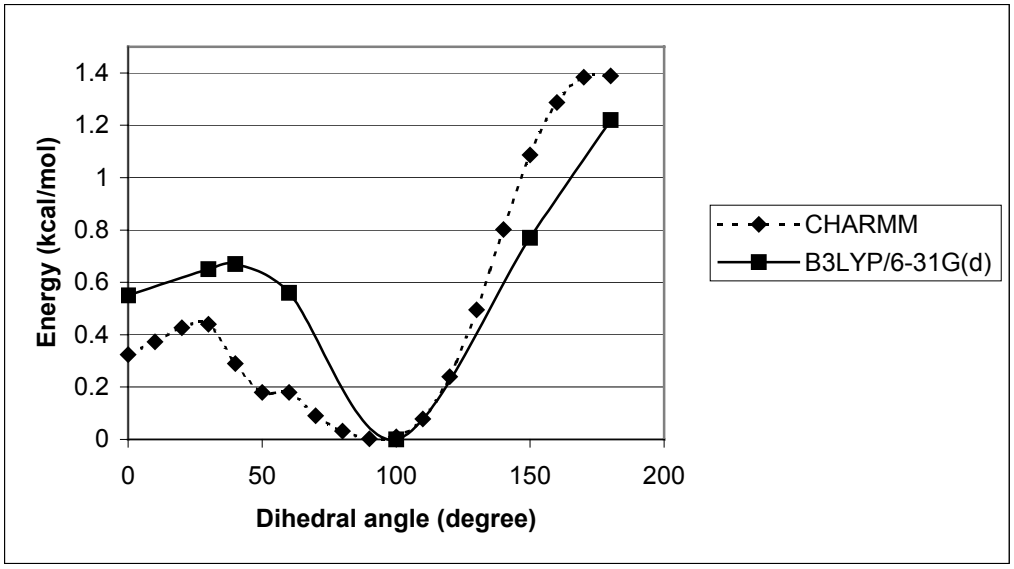

Figure 5.11. *Potential energy surface plot for rotation about the C1-N3-C7-C8 dihedral angle.*

5.4 Future Directions and Preliminary Data

While the focus of this chapter has been on the use of choloroaluminate ionic liquids composed of EMIC, another organic chloroaluminate ionic liquid, N-1-butylpyridinium chloride (BPC), see Scheme 5.1, has been shown to exhibit the same stereoselective and rate-enhancing properties. The composition of the BPC ionic liquid can be varied from basic to acidic in the same fashion as EMIC. Following the same procedures used for EMIC, a systematic study of BPC has been started. The 1:1 ratio of cation to anion has been calculated using the B3LYP/6-31G(d) level of theory, shown to be an appropriate level of theory in the EMIC system. The Diels-Alder reaction between cyclopentadiene and methyl acrylate was used. The four stereospecific transition structures complexed to the BP^+ cation, in the absence of counterions, has been calculated at the B3LYP/6-31G(d) in order to determine the correct orientation of the cation to the dienophile. Preliminary structures of the 1:1 acidic and basic melts complexed to the transition structures have been started.

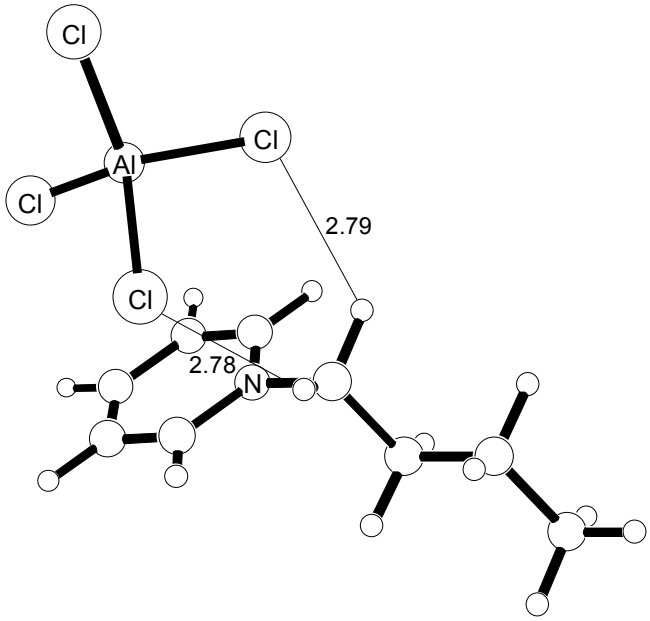

"Basic"

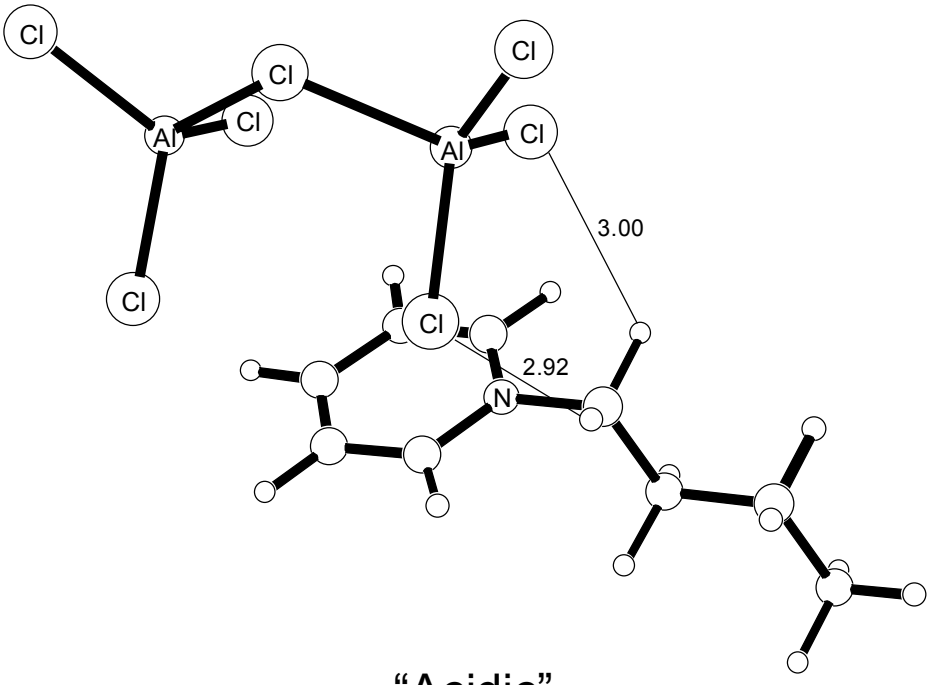

"Acidic"

Figure 5.12. *B3LYP/6-31G(d) optimized structures of 1:1 basic and acidic BP ionic liquid complexes.*

Table 5.16. *Binding enthalpies of 1:1 BPC ionic liquid complexes using the HF/6-31G(d), B3LYP/6-31G(d) and MP2/6-31G(d) level of theory (in kcal/mol).*

	Binding Enthalpy
HF	
$AlCl_4^{-}\cdots BP^{+}$	64.1
$Al_2Cl_7^{-}\cdots BP^{+}$	58.3
B3LYP	
$AlCl_4^{-}\cdots BP^{+}$	66.7
$Al_2Cl_7^{-}\cdots BP^{+}$	61.2
MP2	
$AlCl_4^{-}\cdots BP^{+}$	72.7[a]

[a] Single point MP2 energy from an MP2/6-31G(d) optimized structure.

The B3LYP/6-31G(d) level of theory (along with HF/6-31G(d) and MP2/6-31G(d)) has been employed to compute the isolated ions, which form in the melts ($AlCl_4^{-}$, $Al_2Cl_7^{-}$ and BP^{+}) along with their 1:1 complexes ($AlCl_4^{-}\cdots BP^{+}$ and $Al_2Cl_7^{-}\cdots BP^{+}$). It has been determined that the binding energy for the $AlCl_4^{-}\cdots BP^{+}$ complex is 66.7 kcal/mol, while the binding energy of the acidic melt, $Al_2Cl_7^{-}\cdots BP^{+}$ is 61.2 kcal/mol, as shown in Table 5.16. The trend where the binding energy decreases significantly as the chloroaluminate ion becomes larger, is once again seen as compared to the 1:1 and 2:1 EMI^{+} complexes. This follows our hypothesis of a weaker binding energy for the complexes as the Lewis acidity increases, regardless of level of theory.

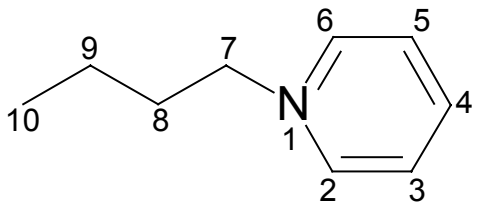

Scheme 5.7. *N-1-butylpyridinium cation.*

Table 5.17. *Comparisons of x-ray and theoretical data for BP^+.*[a]

Geometry	*x-ray*[b]	*HF*	*B3LYP*	*MP2*
N_1C_2	1.352	1.338	1.354	1.354
N_1C_6	1.348	1.338	1.354	1.354
N_1C_7	1.497	1.492	1.497	1.492
C_2C_3	1.358	1.373	1.395	1.398
C_3C_4	1.371	1.397	1.396	1.395
C_4C_5	1.374	1.397	1.397	1.395
C_5C_6	1.359	1.373	1.395	1.398
C_7C_8	1.491	1.527	1.532	1.524
C_8C_9	1.358	1.532	1.537	1.530
C_9C_{10}	1.485	1.529	1.532	1.526
$\angle C_2N_1C_6$	120.4	120.6	120.5	121.1
$\angle C_2N_1C_7$	119.3	119.7	119.5	119.3
$\angle C_6N_1C_7$	120.2	119.7	120.0	119.4
$\angle N_1C_2C_3$	120.3	121.1	120.8	120.3
$\angle C_2C_3C_4$	119.9	118.9	119.5	119.7
$\angle C_3C_4C_5$	119.2	119.6	119.2	118.7
$\angle C_4C_5C_6$	119.8	118.6	119.2	119.6
$\angle N_1C6C_5$	120.3	121.2	120.9	120.5
$\angle N_1C_7C_8$	111.9	111.8	112.1	110.9
$\angle C_7C_8C_9$	125.3	111.4	111.3	111.1
$\angle C_8C_9C_{10}$	120.6	112.2	112.2	111.8

[a] Bond distances (Å) and bond angles (º) defined in Scheme 5.7. [b] Taken from ref. 52.

An x-ray crystal structure of the acidic melt involving a BPC and $AlCl_3$, where the mole fraction of $AlCl_3$ compared to EMIC was 55:45 mol%, has been previously reported.[52] The bond lengths and angles for BP^+ are presented in Table 5.3, along with our calculations using the HF/6-31G(d), B3LYP/6-31G(d) and second-order MP2/6-31G(d) levels of theory. In general the comparison between experimental data and all three levels of theory is good. However, there seems to be an unusual distortion at the n-butyl chain in the crystal structure. The crystallographic C_8C_9 and C_9C_{10} distances are shorter than that expected for a single bond. One reason behind the instability arises from the least-squares refinement of the H atoms bonded to the C_8, C_9 and C_{10} atoms.[52] The

$C_7C_8C_9$ and $C_8C_9C_{10}$ angles also suffer from the same forces which caused the bonds to seem shortened.

A frequency analysis on the BP^+ ion was carried out and the 1:1 acidic and basic melt models at B3LYP/6-31G(d) and compared specific stretches to experimental data in Table 5.17. The scaled vibrational frequencies are within 1.6% of experimental frequencies of vibration. The B3LYP/6-31G(d) level of theory, in agreement with previous structural, vibrational and energetic ionic melt studies, is an appropriate level of theory to describe chloroaluminate ionic liquids.

Table 5.18. *Comparison of peak frequency (cm^{-1}) changes occurring with melt acidity, calculated at the B3LYP/6-31G(d) level of theory.*

melt	*aromatic C-H str/b*	*Me C-H str sym*	*aliphatic C-H str*	*aromatic str/deform*	*ring i/p asym*	*ring b o/p*
BP^+	3105	2939	2928	1470	1142	933
acidic						
BP-Al_2Cl_7	3117	2932	2924	1473	1149	938
1.8:1 melt[a]	3048	2968	2938	1489	1176	956
basic						
BP-$AlCl_4$	3104	2931	2912	1473	1144	935
0.8:1 melt[a]	3054	2967	2940	1488	1175	955

All calculations scaled by 0.9614.[43] [a]Experimental data taken from ref. 41.

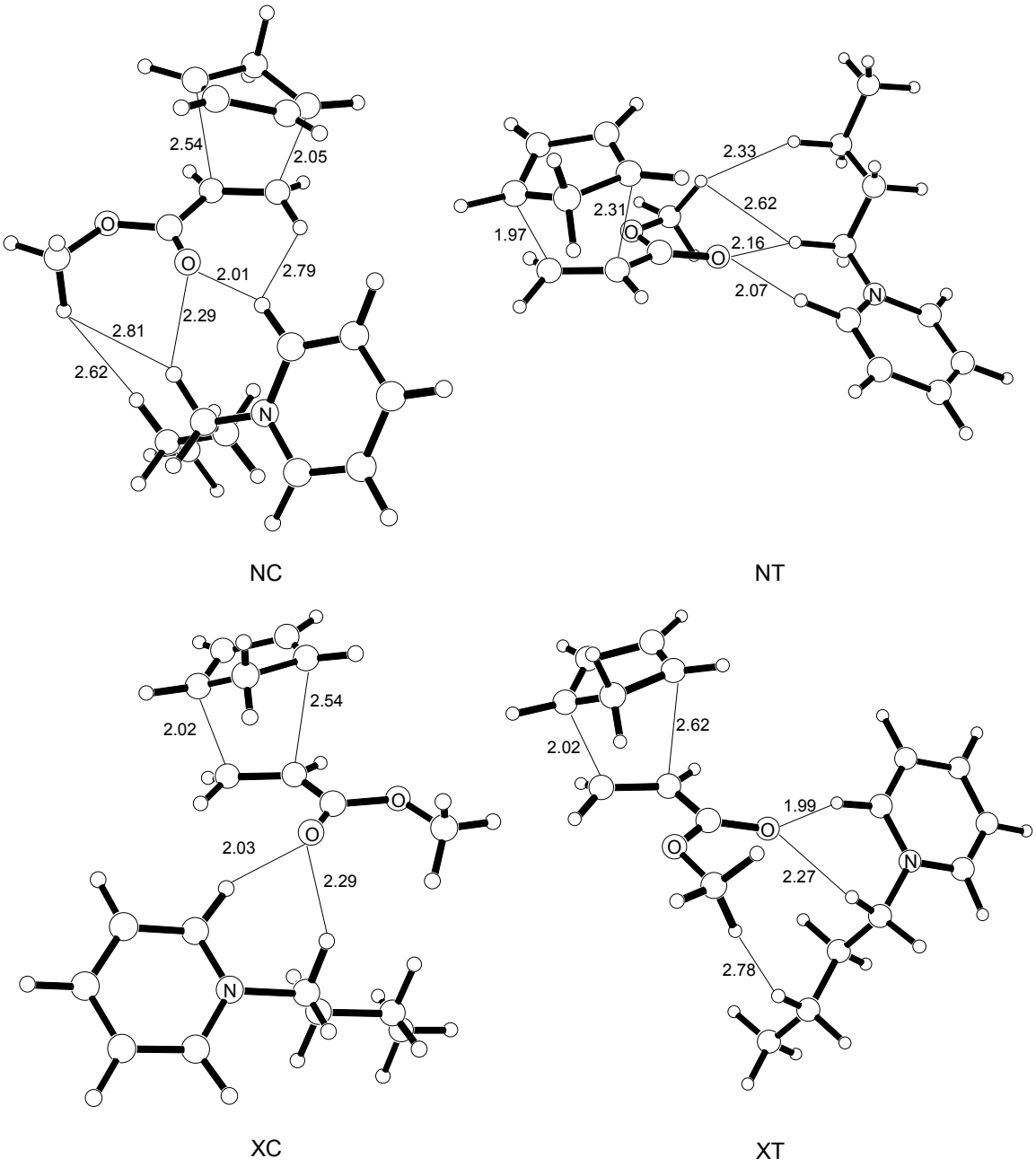

Figure 5.13. *The four stereospecific transition structures with the BP^+ cation, optimized using the B3LYP/6-31G(d) level of theory.*

The four stereospecific (NC, NT, XC and XT) transition structures have been located for the cyclopentadiene and methyl acrylate Diels-Alder reaction configurations with the BP^+ cation, as shown in Figure 5.13. The configurations were selected to orient the most acidic pyridinium protons towards the carbonyl oxygen of methyl acrylate. Complexation of BP^+ to each of the four transition structures are concerted and asynchronous, as indicated by the lengths of the breaking and forming bonds (~2.05 and ~2.54 Å in the NC structure). Although the complexation of the BP+ to the transition structure matches chemical intuition, this analysis is an oversimplification of the environment found in an ionic liquid. In this explicit ionic liquid cation model, the activation energies in Table 5.19 are computed by subtracting the isolated cyclopentadiene and the hydrogen bonded methyl acrylate and ion complex energies from the total transition structure energy, however the structures have not been thermodynamically corrected.

Table 5.19. *Computed electronic activation energies for BP^+ and the four stereospecific transition structures from the B3LYP/6-31G(d) level of theory (in kcal/mol).*

TS	$\Delta E^{\ddagger}_{elec}$
NC	13.0
NT	23.8
XC	-
XT	12.4

Further work is currently being carried out, where the 1:1 and 2:1 anion to cation complexes will be included in the transition structure, in order to model the acidic and basic melts. Figure 5.14 is a partially optimized structure of the 1:1 basic melt approximation.

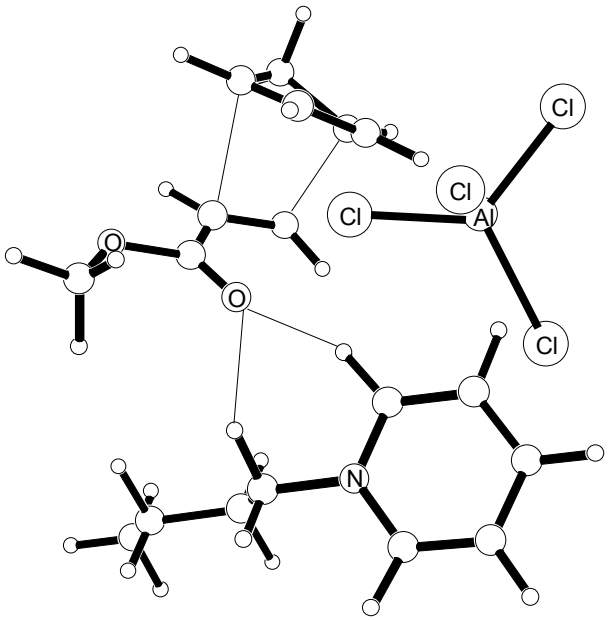

Figure 5.14. *The partially optimized NC transition structure for cyclopentadiene and methyl acrylate with a basic approximated 1:1 ratio anion-cation environment computed using the B3LYP/6-31G(d) level of theory.*

5.5 References

(1) Welton, T. *Chem. Rev.* **1999**, *99*, 2071; Seddon, K. R. *J. Chem. Tech. Biotechnol.* **1997**, *68*, 351; Freemantle, M. In *C&EN*, 2001, pp 21.

(2) Hébant, P.; Picard, G. *J. Mol. Struc. (Theochem)* **1995**, *358*, 39; Picard, G.; Bouyer, F. C.; Leroy, M.; Bertaud, Y.; Bouvet, S. *J. Mol. Struc. (Theochem)* **1996**, *368*, 67; Ribeiro, M. C. C.; Almeida, L. C. J. *J. Chem. Phys.* **2000**, *113*, 4722; Bock, C. W.; Trachtman, M.; Mains, G. J. *J. Phys. Chem.* **1994**, *98*, 478; Acevedo, O.; Evanseck, J. D. In *Ionic Liquids as Green Solvents: Progress and Prospects*; Estill, D. R., Ed.; ACS Symposium Series, 2003.

(3) Takahashi, S.; Suzuya, K.; Kohara, S.; Koura, N.; Curtiss, L. A.; Saboungi, M. L. *Z. Phys. Chem.* **1999**, 209.

(4) Wilkes, J. S.; Leveisky, J. A.; Wilson, R. A.; Hussey, C. L. *Inorg. Chem.* **1982**, *21*, 1263.

(5) Hussey, C. L. *Pure & Appl. Chem.* **1988**, *60*, 1763.

(6) Gale, R. J.; Gilbert, B. P.; Osteryoung, R. A. *Inorg. Chem.* **1978**, *17*, 2728.

(7) Wilkes, J. S.; Frye, J. S.; Reynolds, G. F. *Inorg. Chem.* **1983**, *22*, 3870.

(8) Ackermann, B. L.; Tsarbopoulos, A.; Allison, J. *Anal. Chem.* **1985**, *57*, 1766; Wicelinski, S. P.; Gale, R. J.; Pamidimukkala, K. M.; Laine, R. A. *Anal. Chem.* **1988**, *60*, 2228.

(9) Gray, J. L.; Maciel, G. E. *J. Am. Chem. Soc.* **1981**, *103*, 7147.

(10) Franzen, G.; Gilbert, B. P.; Pelzer, G.; Depauw, E. *Org. Mass Spectrom.* **1986**, *21*, 443.

(11) Davis, L. P.; Dymek Jr., C. J.; Stewart, J. J. P.; Clark, H. P.; Lauderdale, W. J. *J. Am. Chem. Soc.* **1985**, *107*, 5041.

(12) Fannin Jr., A. A.; King, L. A.; Leveisky, J. A.; Wilkes, J. S. *J. Phys. Chem.* **1984**, *88*, 2609.

(13) Garner, P. P. In *Organic Synthesis in Water*; Grieco, P. A., Ed.; Blackie Academic and Professional: London, 1998.

(14) Meijer, A.; Otto, S.; Engberts, J. B. F. N. *J. Org. Chem.* **1998**, *63*, 8989.

(15) Wijnen, J. W.; Engberts, J. *Journal of Organic Chemistry* **1997**, *62*, 2039.

(16) van der Wel, G. K.; Wijnen, J. W.; Engberts, J. B. F. N. *J. Org. Chem.* **1996**, *61*, 9001; Engberts, J. B. F. N. *Pure & Appl. Chem.* **1995**, *67*, 823; Otto, S.; Blokzijl, W.; Engberts, J. B. F. N. *J. Org. Chem.* **1994**, *59*, 5372; Blokzijl, W.; Engberts, J. B. F. N. In *Structure and Reactivity in Aqueous Solution*; Cramer, C. J., Truhlar, D. G., Eds.;

American Chemical Society: Washington, DC, 1994; Vol. 568, p 303; Blokzijl, W.; Engberts, J. B. F. N. *J. Am. Chem. Soc.* **1992**, *114*, 5440.

(17) Blokzijl, W.; Engberts, J. B. F. N. *Angew. Chem. Int. Ed. Engl.* **1993**, *32*, 1545.

(18) Blokzijl, W.; Blandamer, M. J.; Engberts, J. B. F. N. *J. Am. Chem. Soc.* **1991**, *113*, 4241.

(19) Chandrasekhar, J.; Shariffskul, S.; Jorgensen, W. L. *J. Phys. Chem. B* **2002**, *106*, 8078.

(20) Kong, S.; Evanseck, J. D. *J. Am. Chem. Soc.* **2000**, *122*, 10418.

(21) Furlani, T. R.; Gao, J. *J. Org. Chem.* **1996**, *61*, 5492; Jorgensen, W. L.; Blake, J. F.; Lim, D.; Severance, D. L. *J. Chem. Soc., Faraday Trans.* **1994**, *90*, 1727.

(22) Blake, J. F.; Lim, D.; Jorgensen, W. L. *J. Org. Chem.* **1994**, *59*, 803.

(23) Jorgensen, W. L.; Lim, D.; Blake, J. F. *J. Am. Chem. Soc.* **1993**, *115*, 2936.

(24) Blake, J. F.; Jorgensen, W. L. *J. Am. Chem. Soc.* **1991**, *113*, 7430.

(25) Acevedo, O.; Evanseck, J. D. *Org. Lett.* **2003**, *5*, 649.

(26) Breslow, R. *Acc. Chem. Res.* **1991**, *24*, 159; Breslow, R.; Rizzo, C. J. *J. Am. Chem. Soc.* **1991**, *113*, 4340; Breslow, R.; Rideout, D. C. *J. Am. Chem. Soc.* **1980**, *102*, 7816; Breslow, R.; Maitra, U. *Tetrahedron Lett.* **1984**, *25*, 1239; Breslow, R.; Maitra, U.; Rideout, D. *Tetrahedron Lett.* **1983**, *24*, 1901; Hunt, I.; Johnson, C. D. *J. Chem. Soc., Perkin Trans. 2* **1991**, 1051.

(27) Breslow, R.; Groves, K.; Mayer, M. U. *Org. Lett.* **1999**, *1*, 117; Breslow, R.; Connors, R.; Zhu, Z. *Pure Appl. Chem.* **1996**, *68*, 1527; Breslow, R.; Zhu, Z. *J. Am. Chem. Soc.* **1995**, *117*, 9923.

(28) Breslow, R. *Struct. React. Aq. Sol.* **1994**, *568*, 291.

(29) Rideout, D. C.; Breslow, R. *J. Am. Chem. Soc.* **1980**, *102*, 7816.

(30) Grieco, P. A.; Nunes, J. J.; Gaul, M. D. *J. Am. Chem. Soc.* **1990**, *112*, 4595; Lubineau, A. *J. Org. Chem.* **1986**, *51*, 2142; Lubineau, A.; Quenau, Y. *J. Org. Chem.* **1987**, *52*, 1001; Grieco, P. A.; Brandes, E. B.; McCann, S.; Clark, J. D. *J. Org. Chem.* **1989**, *54*, 5849; Dack, M. R. J. *Chem. Soc. Rev.* **1975**, *4*, 211.

(31) Gajewski, J. J.; Peterson, K. B.; Kagel, J. R. *J. Am. Chem. Soc.* **1992**, *109*, 5545; Grieco, P. A. *Tetrahedron Lett.* **1986**, *27*, 1975.

(32) Otto, S.; Engberts, J.; Kwak, J. C. T. *J. Am. Chem. Soc.* **1998**, *120*, 9517; Yoshida, K.; Garner, P. *J. Org. Chem.* **1983**, *48*, 3137; Grieco, P. A.; Garner, P.; Zhen-min, H. *Tetrahedron Lett.* **1983**, *24*, 1897; Grieco, P. A. *J. Org. Chem.* **1983**, *48*, 3137.

(33) Cativiela, C.; García, J. I.; Gil, J.; Martínez, R. M.; Mayoral, J. A.; Salvatella, L.; Urieta, J. S.; Mainar, A. M.; Abraham, M. H. *J. Chem. Soc., Perkin Trans. 2* **1997**, 653; Cativiela, C.; García, J. I.; Mayoral, J. A.; Royo, A. J.; Salvatella, L.; Assfeld, X.; Ruiz-lopez, M. F. *J. Phys. Org. Chem.* **1992**, *5*, 230; Cativiela, C.; García, J. I.; Mayoral, J. A.; Avenoza, A.; Peregrina, J. M.; Roy, M. A. *J. Phys. Org. Chem.* **1991**, *4*, 48; Sangwan, N. K.; Schneider, H.-J. *J. Chem. Soc., Perkin Trans. 2* **1989**, 1223; Schneider, H.-J.; Sangwan, N. K. *Angew. Chem. Int. Ed. Engl.* **1987**, *26*, 896.

(34) Personal *communication with Tom Welton*.

(35) Collaboration *with Dan Singleton*; Singleton, D. A.; Merrigan, S. R.; Beno, B. R.; Houk, K. N. *Tetrahedron Lett.* **1999**, *40*, 5817.

(36) Fannin Jr., A. A.; Floreani, D. A.; King, L. A.; Landers, J. S.; Piersma, B. J.; Stech, D. J.; Vaughn, R. L.; Wilkes, J. S.; Williams, J. L. *J. Phys. Chem.* **1984**, *88*, 2614.

(37) Dieter, K. M.; Dymek Jr., C. J.; Heimer, N. E.; Rovang, J. W.; Wilkes, J. S. *J. Am. Chem. Soc.* **1988**, *110*, 2722.

(38) Couch, T. W.; Lokken, D. A.; Corbett, J. D. *Inorg. Chem.* **1972**, *11*, 357.

(39) Dymek Jr., C. J.; Grossie, D. A.; Fratini, A. V.; Adams, W. W. *J. Mol. Struc.* **1989**, *213*, 25.

(40) Takahashi, S.; Curtiss, L. A.; Gosztola, D.; Koura, N.; Saboungi, M. L. *Inorg. Chem.* **1995**, *34*, 2990.

(41) Tait, S.; Osteryoung, R. A. *Inorg. Chem.* **1984**, *23*, 4352.

(42) Blander, M.; Bierwagen, E.; Calkins, K. G.; Curtiss, L. A.; Price, D. L.; Saboungi, M. L. *J. Chem. Phys.* **1992**, *97*, 2733.

(43) Scott, A. P.; Radom, L. *J. Phys. Chem.* **1996**, *100*, 16502.

(44) Lee, C. W. *Tetrahedron Lett.* **1999**, *40*, 2461.

(45) Ruiz-López, M. F.; Assfeld, X.; García, J. I.; Mayoral, J. A.; Salvatella, L. *J. Am. Chem. Soc.* **1993**, *115*, 8780.

(46) Jaeger, D. A.; Su, D. *Tetrahedron Letters* **1999**, *40*, 257.

(47) Margulis, C. J.; Stern, H. A.; Berne, B. J. *J. Phys. Chem. B* **2002**, *106*, 12017; de Andrade, J.; Böes, E. S.; Stassen, H. *J. Phys. Chem. B* **2002**, *106*, 3546; Morrow, T. I.; Maginn, E. J. *J. Phys. Chem. B* **2002**, *106*, 12807.

(48) Fox, T.; Kollman, P. A. *J. Phys. Chem. B* **1998**, *102*, 8070.

(49) Mayo, S. L.; Olafson, B. D.; Goddard III, W. A. *J. Phys. Chem.* **1990**, *94*, 8897.

(50) Breneman, C. M.; Wiberg, K. B. *J. Comput. Chem.* **1990**, *11*, 361.

(51) MacKerell Jr., A. D.; Bashford, D.; Bellott, M.; Dunbrack, R. L.; Evanseck, J. D.; Field, M. J.; Fisher, S.; Gao, J.; Guo, H.; Ha, S.; Joseph-McCarthy, S.; Kuchnir, L.;

Kuczera, K.; Lau, F. T. K.; Mattos, C.; Michnick, S.; Ngo, T.; Nguyen, D. T.; Prodhom, B.; Reiher III, W. E.; Roux, B.; Schlenkrich, M.; Smith, J. C.; Stote, R.; Straub, J.; Watanabe, M.; Wiorkiewicz-Kuczera, J.; Yin, D.; Karplus, M. *J. Phys. Chem. B* **1998**, *102*, 3586.

(52) Ward, D. L.; Rhinebarger, R. R.; Popov, A. I. *Acta. Cryst.* **1986**, *C42*, 1771.

Chapter 6

Organizing Elements Delivered by Bidentate Copper(II) Based Chiral Lewis Acid Catalysts in Asymmetric Induction

The transition structure "organizing elements" delivered by bidentate copper-based chiral Lewis catalysts in asymmetric induction have been investigated using Becke three-parameter density functional theory with the non-local correlation of Lee, Yang, and Parr. The stereoselective influences of C_2-symmetric bis(oxazoline)-Cu(II) complexes upon cyclopentadiene and acrylate imide Diels-Alder reaction have been explained in terms of three critical factors or organizing elements: the impact of metal coordination geometry, dienophile conformation (s-*cis* vs. s-*trans*), and bis(oxazoline) substituents. Consistent with experiment, our computed B3LYP/6-31G(d) *endo s-cis* transition structure is the preferred reaction pathway for all substituents studied (methyl, Ph, *t*-butyl) which is related back to the three specific organizing elements. It has been computed that *endo/exo* selectivity diminishes depending upon the bis(oxazoline)-Cu(II) C_2 substituent, where

t-butyl>*i*-Pr>Ph. A detailed picture of how the bis(oxazoline)-Cu(II) ion influences organic reactions and stereochemistry is presented to continue the development of chiral Lewis acids as catalysts for enantioselective Diels-Alder reactions.

David Evans and co-workers have designed and synthesized copper(II)-based Lewis acid catalysts, as well as demonstrated the kinetic and synthetic utility of such systems.[1] Chiral Lewis acid Cu(II) catalysts have been applied to many carbon-carbon bond-forming reactions such as aldol, enol amination, ene, Michael, and hetero Diels-Alder reactions with exceptional enantioselectivity.[2-4] The majority of C_2-symmetric bis(oxazoline)-Cu(II) complexes that catalyze Diels-Alder reactions involve α,β-unsaturated carbonyl compounds with electron rich olefins, with high diastero- and enantioselectivity of 94-96%.[5] In the asymmetric Diels-Alder cycloaddition reaction involving chiral α,β-unsaturated N-acyloxazolidinones such as 3-acryloyl-oxazolidin-2-one (acrylate imide), bis(oxazoline)-Cu(II) delivers a product with considerable diastereo-and enantioselectivity, as shown in Scheme 6.1.

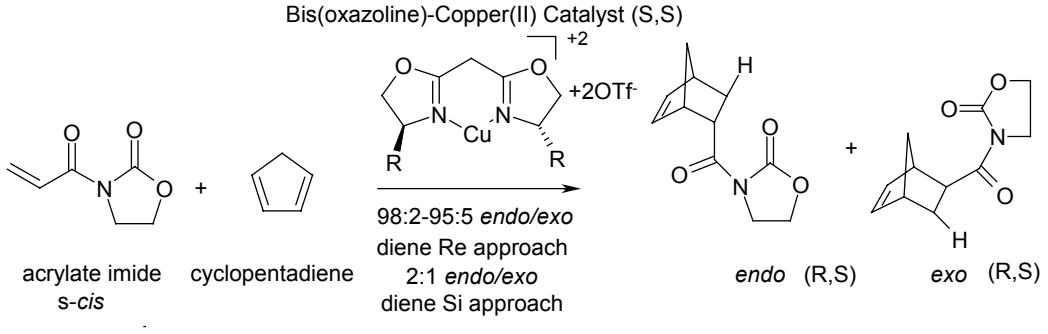

Scheme 6.1. *The acrylate imide and cyclopentadiene Diels-Alder reaction catalyzed by bis(oxazoline)-Cu(II) with representative products of the favorable sterochemical outcome (S) and unfavorable outcome of (R).*[5]

A mechanistic understanding of the elements that control π-facial selectivity in enantioselective reactions is lacking. There are many structural variables, referred to as organizing elements, within a Diels-Alder reaction catalyzed by bis(oxazoline)-Cu(II) that contribute to the observed enantioselectivty: dienophile-catalyst coordination

(tetrahedral vs square planar), dienophile conformation (s-*cis* vs s-*trans*), diene approach (*endo* vs *exo*)[6], and C_2 substituents (Ph, iPr,t-Butyl).[4,7,8] Our efforts illustrate that the overall enantioselective effectiveness of bis(oxazoline)-Cu(II) observed in asymmetric induction encompasses all of these variables and exploits them accordingly.

6.1 Metal Coordination Geometry

The well-documented importance of the attributes of Cu(II) catalyzed Diels-Alder reactions highlight the synthetic utility of such systems.[9] According to Irving-Williams, in comparing order for the stability of transition-metal complexes, Cu(II) shows optimal stability for first row transition metals.[7] Recent studies by Engberts and co-workers have shown the influence of diamine ligands on the rate and enantioselectivity of Cu(II) catalyzed Diels-Alder reactions in water.[8,10] Through the development of bis(oxazoline) complexes a number of different metal centers were explored. Studies by Corey and co-workers established that other ligand-metal complexes using Fe(III) and Mg(II) might also serve as effective chiral catalysts.[11] Evans et al. expanded the range of metals studied by including Ti(IV), Yb(II), Zr(IV), Al(III), Ni(II), and Co(II). These different transition metals could not best the rate and enantioselectivity of the Cu(II) based catalyst.[10] This is due to the chemistry inherent to Cu(II), originating from the Jahn-Teller effect. Coordination in Cu(II) to the four equatorial sites is stronger than that to the two remaining axial positions, this leads to the generally characterized square planar geometry. In a study conducted by Engberts and co-workers, it was reported that certain transition metals such as Zn(II), Ni(II), and Co(II) have no intrinsic preference for axial over equatorial ligand binding.[10] A preference for equatorial coordination is an important

component involved in the deliverance of enantioselectivity in Diels-Alder reactions. A reversal of enantioselectivity delivered by bis(oxazoline)-Cu(II) will occur with a tetrahedral coordination geometry, which will introduce degeneracy in diene facial selectivity (see Scheme 6.2), since both the Re and Si faces have an equal orientation for attack.[12] Low-level PM3 calculations have been carried out on the bis(oxazoline)-Cu(II)-substrate complex that predict a distorted square planar complexation.[4,13] A full density functional theory treatment of this complex has not been reported to date.

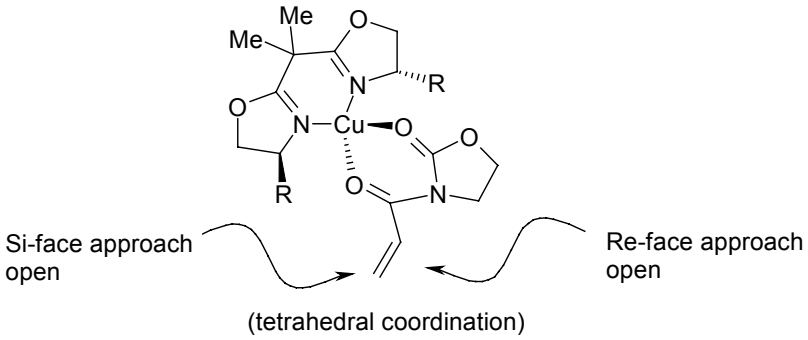

Scheme 6.2. *A tetrahedral coordination to bis(oxazoline)-Cu(II) will result in an arbitrary sense of asymmetric induction and loss of diastereo- and enantioselectivity since both the Re and Si face are equally available for attack.*

Cu(II) (d^9) complexes show great variability in coordination geometry due to the Jahn-Teller effect.[14,15] Octahedral coordination in Cu(II) containing complexes show a Jahn-Teller effect by having lower binding energies of the fifth and sixth axial ligands as compared to the four equatorial ligands.[16] Cu(II) complexes can have square-planar or nearly square-planar geometry due to angular Jahn-Teller distortion.[17] The angle of distortion can vary with ligand field strength, such that, a near tetrahedral coordination geometry can be observed.[14] In particular, $[CuCl_4]^{-2}$ shows structures ranging from tetrahedral through square planar to a distorted octahedral.[18] In order to maximize the

planarity of the Cu(II) metal coordination geometry the substrate must be equipped with favorable ligands such as the carbonyl oxygens of acrylate imide.

The Diels-Alder reaction of cyclopentadiene and acrylate imide complexed to bis(oxazoline)-Cu(II) has the catalyst coordinated to the carbonyl oxygens of acrylate. A working hypothesis is that the imide geometry results in a "twisted" planar conformation that locks the dienophile in place.[19] The C_2-like symmetry of bis(oxazoline)-Cu(II) coupled with the tetrahedral-like metal coordination geometry is proposed to block one face of the dienophile, thus controlling the selectivity.[3] The bulky C_2 substituents on the bis(oxazoline)-Cu(II) catalyst effectively removes the Si face approach for the diene leaving the Re face approach available for attack to form products, illustrated in Scheme 6.3. The incorporation of all these outlined factors (bulky C_2 substituents, square planar) will work in concert to optimize the design of a well-organized catalyst for asymmetric induction.

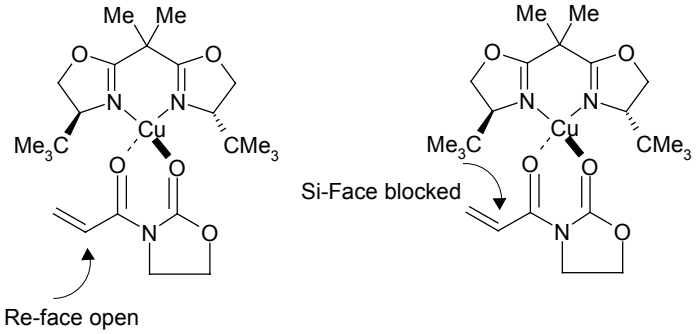

Scheme 6.3. *Nature of distereo-enantioselectivity delivered by bis(oxazoline)-Cu(II).*

Specific groups substituted onto the C_2 positions of the bis(oxazoline)-Cu(II) catalyst such as phenyl, dimethal (analogous to *i*-Pr), and *t*-butyl show differences in *endo/exo* ratios such that *t*-butyl>*i*-Pr>Ph.[20] A quantitative explanation accounting for these observed differences has not been reported to date. Additionally, the role

counterions play in these Cu(II) complexes significantly effects catalytic activity and reaction enantioselectivity. The SbF_6-derived complex is 20 times more reactive than a (OTf)- derived counterpart in the Diels-Alder reaction (Scheme 6.1).[21]

6.2 Bis(oxazoline)-Cu(II) Catalyzed Reaction

The remarkable reactivity and selectivity by the copper (II) based catalytic system provides a basis to design more reactive catalysts that can be extended to other organic reactions. A catalyst could allow for greater flexibility in the nature of the diene, as well as the substitution pattern on the dienophile. Given the synthetic importance and current understanding of the nature of the diastereo- and enantioselectivity delivered by bis(oxazoline)-Cu(II), it is important to further investigate the origin by a comprehensive computational assessment of the catalyzed Diels-Alder reaction. To date, a full density functional study of bis(oxazoline)-Cu(II) upon Diels-Alder reactions have not been reported. Density functional theory is used to include the effects of electron correlation in determining all transition structures. As a result, a more complete understanding of the factors that influence the observed enantioselectivity in Diels-Alder reactions is directly computed.

6.2.1 Bis(oxazoline)-Cu(II)

Previously, the B3LYP/6-31G(d) level of theory has been reported for Cu(I) binding to small organic systems. Luna and co-workers found the B3LYP method is in the best agreement with experiment compared to G2-based methods and CCSD(T) formulism by predicting binding energies to nitrogen or oxygen within 7 kcal/mol compared to experiment.[22] From the previous studies on copper(I), the necessity of including the effects of electron correlation, especially on the core electrons, has been well documented. Additionally, Tan and co-workers have shown that the $3s^2$ shell of copper is extremely sensitive to the inclusion of electron correlation.[23] By including electron correlation effects, we find that the UB3LYP/6-31G(d) geometry optimized bis(oxazoline)-Cu(II)-water ground state structure in terms of bonds, angles, and dihedrals are within 0.01 ± 0.06Å of the reported x-ray structure, (see Figure 6.1).[20] The x-ray structure is of the t-butyl-substituted bis(oxazoline)-Cu(II) system complexed to water. The dihedral angle between the O1-Cu2-N3-C4 in Figure 6.1 was found to be 35.2, which was in good agreement with experiment. The bis(oxazoline)-Cu(II) system was also complexed to two Cl atoms and 2 NH_2 molecules and carried out using the same level of theory, which gave the Cl-Cu2-N3-C4 dihedral angle of 36.8 and a N-Cu2-N3-C4 dihedral angle of 39.4 which is in excellent agreement with experiment as well.

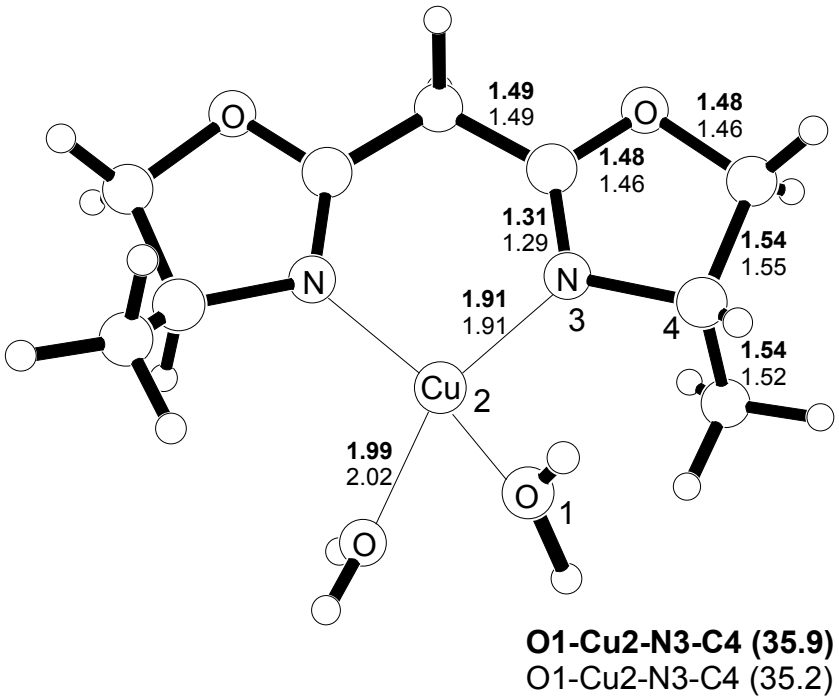

Figure 6.1. *Optimized ground state of Bis(oxazoline)-Cu(II) coordinated to water. Bold numbers are crystallographic data.*[24]

6.2.2 Parent System Transition Structure Geometries

The parent system, acrylate imide and cyclopentadiene, will serve as a model for the insertion of the bis(oxazoline)-Cu(II) catalyst. Four reaction pathways are possible for the concerted asynchronous Diels-Alder reaction between acrylate imide and cyclopentadiene. The transition structures are denoted NC (endo-*cis* acrylate imide), XC (exo-*cis* acrylate imide), NT (endo-*trans* acrylate imide), and XT (exo-*trans* acrylate imide) shown in Figure 6.2.

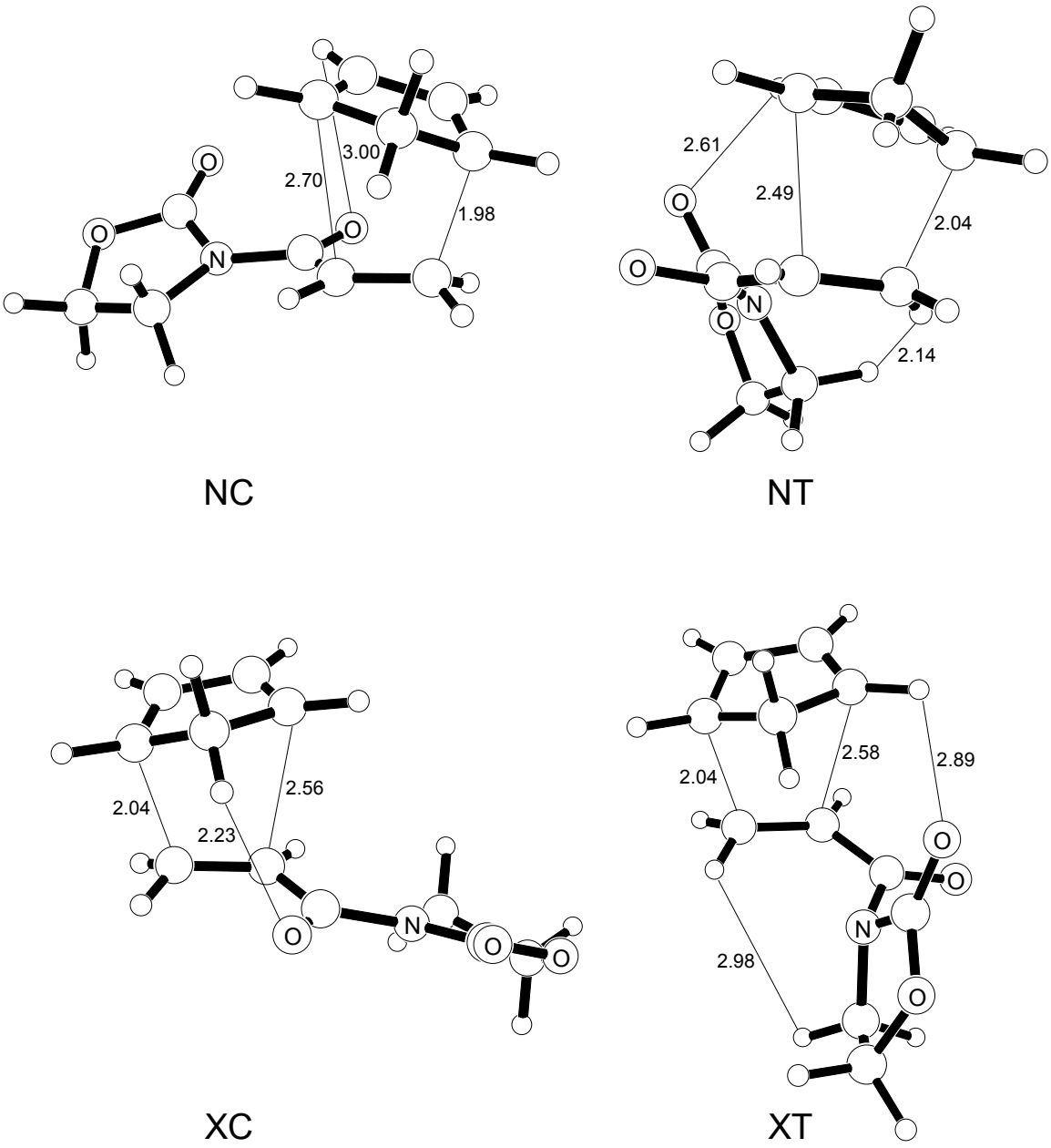

Figure 6.2. *Transition structures of the parent reaction between cyclopentadiene and acrylate imide in the gas phase, which models the strain produced by the s-trans geometry. Bond lengths (Å) are given for vacuum.*

The NC and XC transition structures have a favorable dienophile geometry compared to the NT and XT, where unfavorable steric interactions occur on the hydrogens between the double bonded carbon group and the ring, particularly for the NT, where the distance is only 2.14 Å. The NT and XT transition structures torsionally strain the imide functional group in order to form a favorable through space electrostatic interaction, reported in our earlier papers, of 2.61 Å and 2.89 Å respectively as shown in Figure 6.2.[25]

6.2.3 Parent System Activation Energies

The absolute energies and thermodynamic corrections from frequency analyses at 298.15K and 1 atm from acrylate imide, cyclopentadiene, and transition structures have been calculated. The computed activation energies, enthalpies, and Gibbs energies in vacuum are given in Table 6.1. The calculated activation energies are determined by subtracting each of the isolated ground state energies from the total transition structure energy. In our recent report on the cycloaddition of acrolein and butadiene in water, the effect of solvent on the activation energies and *endo/exo* selectivity observed by experiment was computed accurately only when the discrete-continuum model approximated solvation forces.[6] We found that the inclusion of two explicit water molecules accounted for roughly 50% of the rate and *endo/exo* selectivity enhancements observed by experiment. Consequently, we have adopted the strategy of using the bis(oxazoline)-Cu(II) to account for the local effects and using the polarizable continuum model (PCM) by Tomasi[26] to understand how solvent and Lewis acids impact chemical

reactivity. Single point calculations have been carried out with dichloromethane solvent being simulated by PCM ($\varepsilon = 8.93$).

Table 6.1. *Activation energies, enthalpies, and Gibbs energies (kcal/mol) of the reaction between cyclopentadiene and acrylate imide in vacuum and single point PCM using the B3LYP/6-31G(d) level of theory.*

TS	$\Delta E^{\ddagger}_{0}$	$\Delta E^{\ddagger}_{298}$	$\Delta H^{\ddagger}_{298}$	$\Delta G^{\ddagger}_{298}$
		Vacuum		
NC	15.3	15.1	14.5	28.4
NT	21.4	21.2	20.6	34.8
XC	16.0	15.4	14.8	28.8
XT	20.5	20.3	19.7	33.9
		PCM		
NC	7.13	7.80	6.80	12.7
NT	10.9	10.9	10.6	16.7
XC	8.2	7.85	7.69	13.8
XT	11.3	11.2	10.9	16.9

The computed activation energies clearly suggest that an *s-cis* dienophile conformation is favored over *s-trans* by approximately 5 kcal/mol. This is in excellent agreement with population ratios obtained by Lanthanide Induced Shifts (LIS), which indicates α,β-unsaturated amides exist predominately as *s-cis*.[27]

6.2.4 Dienophile Conformation

To confirm the validity of our predicted product ratios using the B3LYP/6-31G(d) level of theory, a systematic study was conducted to confirm acrylate imide's affinity for an *s-cis* conformation. $Cu(H_2O)_2^{+2}$ was used to model the Jahn-Teller distorted square planar coordination to the catalyst bis(oxazoline)-Cu(II). Calculations of acrylate imide with bidentate coordination to $Cu(H_2O)_2^{+2}$ and the non-complexed both show strong tendencies to exist as *s-cis*. An s-*trans* arrangement suffers from a moderate steric

repulsion involving distances of the hydrogen of acrylate and the hydrogens of the imide. The computed ground states of acrylate imide and the acrylate imide + $Cu(H_2O)_2^{+2}$ complex revealed that the distance between the hydrogen on the double bond to the hydrogen on the ring, 2.16 Å and 2.27 Å respectively, are as not ideal as the s-*cis* conformation (see Figure 6.3).

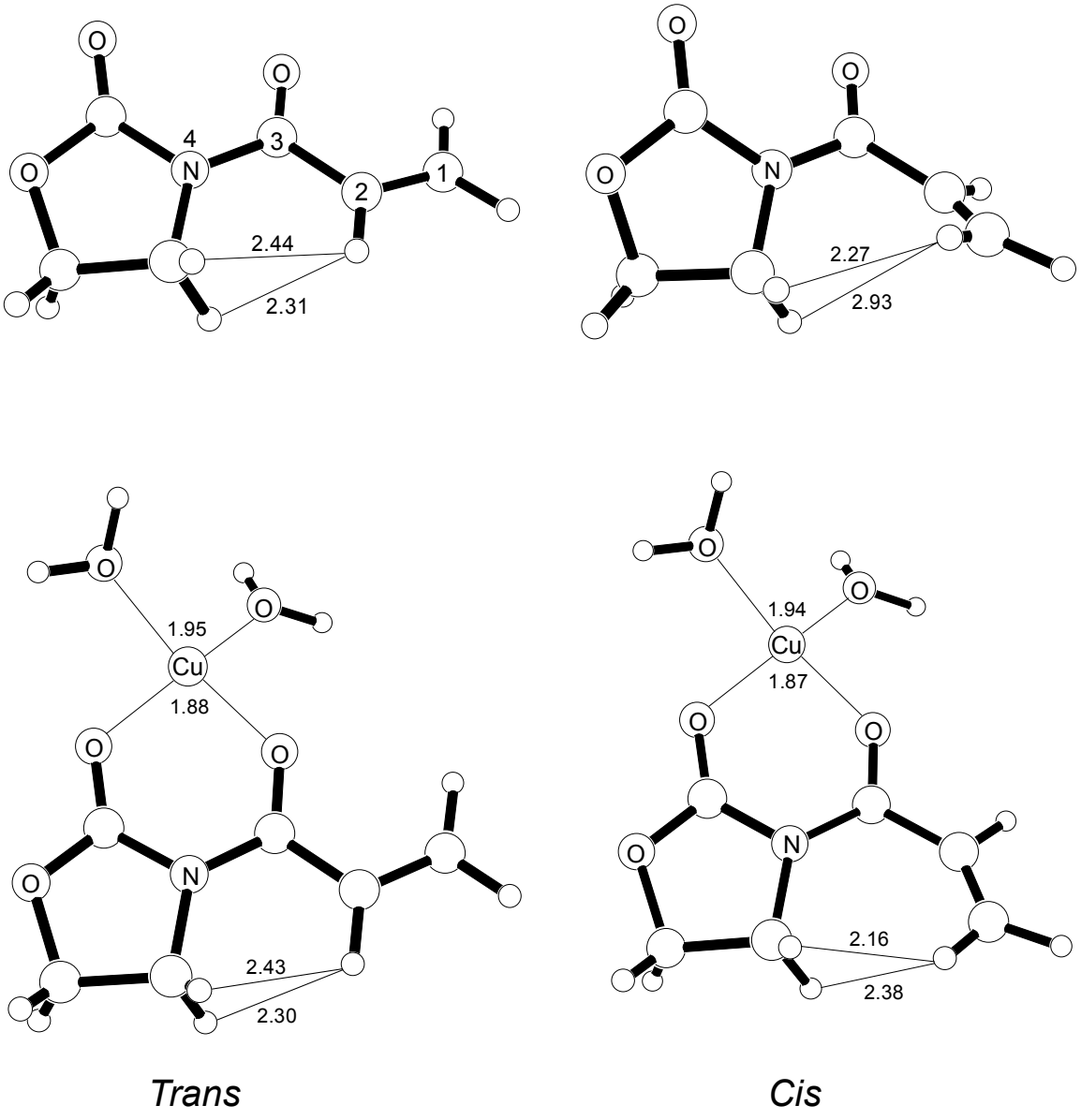

Figure 6.3. *Optimized ground states for acrylate imide and acrylate imide with* $Cu(H_2O)_2^{+2}$.

An inherent deviation in torsional strain on the angle for C1-C2-C3-N4 exists between acrylate imide with $Cu(H_2O)_2^{+2}$ and non-complexed acrylate imide by approximately 15°, with the dienophile having a value of 139° while the complexed system has a value of 155°. Cu(II) coordinated to the carbonyls in acrylate imide draws electron density from the oxygen atoms. In order to maintain conjugation, a more characteristic double bond will form adjacent to the carbonyl leaving more negative charge on the oxygen to form a bond with Cu(II) (see Figure 6.3). Since the degree of steric interaction between the α-hydrogens depends on the planarity of the system, the differences in the conformation of the $Cu(H_2O)_2^{+2}$ + acryl imide ground state compared to the isolated acrylate imide contributes toward this unfavorable interaction, although the distances between the hydrogens are similar for both systems.

6.3 Diels-Alder/Bis(oxazoline)-Cu(II) System

Transition structure and ground state analysis reveals that the Diels-Alder reaction between acrylate imide and cyclopentadiene will greatly favor the NC and XC products. Based on these observances, the acrylate imide, cyclopentadiene, and the bis(oxazoline)-Cu(II) calculated transition structures in vacuum took into consideration only the *s-cis* conformation of the dienophile. The chiral bis(oxazoline)-Cu(II) contributes to the overall observed diastereo- and enantioselectivtive by dictating the diene approach. The Re face diene approach is favored by the bulky C_2 sustituents blocking the Si face of the dienophile substrate. These strong steric interactions contribute to the experimental observed stereo-product (S) (see Scheme 6.1). C_2 substituent effects have been studied using differing functional groups, such as Ph, *i*-butyl, methyl, or *t*-butyl. The four-

stereospecific transition structures for the concerted asynchronous bis(oxazoline)-Cu(II) catalyzed Diels-Alder reaction are seen in Figure 6.4. The NC Si and XC Si transition structures model the strong steric hindrances introduced by a methyl substituted bis(oxazoline)-Cu(II). Diene hydrogens reach as close as 2.73 Å with the C_2 methal group compared to a more favorable 4.24 Å hydrogen interaction in the Re face approach.

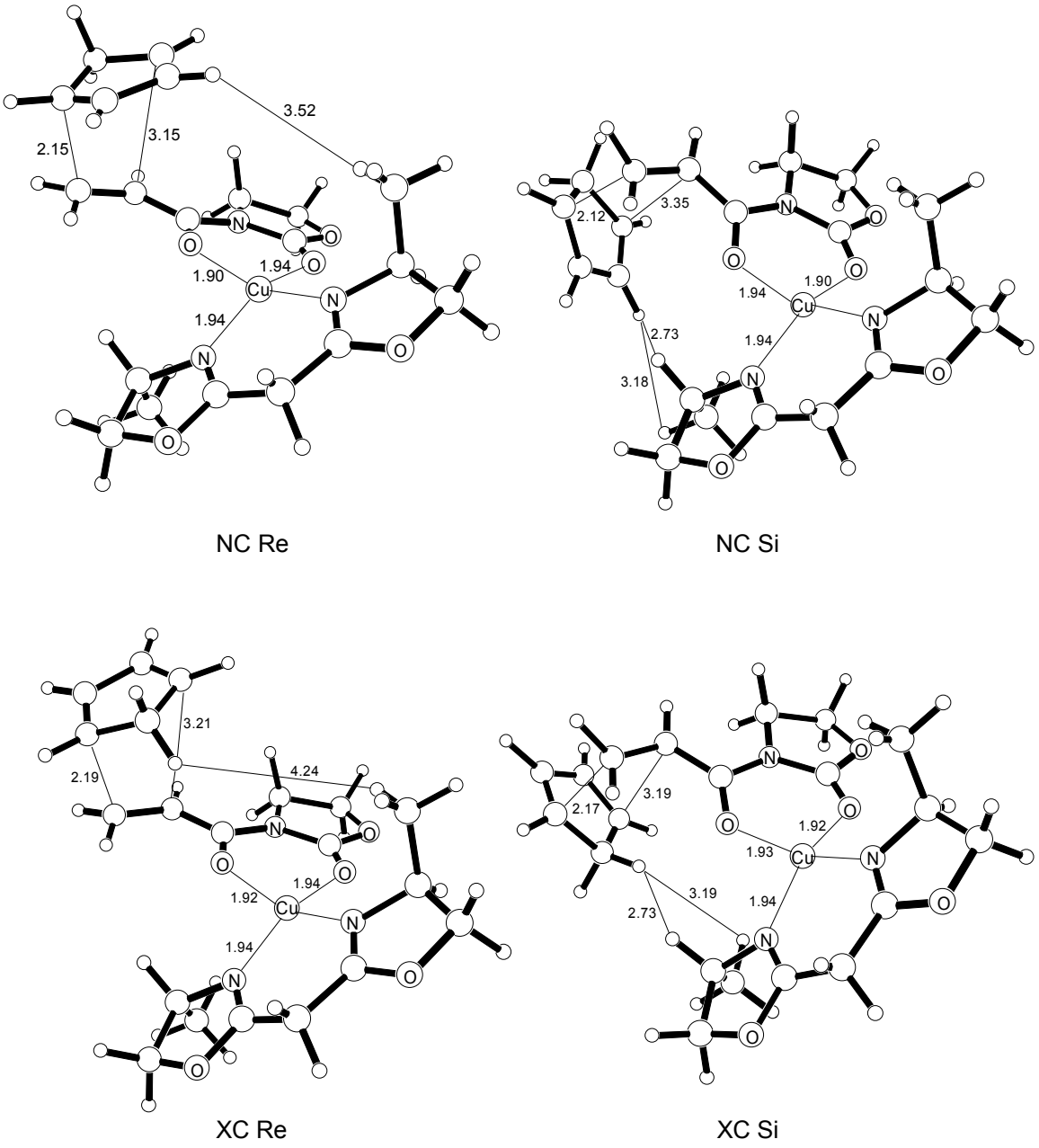

Figure 6.4. *Optimized transition structures of the reaction between acrylate imide, cyclopentadiene, and methyl substituted bis(oxazoline)-Cu(II) Diels-Alder reaction catalyzed by bis(oxazoline)-Cu(II). TS Bond lengths (Å) and dihedral angles given in degrees.*

6.3.1 Activation Energies for Catalyzed Reaction

The calculated vacuum activation parameters are indicative of a negative activation barrier for a bis(oxazoline)-Cu(II) catalyzed Diels-Alder reaction, as seen in Table 6.2. The negative activation barrier could be the result of gas phase calculations, so bulk solvation by the use of the polarizable continuum model (PCM) is currently being investigated.

Table 6.2. *Activation energies, enthalpies, and Gibbs energies (kcal/mol) of the reaction between cyclopentadiene and acrylate imide in the presence of the methyl substituted bis(oxazoline)-Cu(II) in vacuum using the B3LYP/6-31G(d) level of theory.*

TS	C_2 Substituent	Diene Approach	$\Delta E^{\ddagger}_{0}$	$\Delta E^{\ddagger}_{298}$	$\Delta H^{\ddagger}_{298}$	$\Delta G^{\ddagger}_{298}$
NC	methyl	Re	-4.65	-4.47	-5.07	7.78
NC	methyl	Si	-3.19	-3.06	-3.66	9.40
XC	methyl	Re	-4.59	-4.36	-4.95	7.70
XC	methyl	Si	-3.60	-3.44	-4.03	8.92

Another hypothesis for negative activation energies and entropy control for Diels-Alder reactions catalyzed by cation containing systems can be drawn from previous work by Houk and coworkers.[28] Studies of halocarbene cycloadditions indicate that a complex is isolated between reactants and the transition state. Analogous to carbene complexes, we have called the between or betwixt minima "twix" as a mnemonic to aid in the explanation of the negative activation energy observed in the bis(oxazoline)-Cu(II) catalyzed Diels-Alder reaction. A dynamical model can be drawn to explain the computational data by introducing an intermediate or "twix" complex that is more stable in energy than the reactants. We propose that the stability of the twix position will be directly proportional to $-T\Delta S$. This term will be extremely dynamic depending upon the

C_2 substituents on bis (oxazoline)-Cu(II). The -TΔS term will contribute to the observed reactivity. However, the origin of diastereo- and enantioselectivity will be rooted in the most favorable ΔH of reaction. Only when the ΔH term overcomes the -TΔS term is the $\Delta G^{\ddagger}$ reached. The optimal ΔH term will be reached by a combination of factors, including diene approach, dienophile conformation, and C_2 substituent selectivity or "twix-selectivity."

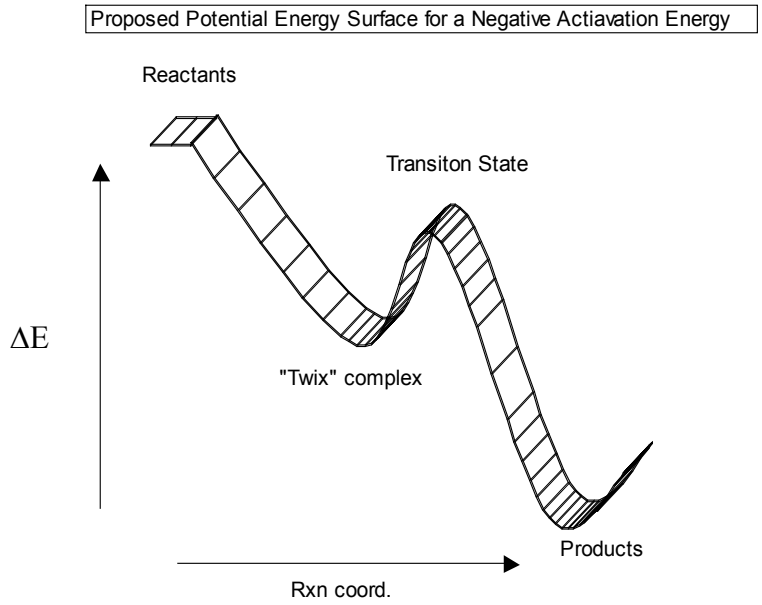

Figure 6.5. *Proposed schematic for a negative activation barrier for a catalyzed bis(oxazoline)-Cu(II) Diels-Alder reaction. The depth of the twix position and transition energy barrier height will be in direct correlation with ΔH.*

Inclusion of solvent may bring the activation energy to a positive activation barrier, removing the "twix" complex altogether. There is a reasonable doubt that the "twix" occurs at all in this system, when compared to carbene systems at different temperatures. At normal temperatures there is no bound complex on the free-energy surface between dichlorocarbene and the alkenes. The potential energy minimum "twix"

is not relevant unless the temperature is low enough that the unfavorable entropy is negligible. The issue of the complex is being addressed with a detailed future investigation and further calculations, described in Section 6.5: Future Directions.

6.3.2 Validation of Computed Results

In order to gain confidence in our computed activation parameters, a direct comparison to experimental rate data provided by Evans and co workers was undertaken.[20] Reaction kinetics is an excellent way to verify usage of a level of theory. For the Diels-Alder reaction between a modified methyl substituted acrylate imide and cyclopentadiene, experimental activation energy of 3.93 kcal/mol was extrapolated from a plot of ln(k) *vs.* 1/t (sec). Our computed $\Delta G^{\ddagger}_{298}$ for the NC transition structure is in reasonable agreement with experiment at 7.78 kcal/mol. In conjunction with the proven reliably of the B3LYP/6-31G(d) level of theory, this agreement with kinetic rata data provides conclusive justification for the UB3LYP/6-31G(d) level of theory and confidence in the computed transition structures and a solid theoretical analysis can be made to explain the origins of endo/exo selectivity in bis(oxazoline)-Cu(II) catalyzed Diels-Alder reactions.

6.4 Conclusion

We have examined the organizing elements involved in a bis(oxazoline)-Cu(II) catalyzed Diels-Alder reaction. Our B3LYP/6-31G(d) calculations confirm a distorted square-planar metal coordination geometry with the substrate dienophile in the transition state and ground state. The level of theory also agrees with previous experimental work,

where α,β-unsaturated ketones, such as acrylate imide, will predominantly exist in the *s-cis* conformer and geometry will be retained in the uncatalyzed transition structure. The origin of diastereo selectivity delivered by bis(oxazoline)-Cu(II) can be explained in terms of steric interactions. The C_2 substituents are responsible for dictating the approach of the diene with respect to the Re face of the dienophile. Since the two Re face transition structures (*endo/exo*) are similar in energy, the observed enantioselectivity may not be solely due to the bulky C_2 substituents.

6.5 Future Directions

The Mulliken overlap population will be used to gauge the strength of noncovalet bonding to examine the secondary orbital interactions that occur at transition structures.[29,30]. Previous work by Woodward and Hoffman[31], Houk[32], Salem[33], Alston[34], and Singleton[29] proposed specific secondary orbital interactions to rationalize the preference of *endo* cycloadditions. The technique will be applied to the methyl substituted transition structures and to the currently running *t*-butyl and phenyl substituted bis(oxazoline)-Cu(II) transition structures. Due to the highly asynchronous nature to the bis(oxazoline)-Cu(II) transition states an exploration of a possible diradical mechanism will be carried out using kinetic isotope effects. Counterions are known have significant effects upon catalytic activity and reaction enantioselectivity,[12] so a detailed investigation of different counterions will be carried out. To explore solvent effects upon the rate and enantioselectivty, an implicit model involving effective Hamiltonian that used continuum distributions to describe the solvent will be applied. The polarizable

continuum model (PCM) by Tomasi and co-workers will be selected.[26] This will aid in confirming our conclusions involving contributions of secondary orbital interactions, steric, and solvent effect upon the rate and enantioselectivity of the bis(oxazoline)-Cu(II) catalyzed Diels-Alder reaction.

6.6 References

(1) Evans, D. A.; Rovis, T.; Kozlowski, M. C.; Downey, C. W.; Tedrow, J. S. *J. Am. Chem. Soc.* **2000**, *122*, 9134; Evans, D. A.; Barnes, D. M.; Johnson, J. S.; Lectka, T.; von Matt, P.; MIller, S. J.; Murry, J. A.; Norcross, R. D.; Shaughnessy, E. A.; Campos, K. R. *J. Am. Chem. Soc.* **1999**, *121*, 7585.

(2) Johnson, J. S.; Evans, D. A. *Acc. Chem. Res.* **2000**, *33*, 325; Ghosh, A. K.; Mathivanan, P.; Cappiello, J. *Tetrahedron: Asymmetry* **1998**, *9*, 1.

(3) Evans, D. A.; Kozlowski, M. C.; Burgey, C. S.; MacMillan, D. W. C. *J. Am. Chem. Soc.* **1997**, *119*, 7893.

(4) Evans, D. A.; Johnson, J. S.; Olhava, E. J. *J. Am. Chem. Soc.* **2000**, *122*, 1635.

(5) Evans, D. A.; Chapman, K. T.; Bisaha, J. *J. Am. Chem. Soc.* **1988**, *110*, 1238.

(6) Kong, S.; Evanseck, J. D. *J. Am. Chem. Soc.* **2000**, *122*, 10418.

(7) Irving, H.; Williams, J. P. *J. Am. Chem. Soc.* **1953**, 3192.

(8) Otto, S.; Boccaletti, G.; Engberts, J. B. F. N. *J. Am. Chem. Soc.* **1998**, *120*, 4238.

(9) Corey, E. J. *Angew. Chem. Int. Ed.* **2002**, *41*, 1650; Ghosh, A. K.; Mathivanan, P.; Capiello, J. *Tetrahedron: Asymmetry* **1998**, *9*, 1.

(10) Otto, S.; Engberts, J. B. F. N. *J. Am. Chem. Soc.* **1999**, *121*, 6798.

(11) Corey, E. J.; Ishinhara, K. *Tetrahedron Lett.* **1992**, *33*, 6807; Corey, E. J.; Imai, N.; Zhang, H. Y. *113* **1991**, 728.

(12) Evans, D. A.; Johnson, J. S.; Burgey, C. S.; Campos, K. R. *Tetrahedron Letters* **1999**, *40*, 2879.

(13) Evans, D. A.; Scheidt, J. N.; Johnston; WIllis, M. C. *J. Am. Chem. Soc.* **2001**, *123*, 4480.

(14) Miessler, G. L.; Tarr, D. A. *Inorganic Chemistry*; 2 ed.; Prentice Hall: New Jersey, 198.

(15) Pasquarello, A.; Petri, I.; Salmon, P. S.; Parisel, O.; Car, R.; Toth, E.; Powell, D. H.; Fischer, H. E.; Helm, L.; Merbach, A. E. *Science* **2001**, *294*, 856.

(16) Stance, A. J.; Walker, N. R.; Firth, S. *J. Am. Chem. Soc.* **1997**, *119*, 10239.

(17) Reinen, D. *Comments on Inorganic Chemistry* **1983**, *5*, 227.

(18) Greenwood, N. N.; Earnshaw, A. *Chemistry of the Elements*; Pergamon Press: Elmsford New York, 1984; Shriver, D.; Atkins, P. *Inorganic Chemistry*; 3 ed.; W.H. Freeman and Company: New York, 1999.

(19) Powell, D. H.; Helm, L.; Merbach, A. E. *J. Chem. Phys.* **1991**, *95*, 9258; Fringuelli, F.; O., P.; Pizzo, F.; L., V. *Eur. J. Org. Chem.* **2001**, 439.

(20) Evans, D. A.; MIller, S. J.; Lectka, T.; von Matt, P. *J. Am. Chem. Soc.* **1999**, *121*, 7559.

(21) Johnson, B.; Evans, D. A. *Acc. Chem. Res.* **2000**, *33*, 325.

(22) Luna, A.; Alcami, M.; Yanez, M. *Chemical Physical Letters* **2000**, *320*, 129.

(23) Tan, X. J.; Zue, W. L.; Cui, M.; Luo, X. M.; Gu, J. D.; Silman, I.; Sussman, J. L.; Jiang, H. L.; Ji, R. Y.; Chen, K. X. *Chemical Physical Letters* **2001**, *349*, 113.

(24) Evans, D. A.; Peterson, G. S.; Johnson, J. S.; Barnes, D. M.; Campos, K. R.; Woerpel, K. A. *Journal of Organic Chemistry* **1998**, *63*, 6541.

(25) Acevedo, O.; Evanseck, J. D. *Organic Letters* **2003**, *5*, 649; Acevedo, O.; Kong, S.; Evanseck, J. D. *J. Am. Chem. Soc.* **2003**, *Submitted*.

(26) Tomasi, J.; Persico, M. *Chem. Rev.* **1994**, *94*, 2027.

(27) Montaudo, G.; Librando, V.; Cacamese, S.; Maravigna, P. *J. Am. Chem. Soc.* **1973**, *95*, 6365.

(28) Houk, K. N.; Rondan, N. G.; Mareda, J. *Tetrahedron* **1985**, *41*, 1555.

(29) Singleton, D. A. *J. Am. Chem. Soc.* **1992**, *114*, 6563.

(30) Birney, D. M.; Houk, K. N. *J. Am. Chem. Soc.* **1990**, *112*, 4127.

(31) Woodward, R. B.; Katz, T. J. *Tetrahedron* **1959**, *5*, 70.

(32) Houk, K. N. *Tetrahedron Lett.* **1970**, 2621.

(33) Salem, L. *J. Am. Chem. Soc.* **1968**, *90*, 553.

(34) Alston, P. V.; Ottenbrite, R. M.; Cohen, T. *J. Org. Chem.* **1978**, *43*.